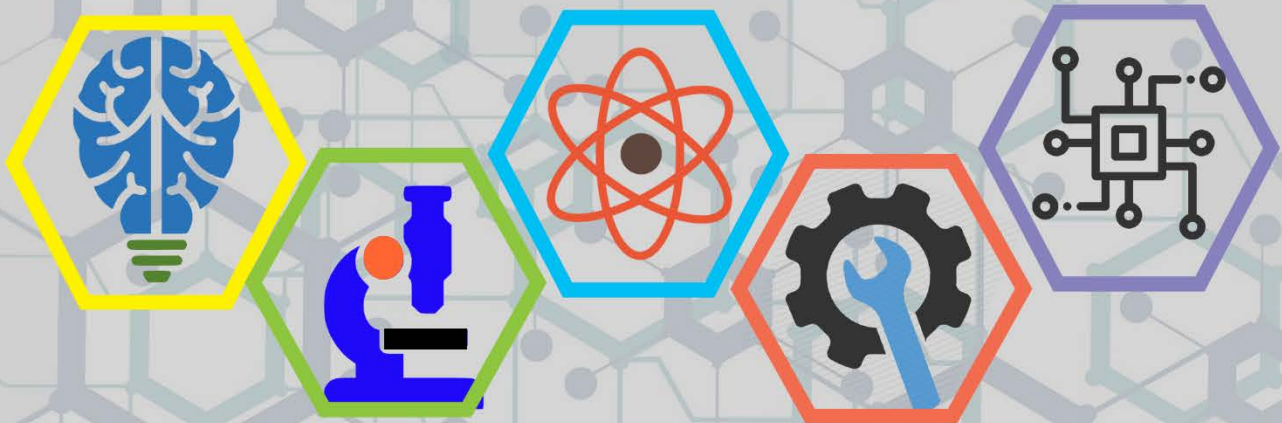# IJEIR

International Journal of Engineering

&

Innovative Research

International Journal of Engineering and Innovative Research (IJEIR)

Editor in Chief

Dr. Ahmet Ali SÜZEN
Isparta University of Applied Sciences

Editorial Board Secretaries

Osman CEYLAN
Isparta University of Applied Sciences

Ziya YILDIZ
Isparta University of Applied Sciences

Correspondence Address

CONTENTS   PAGE

Research Articles

ÇÖZGÜLÜ ÖRME İŞLETMESİNDE TOZ MARUZİYET ÖLÇÜMLERİNİN İŞ SAĞLIĞI VE GÜVENLİĞİ AÇISINDAN DEĞERLENDİRİLMESİ

Murat KODALOĞLU [1]*[ID], Gizem KARAKAN GÜNAYDIN [2][ID]

[1] Isparta Uygulamalı Bilimler Üniversitesi, Yalvaç Teknik Bilimler Meslek Yüksekokulu, Mülkiyet Koruma ve Güvenlik Bölümü, Isparta, Türkiye.
[2] Pamukkale Üniversitesi, Buldan Meslek Yüksekokulu, Moda Tasarım Programı, Denizli, Türkiye.

*Sorumlu Yazar: muratkodaloglu@isparta.edu.tr

ÖZET: Havadaki kirleticilerin, özellikle yüksek maruziyet düzeyinde sıklıkla görülen pnömokonyoz akciğer hastalıkları ile ilişkileri kurulmaktadır. [4] Kişilerin toza maruziyeti söz konusu olduğunda, toza bağlı mesleki hastalıklara yakalanma riskleri de beraberinde ortaya çıkmaktadır. Sanayileşmiş ve sanayileşmekte olan ülkelerde sınır değerlerin de üzerinde toza maruziyet, iş görmezlikler ve ölümlere yol açabilmektedir. Çalışanların, çalışma ortamından kaynaklanan hastalıklarla mağdur edilmesi kabul edilemeyeceği gibi, mesleki hastalıkların ulusal sağlık ve sosyal güvenlik sistemleri üzerine mali yükler oluşturmaktadır. Tüm bu olumsuzluklar, ortadan kaldırılabilir, yönetilebilir veya kontrol altına alınabilir. Toz, sanayileşmenin yoğun olarak yaşandığı pek çok ülkede insan sağlığını ve yaşam kalitesini daha fazla etkileyen önemli bir sorun olma özelliği taşımaktadır. İnsanlar, yaşamın değişik ortamlarında tozlu alanlarda bulunmaktadır. Bununla birlikte tozdan en çok etkilenen kesimi, yüksek düzeyde tozun ortaya çıktığı sanayi kuruluşlarında çalışanlar oluşturmaktadır. Toz, çalışan kişilerin yaptıkları işten yakınmalarına neden olması, çalışma performanslarını olumsuz yönde etkilemesi ve buna bağlı olarak iş gücü kaybına neden olması önem arz etmektedir. Fabrikalarda farklı tozlu ortamlarda çalışan kişilerin tozdan etkilenme durumlarını incelemeyi amaçlayan bu çalışma kapsamında, işletmenin çözgülü örme ve şardon bölümlerinin toz düzeyi ölçümleri yapılarak belirlenmiştir. Örme ve şardon makinalarının ortama yaydıkları toz düzeyi değerleri ölçülmüştür. Ölçüm sırasında; iş analizinde tespit edilen nominal gün şartlarının dışına çıkılmadığı gözlenmiştir. Görevler belirlenen süreler içinde gerçekleştirilmiştir ve tüm toz kaynakları tespit edilen sürelerde çalışılmıştır.

Anahtar Kelimeler: Toz, Çözgülü Örme, Şardon, Maruziyet.

EVALUATION OF DUST EXPOSURE MEASUREMENTS REGARDING TO OCCUPATIONAL HEALTH AND SAFETY IN A WARP KNITTING FACILITY

ABSTRACT: Airborne pollutants are associated with pneumoconiosis lung diseases, which are especially observed at high exposure levels. As the people are exposed to dust, the risks of getting dust-related occupational diseases also arise. Exposure to dust above the limit values in industrialized and industrializing countries can lead to disability and deaths. It is unacceptable for employees to be victimized by diseases caused by the working environment, and occupational diseases create financial burdens on national health and social security systems. All these negativities can be eliminated, managed or controlled. Dust is an important problem affecting human health and quality of life more in many countries where industrialization is intense. People are in dusty areas in different environments of life. However, workers in industrial establishments where high levels of dust are generated constitute the group that is most affected by dust. It is important that dust causes employees to complain

about their work, adversely affect their working performance, and consequently cause loss of workforce. Within the scope of this study, which aims to examine the dust exposure of people working in different dusty environments in factories, the dust level of the warp knitting and raising sections of the enterprise was determined by performing some measurements. Dust level values emitted by knitting and raising machines to the environment were measured. During the measurement; It was observed that the nominal day conditions determined in the job analysis were not exceeded. The tasks were carried out within the specified periods and all dust sources were studied within the determined periods.

Keywords: Dust, Warp Knitting, Raising Machine, Exposure.

1. GİRİŞ

Genel olarak "toz" deyimi belli süre havada asılı kalabilen çeşitli büyüklükteki katı taneler için kullanılır. Tozlar çeşitli organik ve anorganik maddelerden aşınma, parçalanma, öğütme, yanma sonucu oluşan ve büyüklükleri 1 μm ile 100 μm arasında değişen kimyasal özellikleri kendisini oluşturan kimyasal maddenin yapısına benzeyen maddelerdir.[4]

Tekstil sektörü, elyaf ve ipliği kullanım eşyasına dönüştürecek süreçleri kapsayan işlemleri içerir. Her türlü ihtiyaca yönelik elyaf, iplik, örme dokuma kumaş, keçe ve dokusuz yüzeylerin olduğu yüzeyler, ev tekstili ürünleri, tekstil sektöründe yer almaktadır. Tekstil sektöründe, yüksek kalite ve optimum hızda üretim yapabilmek için kullanılan makine ve teçhizat önem taşımaktadır. Tekstil sektörü, emek-yoğun olması bakımından iş gücü etkin bir sektördür.

Makinalaşma ile ortaya çıkan ve iş başarısını olumsuz yönde etkileyen makine etkilerinden birisi tozdur. Toz, birden fazla makinanın bir arada çalıştırıldığı ortam koşullarında, makinaları kullanan işçilere önemli düzeyde rahatsızlıklar verebilmektedir. Bu gibi ortamlarda yüksek toz düzeyi, işçilerin sağlığını ve verimlerini olumsuz yönde etkilemektedir. Çözgülü örme ve şardon makinalarının oluşturduğu tozun işçi sağlığı üzerindeki olumsuz etkileri incelenebilmesi için bu makinaların ortama yaydığı toz düzeyinin saptanması gereklidir. İşletmede toz düzeyi ölçümü yapılmış ve işçi üzerindeki etkileri incelenmiştir.

Sanayileşme arttıkça insan sağlığını olumsuz yönde etkileyecek çevresel etmenler de artmaktadır. Bu çevresel etmenlerden en yoğun olarak etkilenen çalışan grup işçilerdir. Ülkemizde de teknolojik ilerlemelerle birlikte işçilerimizin sağlığı korunmaya çalışılmaktadır. Ülkemizde en önde gelen sektör tekstil sektörüdür. Örme sanayiinde işçiler belli başlı bazı çevresel zararlı etkenlere maruz kalmaktadırlar. Bunlardan en yoğun olanları gürültü, nemin yüksek oluşu ve tozdur. Çevresel etkenlerin yanında işin yürütülmesi ile ilgili etkenler bulunmaktadır. Bunlar vardiyalı çalışma koşulları, sürekli ayakta çalışma gibi faktörler olarak sıralanabilir. İşyeri tozu en iyi bilinen meslek hastalığı nedenidir. Özellikle pamuk tozuna bağlı olarak tanımlanmış bissinozis çok eski dönemlerden beri bilinmektedir [6]. Uzun yıllar iplik üretiminde çalışan işçilerde, solunum fonksiyonlarında etkilenme görülür. Pamuk tozuna 20-25 yıldan uzun süre maruz kalan bireylerde bissinozis geliştiği [5] ve bissinozis sıklığı çalışılan bölümlere göre farklılıklar gösterdiği belirtilmektedir [2]. Bu çalışmada, çözgülü örme yapan işletmede toz maruziyet düzeyi ve bunun çalıştıkları bölümlerle ve çalışma süreleriyle ilişkisinin incelenmesi amaçlanmıştır. Değişik bölümlerde toz yoğunluğunu ölçerek işçilerin solunum fonksiyonlarındaki değişiklikler işyerindeki toz yoğunluklarıyla ilişkilendirilmesi amaçlanmıştır.

1.1.Toza Bağlı Mesleki Solunum Sistemi Hastalıkları

Havadaki başlıca kirleticilerden biri olan toz, mesleki akciğer hastalıklarının temel nedenlerinden biridir. İnsan sağlığı bakımından önemli olan 0.5 – 100 mikron arasındaki büyüklüklere sahip olan tozlardır. Çünkü bu büyüklükteki tozlar solunum yoluyla alveollere

ulaşıp birikim yaparak "pnömokonyoz" olarak bilinen akciğer toz hastalıklarına neden olurlar. Daha büyük tozlar havada asılı kalmayıp çöktükleri için insan vücuduna giremezler. Mesleki hastalıkların oluşmasında tozun partikül büyüklüğü, fibrojenik potansiyeli, ortamdaki konsantrasyonu ve kişinin maruziyet süresi etkilidir. Tozların akciğerde hastalık meydana getirmesinde tozun özellikleri kadar kişisel faktörlerin de etkili olduğu unutulmamalıdır.

1.1.1. İnorganik tozların neden olduğu hastalıklar
• Asbestosis (Asbestoz)
• Silikosis (Slikoz)
• Kömür Tozu Hastalığı
• Siderosiz

1.1.2. Organik tozların neden olduğu hastalıklar
• Bisinozis

1.1.3. Sık Görülen Diğer Mesleki Akciğer Hastalıkları
• Akciğer Kanseri
• Mesleki Astım (yükümlülük süresi 1 yıl)
• Ağır metal Hastalıkları
• Kronik Obstrüktif Akciğer Hastalığı (KOAH)

1.1.4. Mesleki Akciğer Hastalıkları
• Akut İnhalasyon Hasarı (Havayolu İrritasyonu , Toksik Pnömonitis , İnhalasyon Ateşi)
• Havayolu Hastalıkları (Bisinozis, Astım, Kronik Bronşit, KOAH)
• Parankimal Bozukluklar (Organik Hipersensitivite Pnömonitisi, İnorganik Pnömokonyoz)
• Enfeksiyon Hastalıkları (Tbc, Virüs, Bakteri)
• Maligniteler (Sinonazal, Akciğer, Plevra (mezotelyoma))[4]

1.2.Tekstil Sektöründe Toz Ölçümleri ve Sınır Değerler

Toz Numuneleri Değerlendirmeleri; Çalışma ortamında toz numune örneklemeleri, TS CEN/TR15230 ve CEN TR 16013-3 standartlarındaki metotlara uygun yapılır.Tozla Mücadele Yönetmeliği (Resmi Gazete Tarihi: 05.11.2013 Resmi Gazete Sayısı: 28812)'ne göre;

Toz: İşyeri ortam havasına yayılan veya yayılma potansiyeli olan parçacıkları,
Toz ölçümü: İşyeri ortam havasındaki toz miktarının gravimetrik esasa veya lifsi tozlarda lif sayısına göre belirlenmesini,
Ölçüm Sonucu Birimi-Zaman Ağırlıklı Ortalama Değer (ZAOD/TWA):
Günlük 8 saatlik zaman dilimine göre ölçülen veya hesaplanan zaman ağırlıklı ortalama değeri ifade eder.
Toza Yönelik Risk değerlendirmesi: İşveren, çalışanlarının sağlık ve güvenliğini tehlikeye atacak, işyerinde bulunan tozlardan kaynaklanan olumsuz etkileri belirlemek üzere, 6331 sayılı İş Sağlığı ve Güvenliği Kanunu ve 29/12/2012 tarihli ve 28512 sayılı Resmî Gazete'de yayımlanan İş Sağlığı ve Güvenliği Risk Değerlendirmesi Yönetmeliği hükümlerine uygun şekilde risk değerlendirmesi yapmakla yükümlüdür. Tozlu işlerde yapılacak risk değerlendirmesinde aşağıda belirtilen hususlar özellikle dikkate alınır:

a) Ortamda bulunan tozun çeşidi,
b) Ortamda bulunan tozun sağlık ve güvenlik yönünden tehlike ve zararları,
c) Maruziyetin düzeyi, süresi ve sıklığı,

ç) Mesleki maruziyet sınır değerleri,

d) Toz ölçüm sonuçları,

e) Alınması gereken önleyici tedbirleri, varsa daha önce yapılmış olan sağlık gözetimlerinin sonuçları.[4]
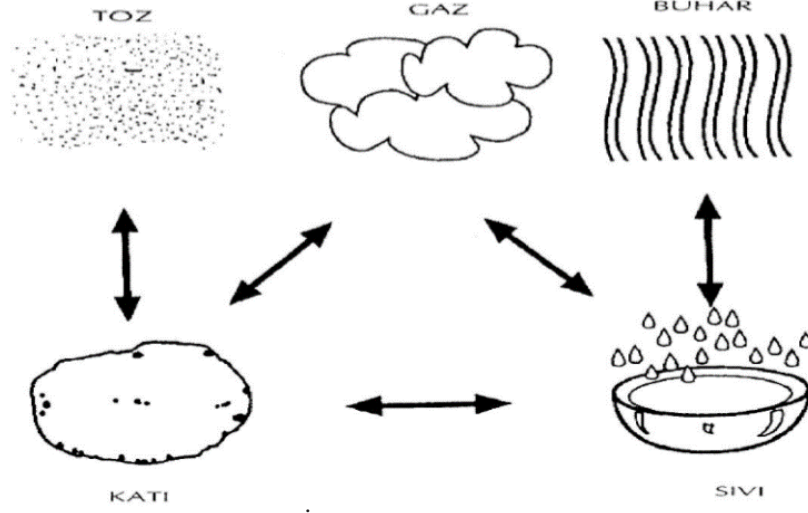
Şekil 1. İş yerlerindeki kirleticiler [7].

İş yerindeki kirleticiler toz, gaz, buhar, katı, sıvı etkileşimleri şekil 1 de verilmiştir.

2. MATERYAL VE YÖNTEM
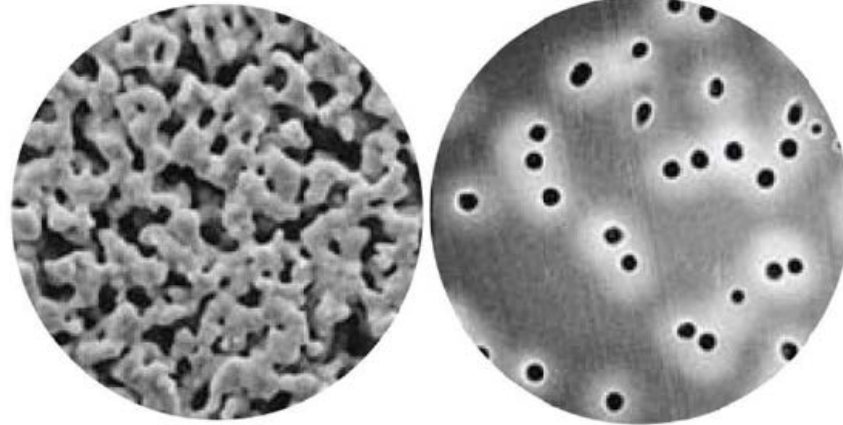
Şekil 2. Gümüş filtre   ve   Polikarbonat filtre [7].

Gravimetrik toz ölçümü için Yaygın kullanılan filtre türleri: pvc, teflon, selüloz, cam fiber, polikarbonat vb. filtreler şekil 2 de gösterilmiştir.
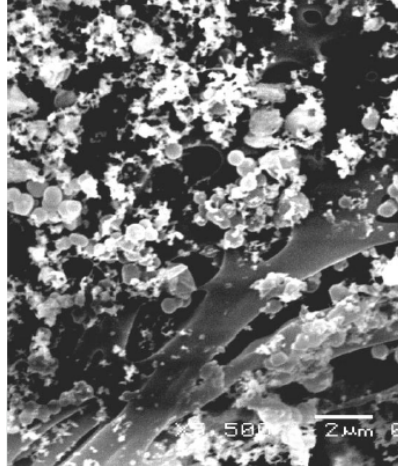
Şekil 3. Solunabilir toz SEM görüntüsü [7].

Polikarbonat filtre üzerine örneklenmiş partiküllerin görüntüsü şekil 3 de verilmiştir.

2.1. Materyal Model

Deneysel çalışmalarda, battaniye fabrikasında kullanılan örme ve şardon tezgahlarında toz ölçümleri yapılmıştır. Tüm maruziyet sınır değerleri şahsi örnekleme esasına dayalı olarak solunum bölgesinde yapılmıştır. Ölçüm cihazının Konumu ; Örnekleme pompası, örnekleme yapılan çalışanın üzerine sabitlenmiştir ve örnekleyici kişinin ağız ve burun bölgesinde 30 cm alan içerisine yerleştirilmiştir. Ölçüm metodolojisi; TS EN 689 İşyeri havası –Solunumla maruz kalınan kimyasal maddelerin sınır değerleri ile karşılaştırılması ve ölçme stratejisi ile değerlendirilmiştir.

Tablo 1. Ölçümlerde Kullanılan Cihazlar

Cihaz Adı	Marka	Model
Hava Örnekleme Pompası	BUCK	LP-5
Dijital Hava Akış Kalibratörü	SENSIDYNE	GO-CAL 4146
Rotametre	DWYER	RMA-26-SSV
Kalibrasyon kavanozu	ZEFON	ZA0085
Hava Örnekleme Kaseti ve 37 mmPVC filtre	ZEFON	725PVC
Basınç, Sıcaklık ve Nem Ölçer	TFA	GAIA

Tablo 2.Ölçüm yapılan Bölümdeki Ortam Şartları

Bölüm/Çalışma Alanı	Sıcaklık (⁰C)	Basınç (hPa)	Nem (%)
Baskı Bölümü	15,0	910,2	66
Yarma ve Kaymaz halı yapıştırma Bölümü	15,0	910,2	66
Çözgülü Örme	18,2	910,5	76
Levet Sarma Bölümü	19,7	910,7	71
Terzihane	18,0	910,6	77
Şardon Bölümü	19,2	910,3	71
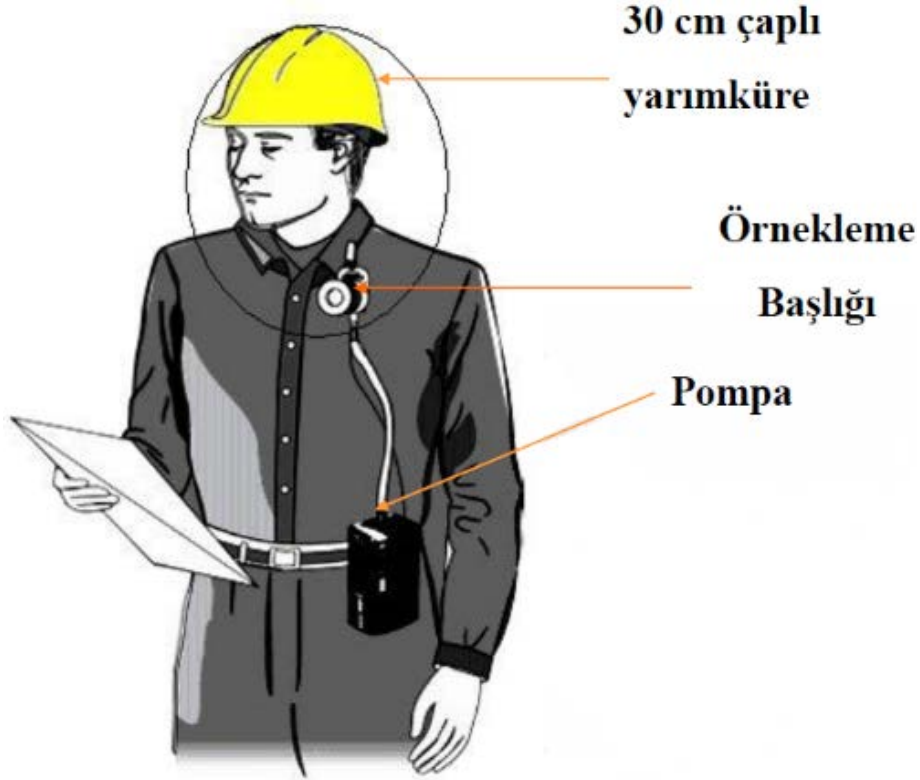
Şekil 4.Toz ölçüm işlemi[7].

Tüm maruziyet sınır değerleri şahsi örnekleme esasına dayalı olarak solunum bölgesinden yapıldığı şekil 4 de gösterilmiştir.

Tablo 3. Bölümlerde yapılan işler ve maruziyet kaynakları.

Bölüm/ Çalışma Alanı	Yapılan İşler	Maruziyet Kaynakları/Yoğunluğu	Maruz kalınan Tozun Türü Hakkında Bilgiler
Baskı Bölümü	Battaniye Desen Basımı, Fiksaj Yıkama ve Kurutma İşleri yapılmaktadır.	Baskı Makinası, fiksaj makinası, Yıkama ve Kurutma Makinası	Ortamda Bulunan istenmeyen toz
Yarma ve kaymaz halı yapıştırma bölümü	Battaniye ayırma, tamirat, keçe yapıştırma, Pvc uygulama işleri yapılmaktadır.	Yarma makinası, keçe yapıştırma makinası, yıkama ve kurutma makinası	Elyaf tozu
Çözgülü Örme Bölümü	Battaniye kumaşı örme işlemi ve levent sarma işlemi yapılmaktadır.	Örme makinası levent sarma makinası	Elyaf tozu
Terzihane	Battaniye kenar dikimi, ovarlok yapımı, oyma işlemi, etiket yapıştırma ve kalite kontrol işleri yapılmaktadır.	Overlok makinası, dikiş makinası, oyma makinası,taş yapıştırma makinası	Elyaf tozu
Şardon bölümü	Battaniye fırçalam işlemi, Kesim işlemi ve sıcak baskı işleri yapımaktadır.	Şardon makinası, Kesim makinası, sıcak baskı makinası	Elyaf tozu

Şekil 4. Baskı bölümü.

Şekil 5. Örme bölümü.

Şekil 6. Şardon bölümü.

Şekil 7. Terzihane.

Tablo 4.Ölçüm sırasındaki çalışma şartları ve işyeri faktörlerinin tanımlanması

Bölüm/Çalışma Alanı	Günlük Çalışma/ Mola Süresi	Maruziyet Süresi	İşin Türü	Bölümde çalışan Kişi Sayısı/Vardiya Sayısı	Havalandırma Şartları	Kaynağa yakınlık durumu	Çalışanın KKD Kullanımı
Baskı Bölümü	9,5 Saat/1 saat	8,5 saat	Battaniye desen basımı, Fiksaj yıkama ve Kurutma işleri yapılmaktadır.	5 Kişi/ 1 vardiya	Havalandırma sistemi bulunmaktadır.	Yakın	Var
Yarma ve Kaymaz halı yapıştırma Bölümü	9,5 Saat/1 saat	8,5 saat	Battaniye ayırma , tamirat, keçe yapıştırma,	2 Kişi /1 vardiya	Havalandırma sistemi bulunmaktadır.	Yakın	Var

8

			işleri yapılmaktadır.				
Çözgülü Örme Bölümü	9,5 Saat/1 saat	8,5 saat	Battaniye kumaşı örme işlemi ve levet sarma işlemi yapılmaktadır.	8 Kişi /1 vardiya	Havalandırma sistemi bulunmaktadır.	Yakın	Var
Terzihane	9,5 Saat/1 saat	8,5 saat	Battaniye kenar dikimi, ovarlok yapımı oyma işlemi etiket yapıştırma ve kalite kontrol işleri yapılmaktadır.	11 Kişi /1 vardiya	Havalandırma sistemi bulunmaktadır.	Yakın	Var
Şardon	9,5 Saat/1 saat	8,5 saat	Battaniye fırçalama işlemi, kesim işlemi yapılmaktadır.	8 Kişi /1 vardiya	Havalandırma sistemi bulunmaktadır.	Yakın	Var

Çeşitli çalışma alanlarında nisan, mayıs, haziran, temmuz aylarında iki adet ölçümler yapılarak değerlendirmelerde bulunulmuştur.

Tablo 5.Ölçüm sonuçları ve değerlendirme

Bölüm/Çalışma Alanı	Yapılan Ölçüm	Çalışan Adı	Yapılan İşin Tanımı	Tozun Türü	Ölçüm Tarihi	Ölçüm sonucu Konsatrasyon (mg/m³)	Ölçüm Sonucu TWA (mg/m³)
Baskı Bölümü	İç Ortam Solunabilir Toz	A	Battaniye desen basımı, Fiksaj yıkama ve Kurutma işleri yapılmaktadır.	İstenmeyen Toz	Nisan 2020	0,86	
						0,87	
					Mayıs 2020	0,83	
						0,85	
					Haziran 2020	0,91	
						0,89	
					Temmuz 2020	0,80	
						0,82	
Yarma ve Kaymaz halı yapıştırma Bölümü	İç Ortam Solunabilir Toz	B	Battaniye ayırma , tamirat, keçe yapıştırma, PVC uygulama işleri yapılmaktadır.	İstenmeyen Toz	Nisan 2020	1,37	
						1,36	
					Mayıs 2020	1,41	
						1,40	
					Haziran 2020	1,32	
						1,33	
					Temmuz 2020	1,35	
						1,36	
Çözgülü Örme Bölümü	İç Ortam Solunabilir Toz	C	Battaniye kumaşı örme işlemi ve	İstenmeyen Toz	Nisan 2020	2,7	
						2,6	

Bölüm	Toz Türü	Kod	İşlem	Toz	Ay		
			levet sarma işlemi yapılmaktadır.		Mayıs 2020	2,4	
						2,4	
					Haziran 2020	2,2	
						2,3	
					Temmuz 2020	2,1	
						2,2	
Levet Sarma Bölümü	Kişisel Solunabilir Toz	D	Levent Sarma İşlemi yapılmaktadır.	İstenmeyen Toz	Nisan 2020		1,93
							1,92
					Mayıs 2020		1,82
							1,83
					Haziran 2020		1,96
							1,95
					Temmuz 2020		1,91
							1,92
Terzihane	İç Ortam Solunabilir Toz	E	Battaniye kenar dikimi, ovarlok yapımıoyma işlemi etiket yapıştırma ve kalite kontrol işleri yapılmaktadır.	İstenmeyen Toz	Nisan 2020	1,42	
						1,43	
					Mayıs 2020	1,36	
						1,37	
					Haziran 2020	1,48	
						1,47	
					Temmuz 2020	1,39	
						1,38	
Şardon	Kişisel Solunabilir Toz	F	Battaniye fırçalama işlemi, kesim işlemi yapılmaktadır.	İstenmeyen Toz	Nisan 2020		1,72
							1,73
					Mayıs 2020		1,65
							1,66
					Haziran 2020		1,78
							1,76
					Temmuz 2020		1,71
							1,73

Toz ölçüm yapılan yerler ve sayılar çalışan işçilerin maruziyet durumları göz önüne alınarak belirlenmiştir. Ölçüm yapılan dokuma/örme bölümü, levent sarma alanı, şardon bölümü ve kesimhane bölümlerinde sınır değerlerin aşılmadığı tespit edilmiştir.

3. SONUÇ VE TARTIŞMA

Çözgülü örme işletmesindeki yüksek toz düzeyinde çalışılması, sağlığı olumsuz yönde etkilemektedir. Bu çalışmada örme ve şardon makinasının ortama yaydığı toz düzeyi değerleri tespit edilmiştir. İnsan sağlığına doğrudan etkili olan tozun oluştuğu iş yerlerindeki işçiler tarafından, tozun etkisini azaltan maske vb. koruyucuların yaygın olarak kullanıldığı belirlenmiştir. Örme ve şardon makinasının oluşturduğu tozun çevreye yayılmasını önlemede

en iyi yöntem kaynağında korumadır yani makinanın tozunun azaltılmasına yönelik alınan önlemlerdir. Kişisel önlemlerden önce üretim yerlerindeki tozun düzeylerini azaltılması işçilerin tozdan etkin biçimde korunması için önem taşımaktadır.

Toz yoğunluğunun ölçülmesi, işyerinin işçilere ne düzeyde zarar verdiğini anlamamıza yardımcı olabilecek bir yoldur. Çalışmada işyeri toz yoğunlukları vertikal ayırıcılı gravimetrik ölçüm yapan partikül ölçüm aleti ile yapılmıştır. Baskı bölümünde 0,80-0,91(mg/m^3) ,yarma bölümünde 1,32-1,41 (mg/m^3), örme bölümü 2,1-2,7 (mg/m^3), levent bölümünde 1,82-1,96 (mg/m^3), terzihane 1,36-1,48 (mg/m^3) şardon bölümünde 1,65-1,78 (mg/m^3) olarak tespit edilmiştir. Çalışmamızda, saptanan değerler sınır düzeylerin altında bulunmuştur. Toz yoğunluğu ile Bissinozis görülme sıklığı arasında ilişki olduğu belirtilmektedir [1].Elde ettiğimiz değerler ile literatürde yapılan çalışmalar kıyaslandığında yapmış olduğumuz çalışmayı destekleyici sonuçlar elde edilmiştir. Zuskin E ve arkadaşları [8] toz yoğunluğu 0.97 mg/m3 olan pamuk tekstil fabrikasında bissinozis sıklığının %42.9 ile %51.6 arasında değiştiğini saptamıştır.

Toz yoğunluğu azaldıkça solunum fonksiyonlarındaki bozulma sıklığı artmaktadır. Bu bağlamda işyerlerinde toz yoğunluğunun azaltılmasına yönelik çalışmalar yürütülmesi gerekliliği ortaya konmuştur. Bu önlemler; uygun havalandırma (Yerel-Genel), ıslak çalışma yöntemi , düzenli toz ölçümleri, periyodik kontrol muayeneleri (röntgen ve SFT), işe giriş muayenesi (Akciğer rahatsızlığı yönünden riskli olanlar, aşırı sigara içenler belirlenmeli ve toz maruziyeti olan işlerde çalışması önlenmeli), çalışanlara gerekli eğitimin verilmesidir.[3]

Sonuç olarak fabrikada işçiler önemli düzeyde toza maruz kalmadıkları, bu maruziyetin sonucu olarak solunum fonksiyonlarında etkilenme olmadığı saptanmıştır. İşyeri toz yoğunluğunun azaltılmasına yönelik çalışmaların her geçen gün önemli olduğu anlaşılmıştır. Çalışma hayatı süresince giderek artan etkilenmenin önceden belirlenmesi için çalışanların periyodik muayeneleri gerekmektedir. Bu muayenelerin solunum fonksiyon testlerini içermelidir. Toza maruz kalan çalışanlarda tozların temas ettiği deride ısı artışı, kızarıklık, yanma, kaşınma, şişme, su toplaması, belirtileri görülebilir. Periyodik muayene sadece işyerindeki risklere göre değil ayrıca işyerindeki risk gruplarına ve işçilerin özel durumlarına göre de yapılmalıdır.

KAYNAKLAR

[1]. Bronchopulmonary Diseases Caused by Cotton, Flax, Hemp or Sisal Dust. In:Early Detection of Occupational Diseases. WHO, Geneva, 1986.

[2]. Cotton. Recommended Health-Based Occupational Exposure Limits for Selected Vegetable Dusts. Technical Report Series no: 684. Geneva 1983.

[3]Ertem, M., İlçin E., Kelle, K., Topçu, F.,(2000) Diyarbakır Sümerbank Halı ve İplikFabrikalarında Çalışan İşçilerin Solunum Fonksiyonlarının İncelenmesi Solunum Hastalıkları; 11: 126-134
Dicle Üniversitesi Tıp Fakültesiı, DİYARBAKIR

[4].Kaplan E., (2016)Tekstil Sektöründe Tozla Mücadele Rehberi Çalışma ve Sosyal Güvenlik Bakanlık yayınları İş Sağlığı ve Güvenliği Genel Müdürlüğü Ankara

[5]. Niven RML, Pickering CAC. Byssinosis: A Review, Thorax 1996;51:632-7.

[6]. Schilling RSF. Byssinosis. In: Encyclopedia of occupational health and safety Parmeggiani L, ed. 3th ed. Geneva:International Labor Office (ILO), 1983;351-3.

[7].Yılmaz E.,(2015) Çalışanların Toz Maruziyet Tespitine Yönelik Çalışmalarda Dikkat Edilecek Hususlar Çalışma ve Sosyal Güvenlik Bakanlık yayınları İş Sağlığı ve Güvenliği Genel Müdürlüğü Ankara

[8]. Zuskin E, Jacobs JJ, Schachter EN, (1991) Witek TJ. A ten year follow-up study of cotton textile workers. Am Rev Respir Dis;143:301-5.

International Journal of Engineering and Innovative Research

http://dergipark.gov.tr/ijeir

RESNET34 DERİN ÖĞRENME MİMARİSİ KULLANILARAK YÜZ GÖRÜNTÜLERİNDEN VÜCUT AĞIRLIĞI TAHMİNİ UYGULAMASI

Bekir AKSOY[1*] , Hamdi SAYIN[1] , Osamah SALMAN[1]

[1] Isparta Uygulamalı Bilimler Üniversitesi, Teknoloji Fakültesi, Mekatronik Mühendisliği, Isparta, Türkiye.

*Sorumlu Yazar: bekiraksoy@isparta.edu.tr

ÖZET: Görüntü işleme teknolojileri günlük hayatımızda sıklıkla kullanılan yöntemlerden birisidir. Özellikle yapay zeka teknolojisinin hızla gelişmesi ile birlikte görüntü işleme teknolojilerinde yapay zeka yöntemleri kullanılmaya başlanmıştır. Örneğin biyomedikal görüntülerden hastalık teşhisi yapılması, yüz görüntülerinden kişilerin duygu analizlerinin yapılması, tarım alanında bitkilere ait görüntüler üzerinden hasat zamanı ve miktarının belirlenmesi gibi birçok alanda yapay zeka yöntemleri kullanılmaktadır. Çalışmada açık erişimli internet sitesi https://academictorrents.com'dan 61110 kişiye ait yüz görüntüleri ve bu görüntülere ait vücut ağırlığı veri seti alınmıştır. Alınan veri seti üzerinde ResNet34 derin öğrenme yöntemi kullanılarak yüz görüntülerinden bu görüntülere ait vücut ağırlığı değerlerini tahminlenme için bir model oluşturulmuştur. Oluşturulan ResNet34 modeli RMSE performans değerlendirme ölçütüne göre değerlendirilerek 0.071797 hata değeri elde edilmiştir. Elde edilen hata değeri ResNet34 modelinin kullanılan veri seti üzerinde başarılı olduğunu göstermektedir.

Anahtar Kelimeler: Resnet34; Regresyon; Vücut Ağırlık Tahmini; Yapay Zeka.

BODY WEİGHT ESTİMATİON APPLİCATİON FROM FACE IMAGES USİNG RESNET34 DEEP LEARNİNG ARCHİTECTURE

ABSTRACT: Image processing technologies are one of the methods used in daily life. With the rapid development of artificial intelligence technology in technology, artificial intelligence methods have been used. For example, diagnosis of diseases from biomedical images, confident emotion analysis of facial images, artificial intelligence methods are used in various fields of harvest time and amount of images of plants in agriculture. In the study, faces of 61110 people and body weight data set of these images were obtained from the open access website https://academictorrents.com. A model was created for the body weight estimation of these images to learn ResNet34 on the data set. The ResNet34 model created was evaluated according to the RMSE performance criteria and an error value of 0.071797 was obtained. The error value obtained indicates that the used data set of the ResNet34 model is successful.

Keywords: Resnet34; Regression; Body Weight Estimation; Artificial Intelligence.

1. GİRİŞ

Görüntü işleme, insan gözü ile yapılabilen işlemlerin bilgisayar ortamında çeşitli arayüz yazılımlarıyla gerçekleştirilmesi ile hızlı sonuçlar üreten bir teknolojidir. Bu teknolojide farklı tanıma modelleri geliştirilmiş ve bu modeler kullanılarak yapılan çalışmalar bilime önemli ölçüde katkıda bulunmuştur. Görüntü işleme ve sınıflandırma yöntemleri kullanılarak, görüntü üzerinde; nesne algılama, etiketli sınıflandırma, nesne ayırma, alt sınıflara bölme gibi birçok kategoride analizler yapılabilmektedir [1]. Görüntü işleme uygulamaları geliştirilirken

problemin türüne ve istenen sonuca göre çeşitli derin öğrenme algoritmaları kullanılmaktadır [2]. Makine öğrenmesine göre çok katmanlı bir yapıya sahip olan ve insan beyninin işleyişinden esinlenen derin öğrenmenin kullanımı, birçok alanda giderek artmaktadır [3]. Derin öğrenme ile ilgili ilk çalışmalar 1950'li yılların sonlarına dayanmasına rağmen son yıllarda başarılı bir şekilde kullanılmasının başlıca sebebi teknolojik cihazların çeşitliliği ile giderek artan büyük veri miktarıdır [4,5]. Derin öğrenmenin geleneksel makine öğrenmesi yöntemlerinden farkı, kodlanmış kurallar ile öğrenmek yerine; resim, video, ses ve metinlere ait veri simgelerinden otomatik olarak öğrenebilme özelliğine sahip olmasıdır [6].

Derin öğrenmenin önemli kullanım alanlarından birisi de bilgisayarlı görüdür. Bilgisayarlı görü; bir görüntüdeki nesneleri tanıma amacıyla, kamera görüntülerindeki özniteliklerin analiz edilerek görüntüden bilgi çıkarma işlemidir[7]. Nesne tanıma, görüntü üzerinde bulunan nesnelerin, insan algısına en yakın şekilde tanımlanabilmesini sağlamak amacıyla gerçekleştirilen işlemlerdir. Yüz tanıma sistemleri ise nesne tanıma uygulamaları arasında en çok ilgi gören ve en sık kullanılan sistemlerden birisidir [8]. Yüz tanıma özellikle kimlik doğrulaması için önde gelen biyometrik tekniktir. Bu teknik askeri uygulamalar, finans, kamu güvenliği gibi birçok alanda yaygın olarak kullanılmaktadır [9]. Özellikle havaalanları, iş yerleri, oteller ve hastaneler gibi halka açık alanlarda güvenliğin sağlanması ve kimlik tespiti yapma amacıyla yoğun olarak kullanılan yüz tanıma sistemleri, aynı amaç doğrultusunda pasaport, kimlik kartı ve sürücü belgesi gibi devlet uygulamalarında da tercih edilmektedir [10]. Yüz tanıma sistemlerinde yüz görüntülerinin birbirine benzerliğinden dolayı sınıflandırma işlemlerinin hassas bir şekilde yapılması gerekmektedir [11]. Biyometri tabanlı sistemler kişinin parmak izi, yüz tanıma gibi dış görünüm veya imza yürüyüşü gibi davranış özelliklerini inceleyen sistemlerdir [12] Yakın zamanda, cinsiyet, yaş, boy ve kilo gibi özellikleri içeren biyometri uygulamaları [13-17], semantik yorumlarından dolayı sıklıkla kullanılan uygulamalardan birisi olmuştur. Yüz tanıma sistemlerinin sınıflandırılmasında genellikle derin öğrenme modelleri kullanılmaktadır.

Çalışmada açık kaynak erişimli internet sitesinden (https://academictorrents.com) alınan toplam 61110 insan yüzü görüntüsü ve bu görüntülere ait vücut ağırlığı verilerinden oluşan veri seti kullanılmıştır. Veri seti 48888 eğitim ve 12222 doğrulama verisi olmak üzere rastgele şekilde ikiye ayrılmıştır. Eğitim veri seti Resnet34 derin öğrenme modeli ile eğitilerek fotoğraf bilgisinden kişinin vücut ağırlığı tahminlenmiştir. Eğitilen model doğrulama veri seti ile değerlendirilmiştir. Elde edilen sonuçlar karekök ortalama hata (Root Mean Square Error-RMSE) performans değerlendirme ölçütüne göre değerlendirilerek 0.071797 hata değeri elde edilmiştir.

2. MATERYAL VE YÖNTEM

Çalışmada açık kaynak erişimli internet sitesinden (https://academictorrents.com) temin edilen 61110 adet insan yüzü fotoğrafı ve bu insanlara ait kişisel bilgilerini içeren csv dosyası veri seti olarak kullanılmıştır [18]. Kullanılan veri seti ve ResNet34 derin öğrenme modeline ait detaylı bilgiler çalışmanın materyal bölümünde verilmiştir.

2.1. Materyal

2.1.1. Çalışmada kullanılan veri seti

Çalışmada kullanılan veri seti, iki bölümden oluşmaktadır. İlk bölüm; ABD İlinois eyaletinde tutuklu bulunan farklı yüz özelliklerine sahip erkek ve kadın toplam 61110 adet mahkûma ait

yüz fotoğrafından oluşmaktadır.


Şekil 1. Veri seti fotoğraf örnekleri.

İkinci veri seti ise yüz görüntüleri verilen mahkumlara ait kişisel bilgileri(ad, soyad, doğum tarihi, ağırlık, boy, saç rengi, göz rengi, ten rengi, cinsiyet vb.) içeren metinsel bilgilerden oluşmaktadır.

	ID	Adı Soyadı	Doğum Tarihi	Kilo	Saç Rengi	Cinsiyet	Boy	Irk	Göz Rengi
0	A00147	MCCUTCHEON, JOHN	06/14/1949	185.0	Brown	Male	67.0	White	Blue
1	A00220	WALKER, ISIAH	03/30/1957	155.0	Black	Male	73.0	Black	Brown
2	A00360	BELL, HOWARD	12/18/1946	167.0	Gray or Partially Gray	Male	69.0	White	Green
3	A00367	GARVIN, RAYMOND	1.12.1954	245.0	Black	Male	72.0	Black	Brown
4	A01054	TIPTON, DARNELL	03/25/1954	166.0	Salt and Pepper	Male	67.0	Black	Brown

Şekil 2. Veri setinde yer alan kişisel bilgiler,

2.1.2. ResNet(residual network) mimarisi

ResNet mimarisi derin ve kompleks sınıflandırma problemlerini çözmek için önerilmiş olan bir evrişimli sinir ağı CNN(Convolutional Neural Network) mimarisidir [19] ResNet, VggNet, AlexNet gibi geleneksel ardışık ağ mimarilerinden farkı mikro mimari bir modül yapısına sahip olmasıdır [20]. Microsoft ekibi tarafından oluşturulan bu model [21], çok katmanlı derin ağlarda gradyan değerlerinin sıfıra yakınsama problemini ortadan kaldırmak için geliştirilmiştir. ResNet mimarisinde, alt katmanlardan elde edilen öznitelik bilgileri sıralı olarak üst katmanlara taşınmasıyla alt ve üst katmanlar arasında bir köprü kurulmaktadır [19]. ResNet mimarisi kullanılan katman sayısına göre farklı mimarilere evrilmiştir. Örneğin; ResNet101 mimarisi, 101 adet katmandan oluşmaktadır. ResNet'te katmanlar arasında yapılan atlama işlemine ResBlock ismi verilir. ResBlock sayesinde bir önceki katmanda bir şey öğrenilmese bile eski katmandaki bilgiyi yeni katmana uygulanarak model daha güçlü hale getirilir. Böylece gradyan silinmesi problemi de ResBlock ile çözülmüş olur. Optimizasyon algoritması olarak eğim düşümü kullanılır [22]. Sıklıkla kullanılan ResNet mimarilerinden birisi de 34 katmandan oluşan ResNet34 mimarisidir. (Şekil 3)[23]
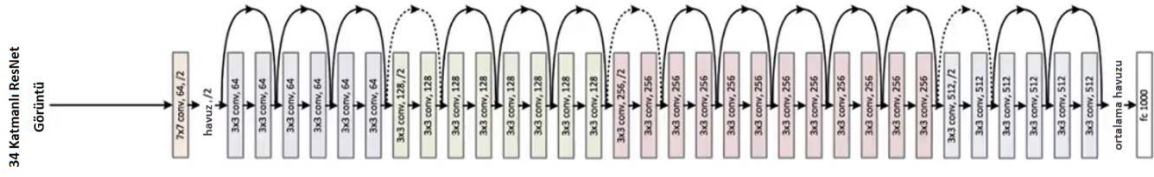
Şekil 3. ResNet-34 mimarisi [23].

Derin öğrenme mimarilerinde ağ derinleşmeye başladığında, bozulma problemi ortaya çıkmaktadır. Bu bozulma yüksek oranda eğitim hatasına yol açmakta, bu da sonuçta tüm sistemin optimize edilmesini zorlaştırmaktadır [19].
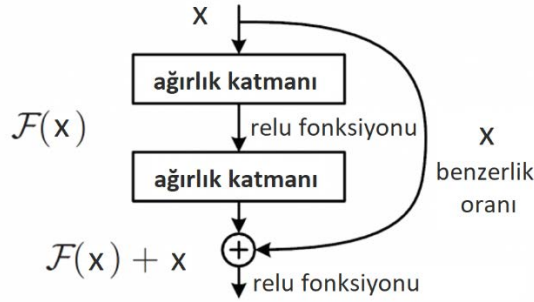
Şekil 4. ResNet mimarisi [18].

Bu problemin çözümü için Microsoft tarafından, derin artık öğrenme modeli oluşturulmuştur. Bu modelde birkaç yığılmış katmanın her birinin doğrudan istenen bir haritaya uymasını beklemek yerine, bu katmanların artık bir haritaya uymasına izin verilmektedir [21]. F (x) + x'in formülasyonu, kısayol bağlantılarına sahip ileri beslemeli sinir ağlar ile gerçekleştirilebilmektedir. Kısayol bağlantıları, Şekil 4'de gösterilen bir veya daha fazla katmanı atlayan bağlantılardır. Kısayol bağlantıları kimlik eşlemesi yapmakta ve bunların çıktıları yığınlanmış katmanların çıktılarına eklenmektedir [22]. Bu sayede kolayca optimize edilebilen ResNet mimarisinin ağdaki derinlik arttıkça daha yüksek eğitim hatası oluşumu önlenmekte ve diğer mimarilerden daha iyi sonuçlar üretebilmektedir [24].

2.1.3. Performans ölçütleri

2.1.3.1 RMSE performans değerlendirme ölçütü

Bir modelde tahminlenen değerler ile gerçek değerler arasındaki uzaklığın hesaplanmasında kullanılan, hatanın büyüklüğünü belirten ölçüttür. RMSE tahmin hatalarının standart sapmasıdır. Yani, kalıntılar, regresyon hattının veri noktalarından ne kadar uzakta olduğunun bir ölçüsüdür; RMSE ise bu kalıntıların ne kadar yayıldığının bir ölçüsüdür. Başka bir deyişle, verilere en iyi uyan çizgi etrafında o verilerin ne kadar yoğun olduğunu söyler. RMSE değeri 0'dan ∞'a kadar değişebilir. Negatif yönelimli puanlar yani daha düşük değerlere sahip tahminleyiciler daha iyi performans gösterir. RMSE, birçok matematiksel hesaplamada istenmeyen mutlak değerin kullanılmasını engeller.

RMSE değerinin sıfıra yakın çıkması, modelin tahmin performansının mükemmele yakın olduğunu ifade etmektedir [25]. Denklem 1 de verilen yi gerçek değeri, $\hat{y}_i$ model tarafından tahmin edilen değeri, n veri miktarını göstermek üzere RMSE matematiksel olarak şöyle ifade edilebilir:

$$RMSE = \sqrt{\frac{\sum_{i=1}^{n}(\hat{y}_i - y_i)^2}{n}} \qquad (1)$$

2.1. Metot

Şekil 5'da çalışmanın iş akış diyagramı verilmiştir. Şekil 6 incelendiğinde ilk aşamada açık erişimli internet sitesinden(https://academictorrents.com) alınan yüz görüntüleri ve bu görüntülere ait veri seti alınmıştır. Çalışmada ilk veri setindeki yüz görüntüleri ile, ikinci veri setindeki bu görüntülere ait vücut ağırlığı bilgisi kullanılmıştır. Veri setinde yer alan diğer kişisel bilgiler analize dahil edilmemiştir. İkinci aşamada ise alınan veri seti üzerinde kayıp veri analizi gerçekleştirilmiştir. Toplam 61110 görüntüden 393 adet görüntüye ait vücut ağırlığı verileri veri setinde bulunamamıştır. Bu durumu çözebilmek için vücut ağırlıklarının ortalama değeri alınarak kayıp veriler ile değiştirilmiştir. Çalışmanın üçüncü aşamasında ise ResNet34 modelinde görüntü verilerini eğitebilmek için tüm yüz görüntüleri eşit boyutlara getirilmiştir. Bir sonraki aşamada ise verilerin ResNet34 modelinde eğitim süresini ve hesaplama gücünü azaltarak modelin performansını arttırmak için veriler 0-1 arasına normalize edilmiştir. Çalışmanın beşinci aşamasında ise eğitime hazırlanan yüz görüntüsü ve bu görüntülere ait vücut ağırlık değerleri rastgele olarak %80 eğitim ve %20 test olmak üzere iki bölüme ayrılmıştır. Eğitim veri seti ResNet34 mimarisi ile eğitilerek öğrenme oranı belirlenerek model üzerinde öğrenme oranı için optimizasyon işlemi gerçekleştirilmiştir. Çalışmanın son aşamasında ise ResNet34 modeli ile eğitilen verilerin test verileri kullanılarak modelin tahminleme doğruluğu belirlenmiştir.
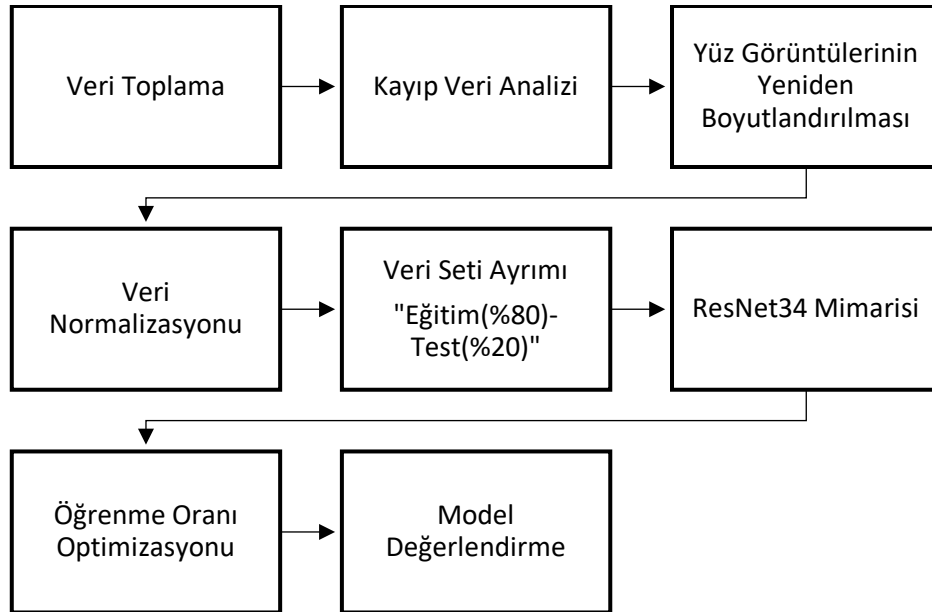
Şekil 5. İş Akış Diyagramı.

3. ARAŞTIRMA BULGULARI

Çalışmada ilk olarak ResNet34 mimarisi kullanılarak eğitilen modelin öğrenme oranı belirlenerek şekil 6'de verilmiştir.
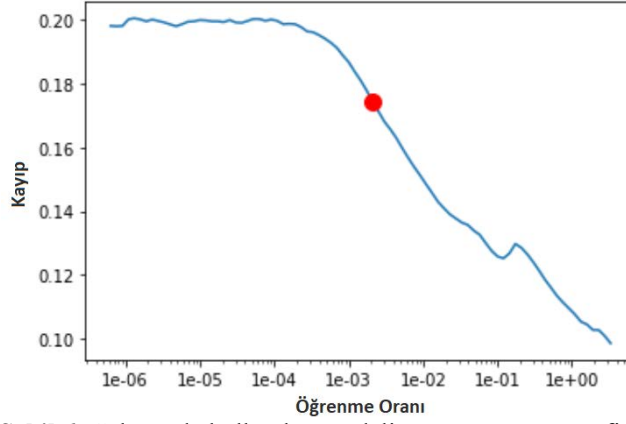
Şekil 6. Çalışmada kullanılan modelin öğrenme oran grafiği.

Şekil 6 incelendiğinde ResNet34 modelinin öğrenme oranını değiştikçe kayıp oranının da değiştiği görülmektedir. Çalışmada kullanılan model için en iyi öğrenme oranın belirleyebilmek için en iyi olan değer en yüksek sabit öğrenme oranına yakın olan değerdir. Ayrıca öğrenme hızı doğrusal yada üstel olarak eğitim boyunca kullanılır. Yerel hata yüzeyinin daha hassas bir şekilde kullanılması uygun öğrenme oranı belirlemede oldukça önemlidir. Bu nedenle şekil 6'de görüldüğü gibi kırmızı işaret ile gösterilen 0.00209 değeri öğrenme oranı olarak belirlenmiştir.

Şekil 7'de çalışmada kullanılan ResNet34 modelinin eğitim ve doğrulama kayıplarına ait grafik verilmiştir. Grafik incelendiğinde eğitim boyunca eğitim ve doğrulama kayıplarının sürekli olarak düştüğü görülmektedir. Mimarinin son tekrarlamada(epoch) eğitim kayıp oranı değeri 0.002624, doğrulama kayıp oranı değeri ise 0.002601'a ulaştığı görülmektedir. Mevcut veri seti için uygulanan Resnet34 modelinin başarılı bir sonuç verdiği görülmüştür.
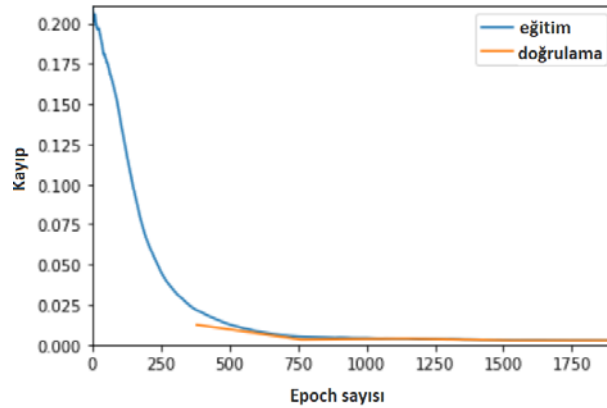
Şekil 7. ResNet34 modeli için eğitim-doğrulama kayıp grafiği.

Çalışmada kullanılan ResNet34 mimarisinin kayıp oranı değeri tablo 1'de verilmiştir.

Tablo 1. ResNet34 model sonuçları.

ResNet34	Eğitim kaybı	Doğrulama kaybı	RMSE hata değeri
	0.002624	0.002601	0.071797

Tablo 1 incelendiğinde oluşturulan ResNet34 modelinin RMSE hata değerinin (0.071797) sıfıra yakın olması modelin kullanılan veri seti için başarılı bir model olduğunu göstermektedir.

Çalışmada kullanılan ResNet34 modeli için örnek yüz görüntülerine ait ağırlık tahminleri şekil 8'de verilmiştir.

Şekil 8. ResNet34 modelinden elde edilen örnek sonuçlar.

Şekil 8'da görüldüğü gibi yüz görüntüleri üzerinde modelin vücut ağırlığı tahmininde oldukça başarılı olduğu görülmektedir.

4. SONUÇLAR

Çağımızda bilgi ve iletişim teknolojilerinin hızla gelişmesi ile birlikte yapay zeka yöntemleri de sıklıkla kullanılmaya başlanmıştır. Özellikle yapay zeka yöntemleri kullanılarak görüntüler üzerinden kimlik tespiti, biyometrik analizler gibi birçok uygulama gerçekleştirilmektedir. Yapay zeka yöntemleri, görüntüler üzerinden tıp, tarım ve hayvancılık gibi alanlarda çeşitli çıkarımlar elde etmek için kullanılmaktadır. Bu çıkarımlardan birisi de yüz görüntüleri üzerinden vücut ağırlığının tahmin edilmesidir. Çalışmada açık erişimli internet sitesinden alınan yüz ve vücut ağırlığı veri seti için kişinin yüz görüntüsünden vücut ağırlığı ResNet34 derin öğrenme mimarisi kullanılarak tahminlenmiştir. ResNet34 modeli RMSE performans değerlendirme ölçütüne göre değerlendirilerek 0.071797 hata değeri elde edilmiştir. Elde edilen bu hata değeri oluşturulan ResNet34 mimarisinin çalışmadaki veri seti ile uyumlu olduğunu göstermektedir.

İlerdeki akademik çalışmalarda farklı yapay zeka modelleri kullanılarak model başarısının arttırılması düşünülmektedir.

KAYNAKLAR

[1] J. Zhang, Y. Xia, Y. Xie, M. Fulham, and D. Feng, "Classification of Medical Images in the Biomedical Literature by Jointly Using Deep and Handcrafted Visual Features," IEEE J. Biomed. Heal. Informatics, vol. 2194, no. 2, pp. 1–10, 2017.

[2] Süzen, A. A., & Cakiroglu, M. A. (2019). Prediction of rebound in shotcrete using deep bi-directional LSTM. Computers and Concrete, 24(6), 555-560.

[3] S. Koitka and C. M. Friedrich, "Traditional feature engineering and deep learning ap [3] Kaya U., Yılmaz A. (2019). Derin Öğrenme, 1-2, ISBN:978-605-2118-399

[4] Rosenblatt, F. (1957). The perceptron, a perceiving and recognizing automaton Project Para. Cornell Aeronautical Laboratory.

[5] Özkan, İ. N. İ. K., & Ülker, E. (2017). Derin Öğrenme ve Görüntü Analizinde Kullanılan Derin Öğrenme Modelleri. Gaziosmanpaşa Bilimsel Araştırma Dergisi, 6(3), 85-104.

[6] Kaya U., Yılmaz A. (2019). Derin Öğrenme, 1-2, ISBN:978-605-2118-399

[7] Çağlayan, A. (2018). Derin Öğrenme Tekniklerini Kullanarak RGB-D Nesne Tanıma. Hacettepe Üniversitesi Bilgisayar Mühendisliği Anabilim Dalı Doktora Tezi

[8] Elmas Ç. 2011. Yapay Zekâ Uygulamaları, Seçkin Yayıncılık, 4.Basım.

[9] Wang, M., & Deng, W. (2018). Deep Face Recognition: A Survey. arXiv, arXiv-1804.

[10] Çetinkaya H. H., ve Akçay M. 2012. Yüz Tanıma Sistemleri ve Uygulama Alanları, XIV. Akademik Bilişim Konferansı Bildirileri, Uşak Üniversitesi.

[11] Aburomman, A. A., & Reaz, M. B. I., 2016. Ensemble of binary SVM classifiers based on PCA and LDA feature extraction for intrusion detection. In 2016 IEEE Advanced Information Management, Communicates, Electronic and Automation Control Conference (IMCEC), 636-640, IEEE. DOI: 10.1109/IMCEC.2016.7867287

[12] Hamdan, B., & Mokhtar, K. (2018). Face recognition using angular radial transform. Journal of King Saud University-Computer and Information Sciences, 30(2), 141-151.

[13] A. K. Jain, S. C. Dass, and K. Nandakumar, "Soft biometric traits for personal recognition systems," in Proc. of ICBA, 2004.

[14] A. Dantcheva, P. Elia, and A. Ross, "What else does your biometric data reveal? a survey on soft biometrics," IEEE Transactions on Information Forensics and Security, pp. 1–26, 2015.

[15] M. S. Nixon, P. L. Correia, K. Nasrollahi, T. B. Moeslund, A. Hadid, and M. Tistarelli, "On soft biometrics," Pattern Recognition Letters, vol. 68, pp. 218–230, 2015.

[16] A. Dantcheva and F. Bremond, "Gender estimation based on smiledynamics," IEEE Transactions on Information Forensics and Security (TIFS), 2016.

[17] C. Chen, A. Dantcheva, and A. Ross, "Impact of facial cosmetics on automatic gender and age estimation algorithms," in Proceedings of IEEE International Conference on Computer Vision Theory and Applications (VISAPP), vol. 2, 2014, pp. 182–190

[18] Yüz ve vücut ağırlığı veriseti, (2020), https://academictorrents.com, Erişim Tarihi: 28.06.2020

[19] He K. Zhang X. Ren S. & Sun J. Deep residual learning for image recognition. In Proceedings of the IEEE conference on computer vision and pattern recognition, pages 770–778. 2016.

[20] Almryad, A. S. S. (2020). Identification Of Butterfly Species Using Machine Learning And Image Processing Techniques (Doctoral Dissertation).

[21] He, K., Zhang, X., Ren, S., Sun, J. (2015). Deep residual learning for image recognition. CoRR, abs/1512.03385.

[22] Figurnov, M., Collins, M. D., Zhu, Y., Zhang, L., Huang, J., Vetrov, D., & Salakhutdinov, R. (2017). Spatially adaptive computation time for residual networks. In Proceedings of the IEEE Conference on Computer Vision and Pattern Recognition (pp. 1039-1048).

[23] Jian, L., Li, Z., Yang, X., Wu, W., Ahmad, A., & Jeon, G. (2019). Combining unmanned aerial vehicles with artificial-intelligence technology for traffic-congestion recognition: Electronic eyes in the skies to spot clogged roads. IEEE Consumer Electronics Magazine, 8(3), 81-86.

[24] Targ, S., Almeida, D., & Lyman, K. (2016). Resnet in resnet: Generalizing residual architectures. arXiv preprint arXiv:1603.08029.

[25] Çınaroğlu, S. (2017). Sağlık harcamasının tahmininde makine öğrenmesi regresyon yöntemlerinin karşılaştırılması. Uludağ Üniversitesi Mühendislik Fakültesi Dergisi, 22(2), 179-200.

International Journal of Engineering and Innovative Research

http://dergipark.gov.tr/ijeir

DESIGN AND SIMULATION OF AN ON-GRID PHOTOVOLTAIC SYSTEM

Wofuru Innocent[1*] , Ekom Abasi Ikoiwak [1] , Big-Alabo Ameze [1]

[1]University of Port Harcourt Choba, Faculty of Engineering, Department of Electrical/Electronic Engineering, P.M.B 5323, Rivers State. Nigeria.

*Sorumlu Yazar: wofurui@yaho.com

ABSTRACT: In this paper, the design and simulation of an On-grid photovoltaic system for the faculty of Engineering, Abuja campus, University of Port Harcourt (Latitude: 4.78°S, Longitude: 7.01°E) was researched in-order to verify alternate power source possibility that can supplement for the inconsistent power from the (Power holding company of Nigeria) grid to the faculty. The system Solar modules are mounted in a fixed tilt orientation in 4-parallel strings of 15 Solar panels in series on the roof-top of the faculty. The photovoltaic system is also designed with a two - parallel string of nine Tesla Powerwall batteries in series for the battery bank storage system. Inverters used for this system are two 9.9kW battery-based grid-tied inverters stacked in parallel with an inbuilt Maximum power point tracker (MPPT). The reinjection system is on-grid as a net-meter is not used since the Power Holding Company of Nigeria, PHCN does not support Net- metering. Thus, power is not injected into the grid from the solar photovoltaic system. In solving the faculty's power lapses and improving power supply quality in the faculty, data collected both within the faculty. These methods include data collection, evaluation of load data, data analysis, suitable design adoption, simulation of data. A solar photovoltaic software application package called PVsyst was employed for various simulations and plots. The end simulation and final work prove the system to be 57% efficient in performance.

Keywords: MPPT, PVsyst, solar, On-grid photovoltaic

1. INTRODUCTION

Renewable energy biggest source on earth so far known to man is the sun. The sun's energy is harvested utilizing a concentrated power system. Photovoltaics directly convert the sun's energy to electrical energy by photovoltaic effect principle. Free electrons are released when certain materials gain light exposure, absorbing photons. This is a photoelectric effect phenomenon. The photovoltaic effect only exists on the photoelectric effect principle. Thus, solar cells are made from this principle. They convert sunlight to direct current (DC) electricity. [6] Single photovoltaic cell does not produce enough electricity as such, a passable number of photovoltaic cells are mounted on a supporting frame, connected electrically to form a photovoltaic module or solar panel. Solar panels or modules specifically designed, supply electric power at a certain potential with produced current indigent on incident light. It is clear that photovoltaic modules produce DC but occasionally we require alternating current, AC. Thus, an inverter and other solar PV components combinations are needed to attain this. [5] Solar energy describes energy amassed from the sun. A complimentary, infinite, inexhaustible, and pollution-free energy.

The energy created when solar radiation is converted to heat(thermal) and electricity(electric). The strength and effect of sun irradiance differ with a change in atmospheric conditions, time of day, latitude, the position and inclination of the earth concerning the sun. [1]

2. MATERIAL AND METHODS

The system designed is to be an on-grid photovoltaic system configuration with back-up batteries with a fixed tilt orientation. The is no solar power injected into the grid since our utility company, PHCN does not support net metering. [8] Hence, the system has no net meter in its system design. System arrangement will constitute PV solar modules 4-parallel strings of 15-modules in series. The array is then tethered to the battery bank via the battery charger which acts as a regulator, automatically disconnects the battery bank from the PV array when the battery is full and also regulates the depths of the battery undercharging. [8] The battery bank is then tethered to two 9.9kW grid-tied inverters which are connected in parallel to increase its power (watts), then to the critical load panel (where the appliance for PV system are all connected). The critical load panel draws specific loads from the building's mains distribution panel and gets isolated from all other loads. [8]

2.1. Software Selection

Numerous Solar PV Software such as heliostat, PVsol, PVsyst were sampled. The decision to adopt the PVsyst software was made based on its reviews, frequency of use by researchers outside Nigeria to design solar systems, simplicity, less complexity and ease of learning than that of other software, ease of accessibility, accuracy, allows for proper calculation of load values and more. PVsyst V6.8.4 is a solar PC software for PV system sizing, design, and analysis. The software contains substantial timely meteorological fact and solar components database. It offers three different configurations of PV system study namely: the grid-connected, Off-grid, and pumping system for the development of an actual solar project. The software permits the export of data from external sources such as google map, simulates values in form tables and graphs of the actual performance of system components. [9]

2.2. Photovoltaic Component Sizing

First and foremost, daily average solar irradiance on horizontal surfaces in Port Harcourt which is measured at 4.04kWh/m2/day. It has been found the panel generation factor of the location to which the PV system will be installed. This factor varies with the variation of the site and has no unit.[11] The daily solar radiation for the location in which the PV plant is sited is divided by the irradiance value of the photovoltaic module at STC. For Port Harcourt city the daily average irradiance value is 4.04kWh/m2/day.

The following formula applies: -

$$\text{Panel Generation Factor} = \frac{\text{Daily Solar Radiation of Location}}{\text{Irradiance of PV at STC}} \tag{1}$$

$$= \frac{4.04 \times 10^3}{1000} = 4.04.$$

The total PV panel energy required is multiplied against the system losses compensation factor known to be a constant of 1.3. Recall that Total energy consumption of appliances,

$= 60,212 \text{Whr/day}$ or $= 60.212 \text{ kWh/day.}$

Energy lost in system $= 1.3$.

Total PV module energy required= (Energy Consumption ×Energy lost in the system).

$= 60.212 \text{kWhr/day} \times 1. \ = 78925.6 \text{Whr/day}$

2.2.1. PV system module sizing.

To size, the PV modules, the total watt peak rating required to operate the PV modules was first determined. The Formula implies

$$P_{pv} \ = \ \frac{E_d}{(PSH) \times \eta_{CR} \times \eta_{inv}} \tag{2}$$

where is the daily energy consumption of the faculty in kWh/day, PSH is the peak sunshine hours (hrs/day), is the charge regulator efficiency, and is the inverter efficiency. For simplification, the formula below is adopted.

$$\text{Total watt peak of PV modules} \ = \ \frac{\text{Energy PVmodules}}{\text{Panel Generation Factor}} \tag{3}$$

$$= \frac{78275.6}{4.04} \quad = 19536.0 \text{Wp.} \ = 19536.0 \text{Wp.}$$

Using the manufacturer's specification, the PV module peak power rated output was obtained and used to calculate system requirements for the number of modules. The modules' peak power is then divided by the panel generation factor PGF. Solar panels with 330Wp rated output are chosen for the design. Then the number of pf PV modules require then becomes: -

$$\text{No. of modules required} = \frac{\text{Total watt peak for PV modules}}{\text{PVmodule peak rated output}} \tag{4}$$

$$= \ \frac{19536.0}{330} \ = \ 59.2 \text{ modules}$$

There are no '.2' modules in the PV module industry thus, the next whole number is chosen, which becomes 60 modules. System configuration will show 60 units of solar panels of 330watts capacity adopted for design. The system will perform better with the 60 modules than 59 modules since more PV modules indicate better system performance and fewer PV modules, the system may not work properly and the battery life cut short. [3,4]

2.2.2. PV system battery sizing.

Battery capacity required is known as Ampere-hour (Ah). The total ampere-hour can be obtained using the following formula:

$$C_{BAH} = \ \frac{E_{db} \times AD}{DOD \times \eta_{BAH} \times V_B} \tag{5}$$

Where is the daily energy required from the battery, DOD is the permissible depth of discharge, AD is autonomy days, is the ampere-hour efficiency of the battery cell, and is the selected nominal DC voltage of the battery block [2,10]. The values of the factors considered while calculating for battery size are battery loss 0.85, 4-days of autonomy, depths of discharge, DOD – 0.8, and battery's nominal voltage. From our battery specification, the nominal voltage is 50.4V. With a similar but simplified calculation, we calculate as follows:

Required battery capacity,

$$(\text{Ah}) = \frac{\text{Total Whr per day used by appliance} \times \text{Days of Autonomy}}{\text{Battery loss} \times \text{depth of discharge} \times \text{nominal battery voltage}} \qquad (6)$$

$$= \frac{19536.0 \times 4}{0.85 \times 0.8 \times 50.4} = \frac{78144}{34.2} = = 2284.9\text{Ah}.$$

Therefore, the total number of batteries for the PV system was found by dividing the required battery capacity by that of 1-battery.

$$\text{No of Batteries} = \frac{\text{Required battery capacity}}{\text{Capcity of 1-battery}} = \frac{2284.9}{134} \qquad (7)$$

$$= 17.05 \text{ batteries} \quad \sim\text{18-batteries}.$$

2.2.3. PV system inverter sizing

To allow for safe and efficient operation the general rule of thumb is that, size of the inverter should be similar to DC rating of solar panel system or solar generator. Therefore, the inverter sizing calculation is: -

Total watts of all appliances = 20,788W

Inverter rating = 20,788W

2.2.4. Combiner box sizing

The size of fuse to use is always determined by the datasheet of the panel. For the grid-tied panel, under 300watts a 15A fuse is usually used. For this PV system, solar panel rating is greater than 300watts therefore, the size of the fuse is calculated as:

Size of Fuse = Solar Panel's Isc x 1.56

$$= 16.302\text{A}$$

The D.C combiner/disconnect box for this system will have 4-16A or 17A fuses to account for the four solar module parallel strings in our design.

3. PV SYSTEM SIMULATION PERFORMANCE

The system's simulation performance considers the system sizing and design, the PV system power generated plus the energy stored in the battery block are used to cover the load demand

when power from PHCN is not available. During the period of grid availability, its power will be used to cover the load demand and to charge the battery block depending on its state of charge. For hourly steps, the simulation software compares the energy demand and the PV energy generated, and according to the difference, the decision to charge or discharge the battery is made. The simulation software takes into cognizance the three following cases for system performance.

First Case: Sufficient energy is being generated by the PV generator array covering the load demand by PV energy will have the priority of charging the battery.

Second Case: the generated PV power is not sufficient to supply the load. The priority here is to utilize grid power if it is available. If grid power is not available, the required load energy is discharged from the battery block.

Third Case: The PV power generated is not sufficient to cover the load and the batteries state of charge, SOC is low. The grid power automatically charges the battery block and covers the load demand at the same time. There is certainty that the grid cut off periods are time-wise irregular depending on the situation with the PHCN and its Distribution companies. Hence the simulation considers the PV system as a standalone system which is the worst-case scenario.

4. RESULTS AND DISCUSSION

Table: 1 refers to the summary of the major parameters, its associated equations and values employed in the design of the design and simulation of an on-grid photovoltaic system An efficient on-grid photovoltaic system is designed and simulated. The results of discrete components, their behavior, and that of the complete model are shown and explained from the software.

Table 1. Parameter used in design and its values.

Parameters	Equations	Values
Panel Generation Factor	$\dfrac{\text{Daily Solar Radiation of Location}}{\text{Irradiance of PV at STC}}$	4.04
Total PV module energy required	Energy Consumption ×Energy lost in the system	78925
Total watt peak of PV modules	$\dfrac{\text{Energy PVmodules}}{\text{Panel Generation Factor}}$	19536.0Wp.
No. of modules required	$\dfrac{\text{Total watt peak for PV modules}}{\text{PVmodule peak rated output}}$	59.2
Required battery capacity	$\dfrac{\text{Total Whr per day used by appliance} \times \text{Days of Autonomy}}{\text{Battery loss} \times \text{depth of discharge} \times \text{nominal battery voltag}}$	
No of Batteries	$\dfrac{\text{Required battery capacity}}{\text{Capcity of 1} - \text{battery}}$	18
Size of Fuse	= Solar Panel's Isc x 1.56	16.302A
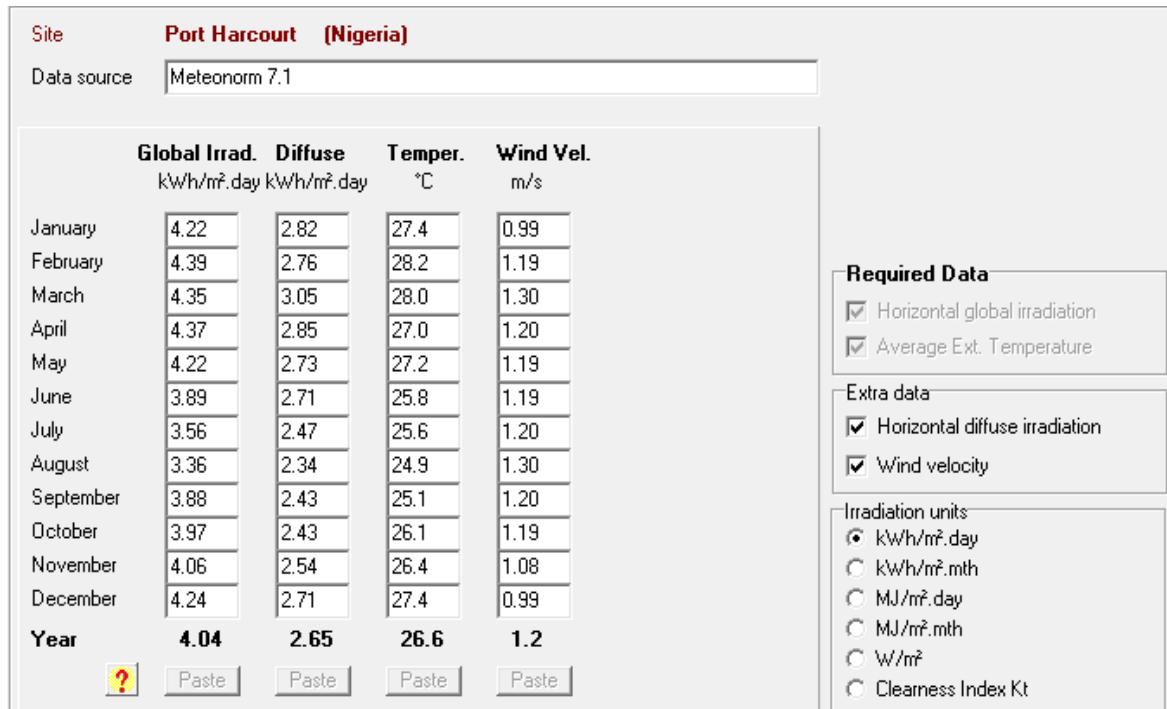
Figure 1. Daily Global Site Irradiance & Temperature Values/Day.

In Figure1, the solar global irradiation of the Faculty per day for the 12-months of the year is generated using the meteonorm 7.1 data site. It shows the average global irradiance as 4.04kWh/m2.day while diffused irradiance is at 2.65kWh/m2.day. The average temperature at 26.60C and wind velocity at 1.2m/s.
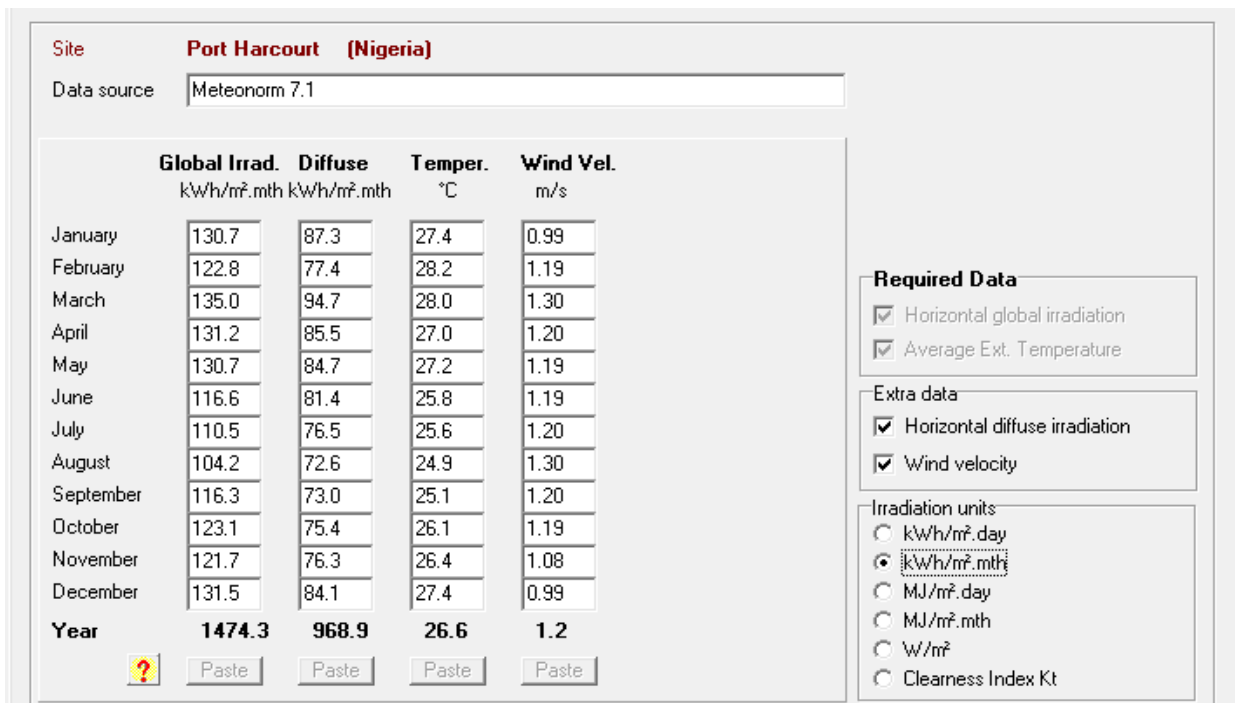
Figure 2. Daily Site Irradiance & Temperature Values/Month.

In Figure 2, the global irradiation of the Faculty per month for the 12-months of the year is generated using the meteonorm 7.1 data site. It shows the average global irradiance per month to be as 1474.3kWh/m2.mth whilst diffused irradiance is at 968.9kWh/m2.mth, average

temperature, and wind velocity correlative to global irradiation per day at 26.60C and 1.2m/s respectively.
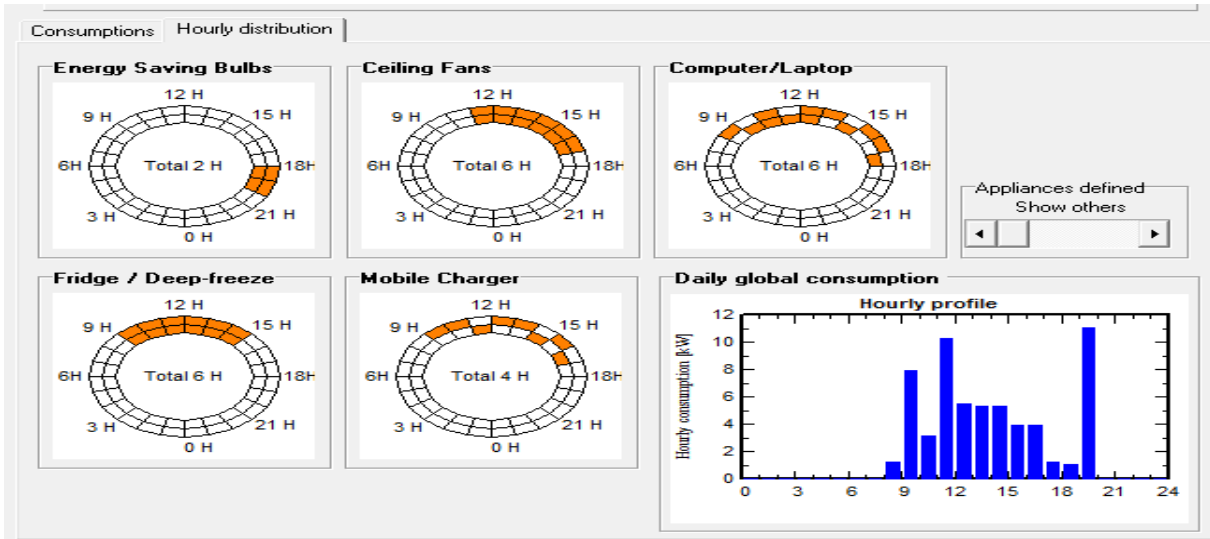
Figure 3. Hourly Load Distribution.
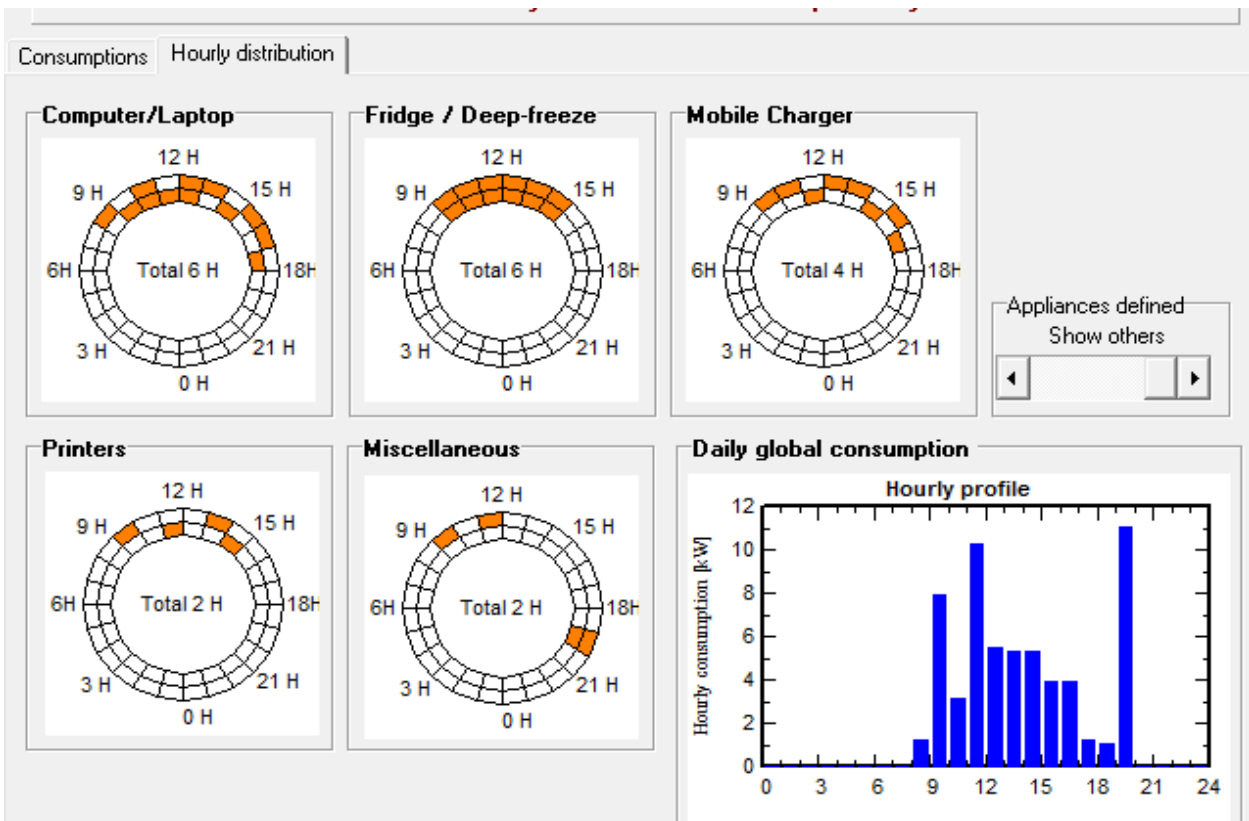
Figure 4. Hourly Load Distribution.

Figures 3 and 4 explain how the load in the faculty are distributed during use. In figure 4, the energy bulbs are switched on between the hours of 6-8 pm, the ceiling fans are in use between 11 am-5 pm, desktop computers, fridges, and mobile chargers are also distributed in certain hourly proportions. The same distribution also applies to fractions of values of daily energy extracted from the annual value of a 24-hr timeline. The results were generated by the software after load values have been inputted into it and the simulation is done. Days of autonomy fixed for the system is 5-days
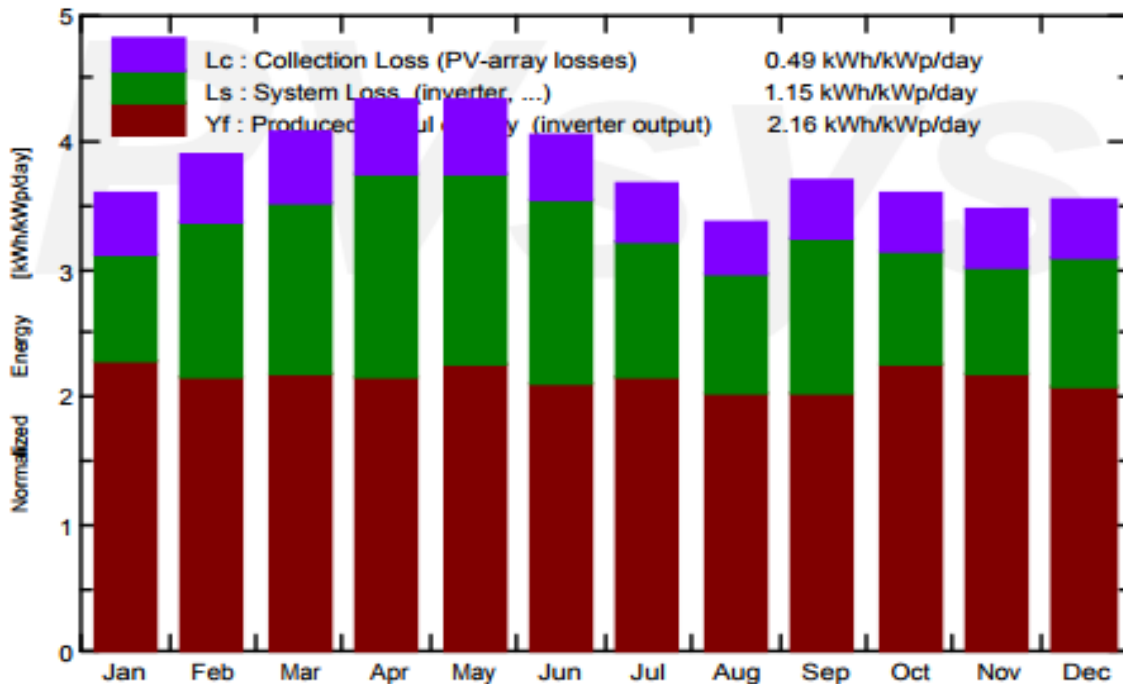
Figure 5. Normalized Energy Production.

In the chart in figure 5, it shows the normalized (kWh/kWp/day) energy plotted against the months of the year to give a response of Collection loss Lc depicted with purple-colored bars with value 0.49kWh/kWp/day, System losses (inverter…) and battery charging Ls depicted in green color with value 1.15kWh/kWp/day and the produced energy (inverter output) Yf is depicted in red-colored bars with a 2.16kWh/kWp/day value.

5. CONCLUSION

The PV system produces energy of 22.76MWh/year and supplies energy of 15.59MWh/year. It, therefore, illustrates PV system power produced to be greater than energy proffered as well as the energy need of the user. This draws to close that, User energy (load) capacity is met and exceeded in the system production. Excess unused energy of 5.608MWh/year (considering losses) noticed, is the disparity in energy values of the system and that of the user. With this result, the software calculates the performance ratio of the system at 56.71%. The system can sustain itself for a period of 25 to 30 years or more if operated within its calculated energy limits. This solar photovoltaic system safes income as it reduces the electricity bill.

In conclusion, the system designed meets the major basic desired objective of this work and surpasses its design expectations.

6. RECOMMENDTIONS

It is recommended that this design should be adopted when plans for a solar photovoltaic system has been drawn.

Also, for the solar photovoltaic system to serve for its appraised lifespan as proposed, it should be used on loads listed in this work, and appliances with thermostat properties should not be utilized on it if not calculated in the energy requirements during a redesigning or expansion phase.

7. ACKNOWLEDGMENT

The authors would like to acknowledge thankfully the continuous support by the Head of the Department of Electrical/ Electrical Engineering University of Port Harcourt as well as the entire member of the staff

REFERENCE

[1] A. Al-Salaymeh, Z. Al-Hamamre (2010) Technical and Economic Assessment of the utilization of Photovoltaic systems in residential buildings: The Case Study of Jordan. Journal of Energy Conversion and Management, August 2010.

[2] C.O.C Oko et al, (2012) Design and Economic Analysis of a Photovoltaic System: A Case Study. International Journal of Renewable Energy Development 1(3) 2012:65-73

[3] D. H. Li, K. L. Cheung, Tony N. T. Lam, Wilco Chan, (2012) A Study of grid-connected photovoltaic (PV) system in Hong Kong. Article in Applied Energy, Feb 2012, pp 90(1).

[4] El-Tallamy, A. Elbaset, (2016) Design and Power Quality Improvement of Photovoltaic Power System. http://www.springer.com>book, 2006.

[5] F. Agai, N. Caka, V. Komoni, (2015). Design Optimization and simulation of buildings in South East Europe. International Journal of Advances in Engineering and Technology, 2011, Vol 1, issue (5), pp 58-68

[6] J. Samimi, E.A. Soleimani, (2015) Optimal Sizing of photovoltaic System in varied climates. Journal of Solar energy 60(2):97-107.Feb 2015

[7] J.C. Hernandez, P. G. Vidal, G. Almonacid, (2010) Photovoltaic in grid-connected buildings. Sizing and Economic Analysis. International Journal of Renewable Energy 15(1):562-565, Sept 2010

[8] L. Fagbile, (2010) Estimation of Total Solar Radiation in Nigeria using meteorological, Nigeria. Journal of Renewable Energy 1. 2010, pp. 1-10.

[9] N. Boullosa. A little background on Solar power. January 2008, https://faircompanies.com

[10] O. W. Westbrook, F.D. Collins, (2013) Energy Model Validation for Large-Scale Photovoltaic systems. In Photovoltaic Specialists Conference (PVSC), 2013 IEEE 39. Pp.0830-0835

[11] W. Muneer, K. Bhattacharya, C. A. Canizares, (2011) Large-Scale Solar PV Investment Models, Tools, and Analysis: The Ontario Case. IEEE Transactions on Power Systems. December 2011, 26(4): pp. 2547-2555

EXPERIMENTAL STUDY ON THE EFFECT OF DIFFERENT COARSE AGGREGATE SIZES ON THE STRENGTH OF CONCRETE

Akanu-Ibiam Ndon[1] , Aniekan Essienubong Ikpe[2*]

[1] Akwa Ibom State University, Department of Civil Engineering, Ikot Akpaden, Mkpat Enin, Nigeria.
[2] University of Benin, Department of Mechanical Engineering, Benin City, Nigeria.

*Sorumlu Yazar: aniekan.ikpe@eng.uniben.edu

ABSTRACT: The purpose of this research work is to compare the effect of coarse aggregate sizes on the strength of concrete. Materials for this study were (water, fine and coarse aggregates and cement). Acceptability criteria for tests on basic materials for concreting were ascertain such as; water according to BS 2690 standard, Fine and coarse aggregates according to BS 812:1975, part 1 to 4 standard and Cement according to BS 12:1991. The acceptability criteria for testing fresh and hardened concrete such as Workability test (slump test in accordance with BS 1881:1983, part 102) and Compressive strength test (cube test in accordance with BS 1881:1983. The specimen size for crushing strength was 150mm x 150mm x 150mm, cured and tested for 7, 14 and 28 days with concrete grade 20 of minimum compressive strength of 14 N/mm2 (mix ratio of 1:2:4). From the result gotten, the concrete strength of aggregate size of 20mm to 28mm after 28 days was higher than that of 13.2mm to 19mm and that of 3.35mm to 10 mm.

1. INTRODUCTION

The strength of concrete depends on many parameters, therefore, an in-depth understanding of appropriate mix ratios for optimum concrete strength is much required by engineers in this field of expertise. Compressive strength of concrete is influenced by age, type of material, and the process of curing, water cement ratio, size of aggregate, type of aggregate, and some other parameters [1, 2]. Emphasis is given to the parameters of the coarse aggregate size and its impact on the strength and workability of concrete. The compressive strength of the aggregate sizes of 3.35mm-10mm,13.2mm-19mm and 20mm-28mm is the main parameter to be examined, the test used to evaluate the compressive strength is non-destructive testing using destructive test on 7,14 and 28 days whichcwill be implemented on the samples and concrete cubes. Both tests are carried out based on the British Standard BS 1881 (1983). Ukala [3] studied the properties of concrete in terms of strength, slump and density by varying aggregate grades. Proportions of 12.7mm, 25.4mm, and 38.1mm and 50.8mm sizes of granite as coarse aggregates were varied in order to create diverse coarse aggregate grading and then combined with a constant fine aggregate gradation and a fixed water/cement (w/c) ratio of 0.7. The results showed that as the coarse aggregate was spread evenly across all four aggregate sizes the strength was maximum as compared to when the aggregates were concentrated towards the 50.8mm size. The workability was observed to be stiffer as more coarse aggregate sizes were introduced into the mix. Finally, the concrete density remained almost constant irrespective of

the aggregate grading. Effects of aggregate sizes on the mechanical properties of lightweight concrete (LC) was investigated by Wei et al. [4]. The absence of medium-sized particles led to decreased in compaction of LC, thereby affecting the density and compressive strength of the concrete. Specimens having medium-sized lightweight aggregate (LAW) showed the highest compressive strength up to 95 MPa. The excessively lower size of expanded shale LWA undermined both the compaction, splitting tensile and flexural strength of LC, while a rational gradation of LWA was beneficial to the splitting tensile and flexural strength. Sneka et al. [5] employed different aggregate sizes in concrete work at constant mix of 1:1.5:3, with water cement ratio of 0.5 throughout the experiment. The mean concrete Compressive Strength and Split Tensile Strength increased with increasing aggregates size. Coarse aggregate sizes of 19, 25 and 37.5 mm gave average Flexural Strengths of 4.59, 4.38 and 3.98N/mm2. The effect of aggregate sizes on the compressive strength of concrete using two nominal mixes (1:2:4 and 1:3:6) was investigated by Ogundipe et al. [6]. Concrete cubes were produced with 6, 10, 12.5, 20 and 25 mm aggregates for the two nominal mixes and they were subjected to compressive strength test. The results indicated that the compressive strength increases with increasing aggregate size up to 12.5 mm, while the concrete produced using 20 mm aggregate had higher compressive strength than those produced using 25 mm aggregate. A synergistic combination of three sizes of coarse aggregates (10mm, 14mm, and 20mm) for concrete work was investigated by Ramonu et al. [7]. Each of the sizes were cast which served as the control. The three aggregate sizes were also combined based on percentage proportion and cast. For each combined sizes of coarse aggregates, 21 cubes (150×150mm) were cast to allow the compressive strength to be monitored at 7, 14 and 28 days. It was observed that the third test of the combined coarse aggregates which contained 30% 10mm, 20% 14mm and 50% 20mm had the highest compressive strength of 25N/mm^2. Obi [8] evaluated the effects of coarse aggregates sizes on concrete quality. It was observed that with proper mixing, the slump test results did not witness shear or collapse type of slump rather there were true slump in all cases of the test. The workability decreased with slight differences when the coarse aggregate size was increased. The increase in the coarse aggregates yielded appreciable increase in the compressive strength. Ekwulo and Eme [9] investigated four concrete specimens made from aggregate size of 9.5mm, 12.7mm, 19.1mm and graded aggregate specimen made from a combination of 9.5mm, 12.7mm and 19.1mm aggregates. A concrete mix of 1:1.5:3 with a constant water-cement ratio (w/c) of 0.6 was used and tested for slump. Concrete cubes were produced from same mix, cured and tested for compressive strength at 14 and 28 days. It was observed that workability (slump) of fresh concrete decreases with increase in aggregate size and that compressive strength increases with increase in aggregate size. It was also observed that grading aggregates using Cement Treated Aggregate gradation procedure does not necessarily increase compressive strength of concrete for rigid pavements. Salau and Busari [10] investigated the effect of different coarse aggregate sizes on the strength characteristics of laterized concrete. The workability of laterized concrete at constant mix ratio of 1:2:4 and water-cement ratio of 0.6 increased as coarse aggregate particle size increased, but decreased with increase in percentage of laterite content. For the two largest coarse aggregate particle sizes (19.5mm and 12.5mm), the workability of laterized concrete at 25% laterite content was almost the same compared to that of normal concrete but was low for 50% laterite content. The density of the hardened concrete (using all granite particle sizes inclusive) increased from 0% to 25% laterite content but later decreases from 25% to 50%. With mixing ratio of 1: 2: 4 and water cement ratio of 0.5, Musa and Saim [11] investigated the effect of concrete strength using coarse aggregate of 10mm, 20mm and fine aggregate 3mm. The results on the 28th day showed the comparison percentage of Cube Test 47.6%, Cylinder Compressive Test 40.5% and Schmidt Hammer Test 48.9%. The results revealed that concrete aggregate size of 20mm had 45.7% higher compressive strength than concrete aggregate size of 10mm. Ajamu and Ige [12] investigated the effect of varying coarse

aggregate size on the flexural and compressive strengths of concrete beam. Concrete cubes and beams were produced in accordance with BS 1881-108 (1983) and ASTM C293 with varying aggregate sizes 9.0mm, 13.2mm, 19mm, 25.0mm and 37.5mm. The water cement ratio was kept at 0.65 with a mix proportion of 1:2:4. The specimen produced were all subjected to curing in water for 28days. Compressive strength of cubes was $21.26N/mm^2$, $23.41N/mm^2$, $23.66N/mm^2$, and $24.31N/mm^2$ for coarse aggregate sizes 13.2mm, 19mm, 25.0mm and 37.5mm. That of flexural strength of test beams were $4.93N/mm^2$, $4.78N/mm^2$, $4.53N/mm^2$, $4.49N/mm^2$ and $4.40N/mm^2$. The objective of this study is to compare the compressive strength of concrete molded with different sizes of crushed stone (i.e. 3.35mm-10mm, 13.2mm-19mm and 20mm-28mm) to determine the difference in strength of the different sizes of crushed stones which were tested after 7days, 14 days and 28 days of crushing.

2. MATERIALS AND METHODS

2.1. Materials

Materials employed in the experimental process of this study are as follows: Fine Aggregate, Coarse Aggregate, Cement, Water, Mould, Slump Cone, Tamping Rod, Tamping Bar, Scooper, Trowel, Compressive Testing Machine, Head-Pan, base plate, weighing balance, brush, A set of sieve.

2.2. Methods

River sand is one of the fine aggregates used for this project work and it was obtained from Ikot Ekong in Mkpat enin L.G.A, Akwa Ibom State, Nigeria. It was clean, sharp and free from clay and other organic matter. Crushed stones which are the largest amount of aggregate used in concrete and are the mineral aggregates. It was obtained from Akamkpa quarry site in Cross River State, Nigeria. Portland cement is manufactured by heating in a kiln mixture of a calcareous and a siliceous, usually argillaceous material. Portland limestone cement was used. The Superset brand of Portland limestone cement of the 42.5N grade produced in Akamkpa was the cement used for this project work and it was well protected from dampness. Workability tests are designed to measure the ease with which concrete can be compacted. To achieve this, concrete was compacted into the mold in three appropriately equal layers with a 16mm diameter tamping rod giving 35 tamps per layer. Top surface was struck off and finished with trowel. The mould was then lifted off vertically and the concrete was allowed to slump.

2.2.1. Acceptability criteria for testing hardened concrete

i. Strength Test: Strength tests are designed to measure the potential strength of concrete when cured and tested in a standard manner. The primary reason for strength test is to maintain control over the batching and mixing of the concrete, thereby checking compliance with specified requirements.
ii. Laboratory Test: Laboratory test in retarder and ordinary Portland cement for the purpose of characterization and determination of their strength when mixed with other constituent was carried out in terms of compressive strength test and slump test respectively.
iii. Curing of Cubes: Mould size of 15cm x15cm was used to cast cubes for compressive strength test. The cubes were cast and tested at the ages of 7, 14 and 28 days after curing.

2.2.2. Preparation of cubes

The Batching of concrete was done by weighing the different constituent materials base on the adopted mix ratio of 1:2:4. The materials were then mixed before adding the prescribed quantity

of water and mixed further to produce fresh concrete. Water cement ratio of 0.4 was adopted. The fleshly mixed concrete was then cast into the mould after mixing for slump test to determine the workability of a fleshly mixed concrete. The concrete poured into the cube mould was compacted in three layers using the tamping rod. The surface of the cubes was made as smooth as practicable by the use of trowel, and the specimen was kept in the mould for 24 hours before demolding it and for it to be ready for curing.

2.2.3. The slump and compressive tests

Before mixing the concrete for the cubes, a trial mix casting was carried out to determine the slump. Slump test is very useful in detecting variations in the uniformity of a mix of a given normal proportions. It is a method used all over the world on day to day, hour to hour variations in the materials being fed into the mixer or manual mixing. The apparatus consisted of a conical mould of 100mm in diameter at the top and 200mm at the bottom and 300mm height and 16mm diameter tamping rod 600mm long and rounded at the end. The inside of the mould was cleaned before each test and the mould placed on a hard surface. The mould was placed in it three layers of concrete of approximately equal depth. Each layer was tamped with 35 strokes using the rounded end of the tamping rod. After the top layer has been tamped, the surface of the concrete was struck off level with the top of the mould using a trowel. The slump is the difference between the highest of the concrete and the height after the removal of the conical mould. After the measurement was taken the concrete that was used in determining slump was thoroughly mix with the fresh concrete before casting into the mould and the surface levelled using a trowel and it was kept for 24 hours in the laboratory before de-moulding and then the cubes were immerged in water for the require curing age. A total of 18 cubes was made. Testing of the hardened cubes was carried out after 7, 14 and 28 days respectively using a Universal compressive testing machine. The cubes were then placed between the hardened steel bearing plates of the Universal compression machine and the load was applied at the rate of $15N/mm^2$ per minutes as specified in BS 1881. The Sample was wiped off from grit and place centrally with load applied steadily to destruction and the highest load reached was determined. This was used to compute the compressive strength and the ratio of the highest load to the cross-sectional area of the samples used for each test and the averages results were adopted as the compressive strength. The slump test experimental process is shown in Figure 1.

Figure 1. Slump test Experiment.

2.2.4. Sieve analysis

The aim of this analysis was to determine the particle size distribution of an aggregate sample. The aggregates were sieved through a set of sieve, the material retained on different sieve is determined. The percentage of material retained on any sieve is given by Equation 1.

$$PN = \underline{Mn} \times 100 \tag{1}$$

Where Mn is the mass of soil retained on each sieve and M is the total mass of sample retained as the commutative.

2.2.5. Procedure for coarse aggregate

The laboratory test procedures for performing a sieve analysis presented here as ASTM. Standard test method particle size distribution of sample

  i.   Take the required quantity of the coarse aggregate, sieve it through a 4.75mm sieve. Take the sieve sample and weight.
  ii.   Determine the initial mass of the sample. Then a stock of the aggregate is assembled. The sieves approximately double that of the next finer. The top sieve must possess openings that are large enough so that the entire sample will fall through the pan.
  iii. The sample was then sieve using a mechanical sieving machine. While sieving through each sieve, the sieve agitated such that the sample rolls in irregular motion over the sieve.
  iv.   The mass of samples in each of the sieve was weigh using a weighing balance. The percentages finer (N) by weight, which is also known as percentage passing in each of the sieve has being plotted.

2.2.6. Procedure for fine aggregate

A Given mass of fine aggregate was measured and washed. This was done so as to remove the clay, silt and dust contained in the sample. The sample being washed became less turbid and a bit transparent. It was then spread outside to dry for about 24 hours and it was put into a set of sieves arranged in decreasing apertures indicated on the chart. The sample retained on each of the sieve was weighed and the results obtained were recorded. The percentage passing through each sieve was computed and plotted against the sieve of aperture sizes to obtain a curve as the particle size distribution curve.

3. RESULTS AND DISCUSSION

The test conducted includes sieve analysis, compressive strength test and slump test. Results obtained from the sieve analysis for fine aggregate sizes and coarse aggregate are presented in Table 1 and 2. The results presented in Table 1 and 2 are further represented in graphical form as shown in Figure 2 and 3.

Table 1. Results of sieve analysis test for fine aggregate.

Sieve sizes (mm)	Weight Retained (kg)	Percentage Retained	Cumulative percentage Retained	Cumulative Percentage Passing
3.35	0.046	3.07	3.07	96.93
1.7	0.108	7.20	10.27	89.73
0.85	0.256	17.07	27.33	72.67
0.425	0.502	33.47	60.80	39.20
0.3	0.296	19.73	80.53	19.47
0.212	0.202	13.47	94.00	6.00

| 0.075 | 0.058 | 3.87 | 97.87 | 2.13 |
| PAN | 0.03 | 2.00 | 99.87 | 0.13 |
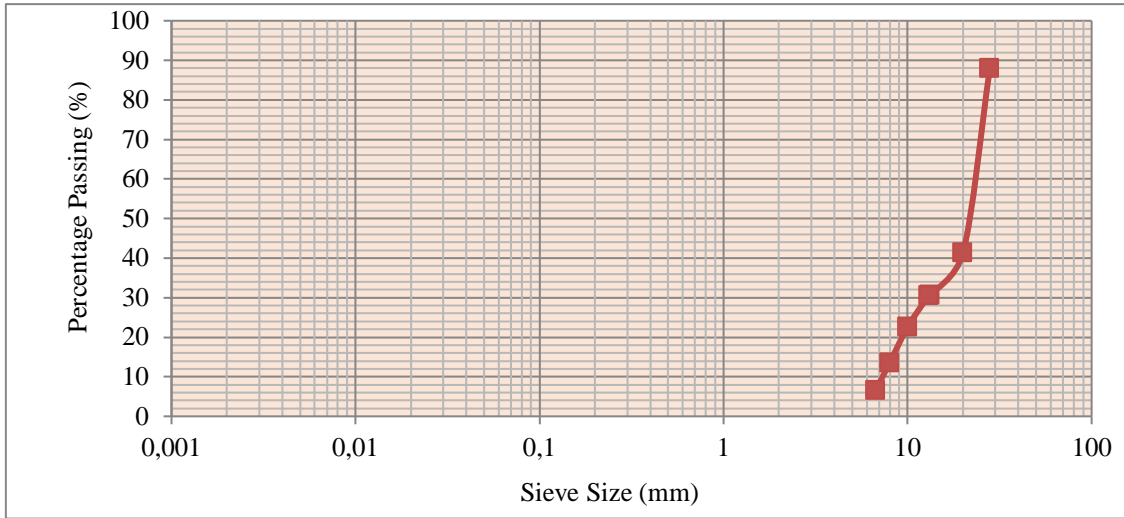
Figure 2. Particle size distribution for fine aggregate.

Table 2. Results of sieve analysis test for coarse aggregate.

Sieve sizes (mm)	Weight Retained (kg)	Percentage Retained	Cumulative percentage Retained	Cumulative Percentage Passing
28	0.18	12.00	12.00	88.00
20	0.7	46.67	58.67	41.33
13.2	0.16	10.67	69.33	30.67
13	0.002	0.13	69.47	30.53
10	0.12	8.00	77.47	22.53
8	0.134	8.93	86.40	13.60
6.7	0.106	7.07	93.47	6.53
3.35	0.09	6.00	99.47	0.53
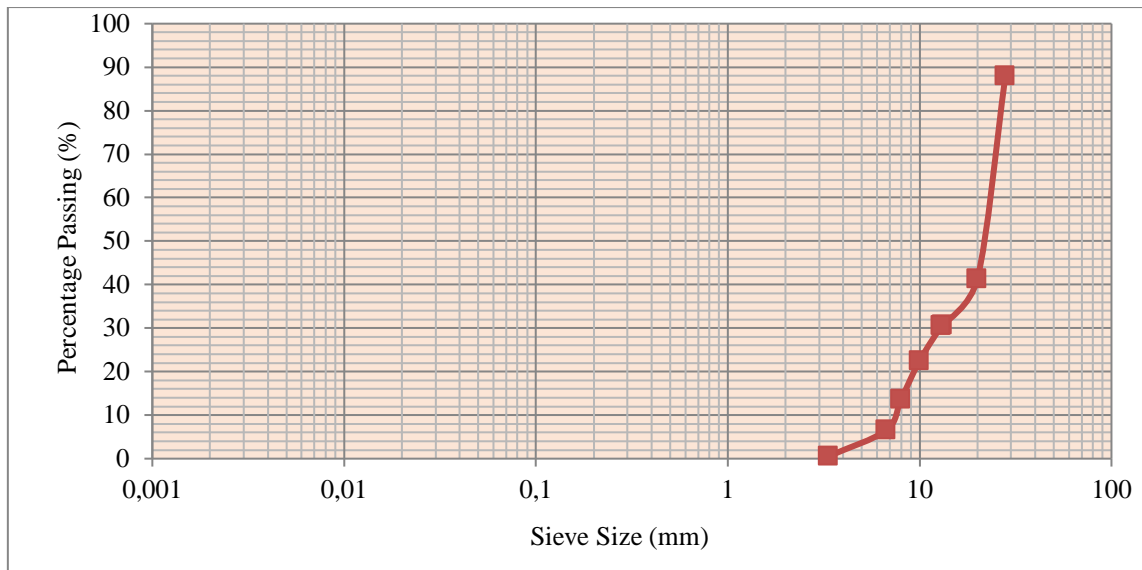
Figure 3. Particle size distribution for coarse aggregate.

Results obtained from the compressive strength test for different coarse aggregate sizes (3.35mm-10mm, 13.2mm-19mm and 20mm-28mm) are presented in Table 3-5. The results presented in Table 3-5 are further represented in graphically as shown in Figure 4-6. Summary

of results for compressive strength for different coarse aggregate sizes is presented in Table 6 and graphically illustrated in Figure 7. Results obtained from slump test experiment is presented in Table 7.

Table 3. Results of compressive strength for 3.35mm-10mm coarse aggregate.

AGGREGATE SIZES = 3.35-10mm;				AREA OF CUBE = 22500mm^2	
Age (Days)	Cube Description	Weight Before Curing (Kg)	Weight After Curing (Kg)	Load (Kn)	Compr. Strength (N/Mm^2)
7	M	7.89	8.00	378.15	14.16
	N	8.27	8.27	258.92	
14	O	7.78	7.78	388.96	17.47
	P	7.88	7.96	397.15	
28	Q	7.87	8.00	357.04	18.64
	R	8.01	8.12	481.79	
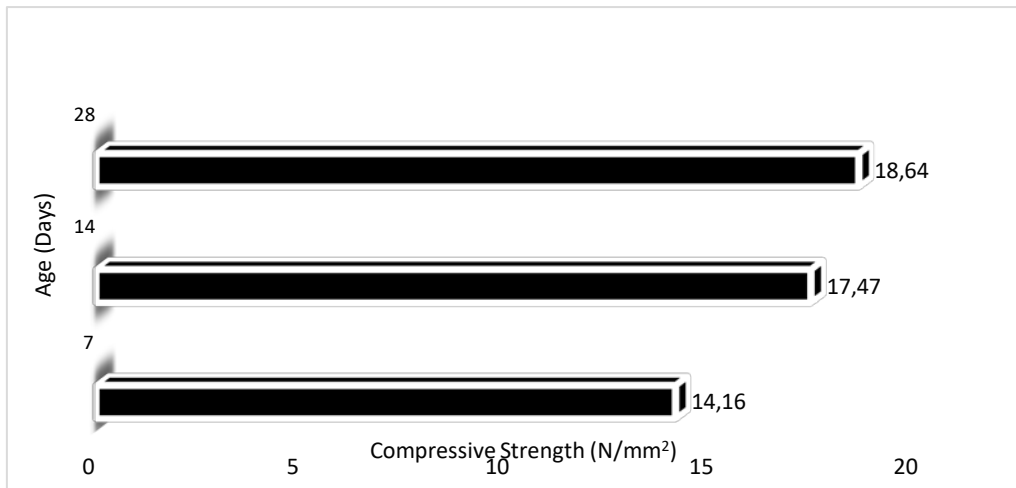
Figure 4. Compressive strength of 3.35-10mm coarse aggregate.

Table 4. Results of compressive strength for 13.2mm-19mm coarse aggregate.

AGGREGATESIZES = 13.2-19mm;AREAOFCUBE = 22500mm^2					
Age (Days)	Cube description	Weight before curing (Kg)	Weight after curing (Kg)	Load (Kn)	Compr. Strength (N/Mm^2)
7	A	8.19	8.24	418.32	19.37
	B	8.54	8.58	453.33	
14	E	8.49	8.55	498.88	24.11
	F	8.39	8.46	585.88	
28	I	8.36	8.46	368.99	24.55
	J	8.58	8.65	735.76	
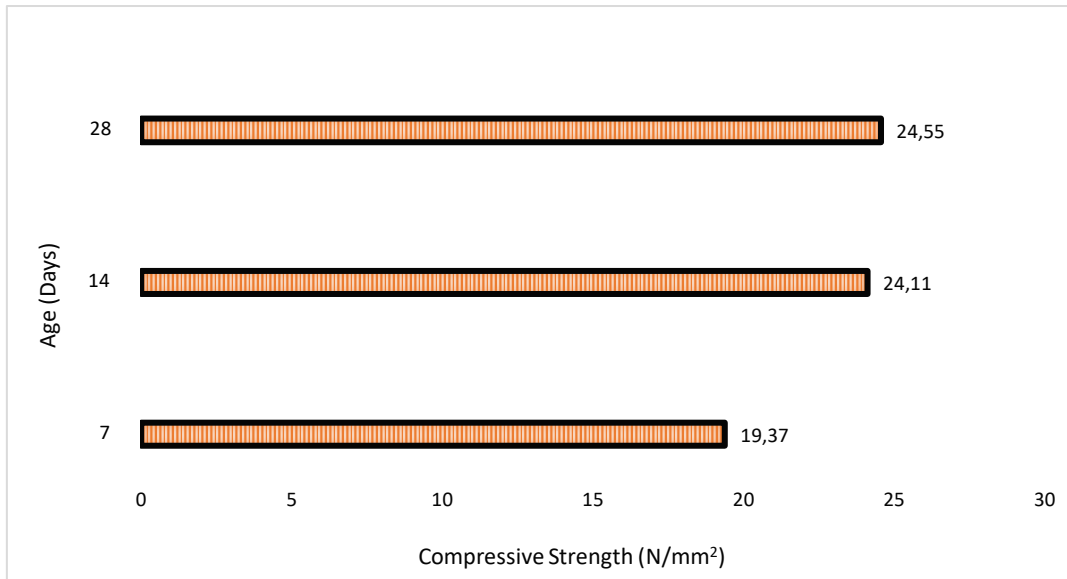
Figure 5. Compressive strength of 13.2-19mm coarse aggregate.

Table 5. Results of compressive strength for 20mm-28mm coarse aggregate.

AGGREGATE SIZES = 20-28mm;				AREA OF CUBE = 22500mm²	
Age (Days)	Cube Description	Weight Before Curing (Kg)	Weight After Curing (Kg)	Load (Kn)	Compr. Strenght (N/Mm²)
7	C	8.47	8.51	344.40	18.31
	D	8.41	8.46	479.33	
14	G	8.54	8.59	633.20	23.68
	H	8.44	8.59	432.29	
28	K	8.37	8.45	588.14	25.25
	L	8.53	8.61	547.90	
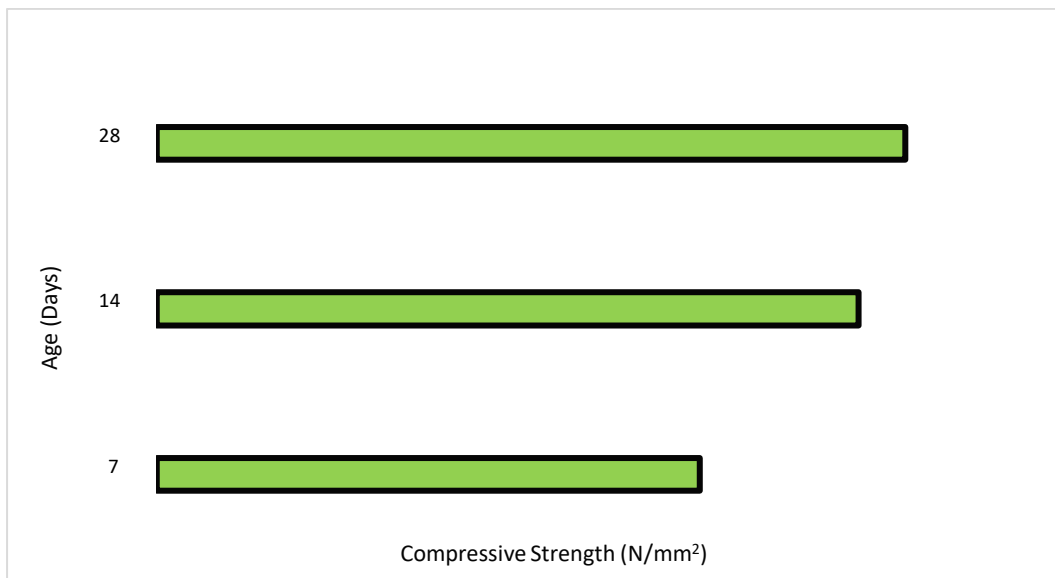
Figure 6. Compressive strength of 20-28mm coarse aggregate.

Table 6. Summary of compressive strength for different coarse aggregate sizes.

Age (Days)	Compressive strength for difference coarse aggregate sizes		
	20-28mm	**13.2-19mm**	**3.35 - 10mm**
7	18.31	19.37	14.16
14	23.68	24.11	17.47
28	25.25	24.55	18.64
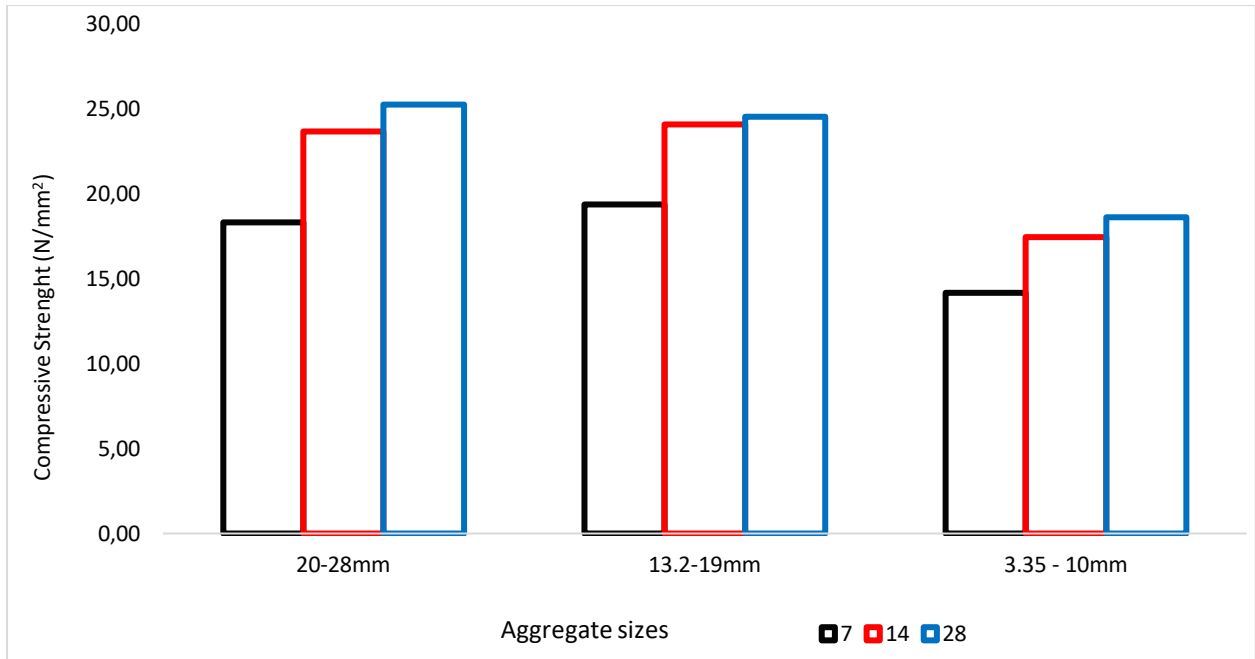
Figure 7. Compressive strength of different sizes of coarse aggregates.

Table 7. Results obtained from slump test experiment.

Sample No.	Mix ratio	W/C	Slump height (mm)	Slump type (mm)
3.35mm-10mm	1:2:4	0.4	10.00	True
13.2mm-19mm	1:2:4	0.4	13.50	True
20mm-28mm	1:2:4	0.4	20.00	True

Results obtained from the laboratory experiment which are shown in Table 6 and graphically in Figure 7, reveals that concrete made with coarse aggregates of sizes ranging from 20mm-28mm (i.e retained on 20mm to that retained on 28mm) had a higher compressive strength as compared to the other two size range. The strength also decreases with aggregate size range of 13.2mm-19mm while those with the range of 3.35mm-10mm showed the least compressive strength. This is in agreement with the findings of Ogundipe et al. [6]. Also in respect to weight of the concrete before and after curing, the concrete with the higher aggregate size range (i.e, 20mm to 28mm and 13.2 mm to 19mm) have a slightly more weight than those produced using the smaller aggregate size range (i.e, 3.35mm to 10mm). This in turn affects the rigidity of concrete and load required to crush them. What this means is that, they can withstand more pressure and thus carry more load. This has also been revealed by the experiment as can be seen in Tables 3, 4 and 5 that concrete made with higher coarse aggregate sizes require more crushing load. It is therefore safe to say, a higher coarse aggregate size will produce a richer concrete.

4. CONCLUSION

In conclusion, results from the experiment revealed that the bigger the coarse aggregate size, the higher the compressive strength produced. It also showed that the strength of concrete increased with the curing days and finally, that with a higher coarse aggregate size, concrete cubes were observed to have more weight than those produced with lesser coarse aggregate size. It was observed that crushed stone is very strong and tough, yet, it has good surface texture that enhanced proper bonding between aggregate and cement paste. Therefore, while evaluating aggregate sizes for optimum concrete strength, the following suggestions should be considered:

i. For construction of foundations, aggregate of larger sizes should be used since it has higher compressive strength.

ii. Proper compaction of the concrete cubes must be ensured, as compaction during the experimental process was observed to improve the strength of concrete.

iii. The workability of concrete is very important since it plays a vital role in the compressive strength of concrete, as such, concrete should be workable enough to achieve the expected strength.

REFERENCES

[1] Abdullahi, M. (2012) Effect of aggregate type on Compressive strength of concrete. International Journal of Civil and Structural Engineering, 2(3), 791-800.

[2] Bamigboye, G. O., Ede, A. N., Egwuatu, C. and Jolayemi, J. (2015) Assessment of Compressive Strength of Concrete Produced from Different Brands of Portland Cement. Civil and Environmental Research, 7(8), 31-38.

[3] Ukala, D. C. (2019) Effects of Combined Aggregate Gradation on the Compression Strength and Workability of Concrete using Fineness Modulus. Journal of Applied Science and Environmental Management, 23(5), 851-856.

[4] Wei, H., Liu, Y., Wu, T. and Liu, X. (2020) Effect of Aggregate Size on Strength Characteristics of High Strength Lightweight Concrete. Material, 13(1314), 1-13.

[5] Sneka, S., Nirmala, M. and Dhanalakshmi, G. (2018) Size Effect of Aggregate in the Mechanical Properties of Concrete. International Research Journal of Engineering and Technology, 5(2), 2093- 2096.

[6] Ogundipe, O. M., Olanike, A. O., Nnochiri, E. S. and Ale, P. O. (2018) Effects of Coarse Aggregate Size on the Compressive Strength of Concrete. Civil Engineering Journal, 4(4), 836- 842.

[7] Ramonu, J. A., Ilevbaoje, J. O. and Olaonipekun O. A., Modupe, A. E. and Saleh, J. Y. (2018) Comparative Analysis of the Combination of Coarse Aggregate Size Fractions on the Compressive Strength of Concrete. International Journal of Civil Engineering and Technology, 9(11), 1447-1457.

[8] Obi, L. E. (2017) Evaluation of the Effects of Coarse Aggregates Sizes on Concrete Quality. European Journal of Engineering Research and Science, 2(10), 1-6.

[9] Ekwulo, E. O. and Eme D. B. (2017) Effect of Aggregate Size and Gradation on Compressive Strength of Normal Strength Concrete for Rigid Pavement. American Journal of Engineering Research, 6(9), 112-116.

[10] Salau, M. A. and Busari, A. O. (2015) Effect of Different Coarse Aggregate Sizes on the Strength Characteristics of Laterized Concrete. IOP Conference Series: Materials Science and Engineering 96(012079), 1-8.

[11] Musa, M. F. and Saim, A. A. (2017) The Effect of Aggregate Size on The Strength of Concrete. The Colloquium, 10, 9-11.

[12] Ajamu, S. O. and Ige, J. A. (2015) Effect of Coarse Aggregate Size on the Compressive Strength and the Flexural Strength of Concrete Beam. Journal of Engineering Research and Applications, 5(1)

International Journal of Engineering and Innovative Research

http://dergipark.gov.tr/ijeir

STRESS MECHANICS OF REINFORCED POLYESTER COMPOSITES

Osaretın M.O [1] , Olodu D.D [1*]

[1] Benson Idahosa University, Faculty of Engineering, Department of Mechanical Engineering, PMB 1100, Benin City, Edo State, Nigeria.

*Sorumlu Yazar: dolodu@biu.edu.ng

ABSTRACT: This research investigates the stress mechanics of reinforced polyester composites when exposure to a sudden impact force, using experimental and analytical methods based on impact and Linear Elastic Fracture Mechanics (LEFM) test procedures. In this study, the stress distribution around crack tip and zone for 14 test samples with geometry 210 mm x 150 mm were investigated. KII stress intensity factors, critical stress, σC, shear stress, τnt the impact energy, E and impact strength, U were determined for each specimen. The mode I fracture toughness, KIC was found to be to be 4.97 MPa.m1/2 at a critical stress of 13.53 MPa while the mode II fracture toughness, KIIC was 1.31 MPa.m1/2 at a shear stress, τnt of 3.71 MPa. The effective thickness was found to be in the range of 80-100mm at fibre volume fraction, Vf of within 0.35-0.50. This was largely found to be as result of fibre bridging and crack arrest mechanisms. This mechanism prevented crack growth direction in specimens containing woven roving not to propagate along the original direction, but change the direction to an inclined path till failure with the exception of those containing soft and hard mat in which the crack grew in the original crack direction as the stress intensity increased. During the impact test, fibre stacking sequence played a vital role, thereby making specimens containing woven roving to resist impact damage and failure, and this resulted in fibre pull-out during fracture. The stress could be seen to concentrated at the crack tip and around the loading pins on a smaller level, compared to the level at the crack tip.

Keywords: Analytical Methods, Critical Stress, Reinforced Polyester Composites, Shear Stress

1. INTRODUCTION

In the analysis of impact damage and fracture of composites, the review of the sources, nature and curvature of impactor and how these fracture initiation takes place, propagate from a microstructural scale at the sites of flaws, and how the coalescence of these flaws leads to a visible separation process that manifests on a macrostructural level before resulting in a catastrophic failure are vital. According to Làszló and George [1], the mechanical and thermal behaviours of a structure depend on the properties of the fibres and the matrix and on the amount and orientations of the fibres. In the structural analysis of composites, the design steps from the micromechanics (which takes into account the fibre and matrix properties) through macromechanics (which treats the properties of the composite) are taken into consideration. Radif and Ali [2] in their studies of the fracture toughness of kenaf mat reinforced polyester composite estimated and analysed the crack criteria by using the mathematical laws that were limited in E1820 standard and the results affirmed by applying the numerical solution of ANSYS to estimate the fracture toughness value , besides the energy release rate of biomass composite. The fracture characterisation of the composites was carried out using the compact tension (CT) specimen that was common used to determine the mode-I fracture properties. The

fracture toughness was found to be independent of pre-crack length while the tests were performed at room temperature. It was found that the numerical simulations of the ANSYS model result demonstrated a good agreement between the experiments computed results of the fracture toughness. Edelugo [3] subjected various ply combinations which were randomly selected and used in laminates to tensile, bending and hardness test after being submerged in alkaline and acidic media of varying molar strength for different times intervals of 24 and 48 hours respectively. Results showed that while some samples combinations increased in strength with increases in timed exposure to the acidic/alkaline environment, while other indicated, instead, a decrease in strength for the same environmental conditions which was a revelation to the fact that there existed certain ply combinations which can exhibit better resistance to harsh environmental conditions than others when put in us. In a study by Dhakal et al. [4], the results on investigation on impact property of non-woven hemp fibre reinforcement, subjected to drop weight impact test was compared with that of chopped strand mat E-glass fibre reinforcement with equal volume fraction. The impact test result showed that the total energy absorbed by 0.21 fibre volume fraction (four layers) of hemp reinforced specimens was comparable to the energy absorbed by the equivalent fibre volume fraction of chopped strand mat E-glass fibre reinforced unsaturated polyester composite specimens. Szekrényes [5] in an overview on the experimental investigations of the fracture toughness in composite materials, several experimental measures of determining the fracture properties of reinforced composites were shown. The aim of the research was to summarize publications about different experimental investigations of the fracture properties of composites materials. From his study, it was observed that fracture and damage in composites could be influenced by many parameters. Williams [6] in his analysis of the fracture mechanics of composites failure reviewed how fracture mechanism can be applied to the various fracture modes observed in composites. It was shown that rather conventional methods may be used for short-fibre composites but that oriented laminates undergo delamination, often parallel to the applied loads, and energy release rate methods must be used to analyse these failures. The importance of delamination toughness in determining composite behaviour was emphasized and details of the various test methods and analysis techniques were given and finally, some discussions of the more complex failures seen in cross-ply laminates were presented. Mandel et al. [7] studied the micromechanical growth of crack in fibre reinforced materials using a 2-D, micromechanical finite element study of stress conditions near crack the tip. The mechanical properties, interface between the fibres and matrix material and the geometry were considered. A close agreement between finite element and experimental values for the loading required for both the initiation of crack growth in the material and arrest by the fibres showed that micromechanical finite element studies are applicable for the development of engineering models for the fracture toughness of fibre reinforced material. It was also shown that the presence of high modulus fibres could significantly reduce the opening mode (mode-I) stresses in the matrix material near the crack tip and could result in crack arrest and an increase in the effective fracture toughness. Further, it was noted that the shear stresses in the matrix material adjacent to the fibre and bond stresses between the fibre and matrix material are larger for a shear mode loading than for an opening mode loading. Although the stresses do not directly result crack growth, they were observed to cause fibre delamination which in turn could result in unstable crack growth.

This research investigates the stress mechanics of reinforced polyester composites when exposure to a sudden impact force, using experimental and analytical methods based on impact and Linear Elastic Fracture Mechanics (LEFM) test procedures.An Introduction should provide a review of the recent literature on the topic and sufficient background information to allow the results of the article to be understood and evaluated.

2. MATERIALS AND METHODS

2.1. Materials

This research is carried out on samples fabricated by randomly varying plies of reinforcements in form of woven roving, hard and soft E-glass fibre mats, combined in unsaturated polyester resin (specific gravity 1.12, viscosity of 65cps and gel time of 25 min) matrix. The catalyst and accelerator used were methyl ethyl ketone peroxide (MEKP) and cobalt respectively due to their compatibility in polyester as curing agents at ambient temperature condition.

2.2. Methods

Impact damage in metal is easily detected as damage starts at the impacted surface; however, damage in composites often begins on the non-impacted surface or in the form of an internal delamination which is immediately preceded by matrix cracking on the impacted surface. The behaviour of fibre reinforced composites when suddenly impacted by a solid object was the subject of much numerical, analytical and experimental research. During the course of analysis in this work, the fracture mechanics of reinforced composites with varied composition of reinforcement forms was critically considered on exposure to suddenly applied impact force. Due to the fracture mechanics consideration, much focus was on the mode and direction of crack propagation, with respect to the stress distribution around the initial crack tip, region and other locations of flaws as the crack grew. The crack growth was found to be a response to the stress intensity around the region of flaw, which was borne out of the stress concentration at the tip of flaw where the maximum stress is present.

3. EXPERIMENTAL

3.1. Linear Elastic Fracture Mechanics

In the analysis of the fracture mechanics of reinforced polyester composite, the Linear Elastic Fracture Mechanic (LEFM) which according to Okorie [8], is concerned with the analysis of elastic stresses in the neighbourhood of pre-existent cracks of specified intensity, for which its purpose is to ascertain the level of applied stress, σ, at which pre-existent cracks of various sizes and geometries will propagate; and impact test approaches were used, where emphasis is focused on exploring the fracture mechanics at the crack tip of the fibre reinforced composite when subjected to impact force. The test was conducted under plane stress condition.

According to Pahizgar et al., [9] the proper way to begin a study of fracture in orthotropic materials (reinforced composite material) is to compare their fracture with the fracture of isotropic materials and then model the fracture mechanism as homogeneous anisotropic materials. Based on the principle of LEFM, the following can be stated that:

a) The crack will advance along the original crack direction.
b) The crack tip displacements can be separated into three different modes: crack-opening mode (Mode I); edge or in-plane sliding mode (Mode II); and crack tearing or out-plane mode (Mode III).
c) The crack tip stress and displacement equation for the above modes are given by Westergaard's equations.

3.2. Analysis of Load-Displacement Records and Calculation of K_I

For the determination of a valid K_I, a conditional value K_Q is obtained first. This involves a geometrical construction on the test record, consisting of drawing a secant line OP as shown below through the origin with slope equal to 0.95 of the slope of the tangent to the initial linear part of the record. The load Ps corresponds to the intersection of the secant with the test record. The load P_Q is then determined as follows: if the load at every point on the record which precedes Ps is lower than P_Q, then $P_Q = Ps$ (type I); if, however, there is a maximum load preceding Ps which is larger than Ps then P_Q is equal to this load (types II and 111) as shown below.
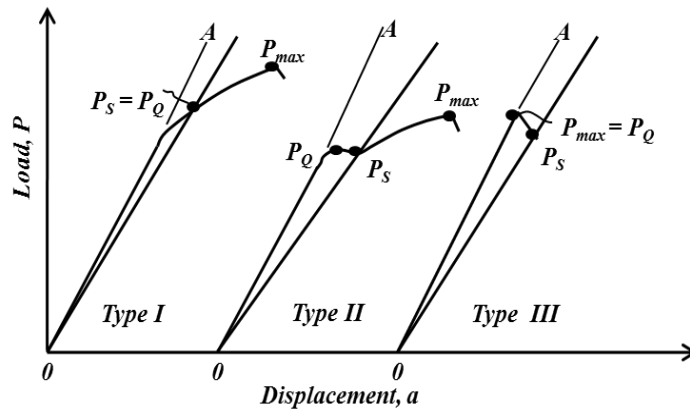
Figure 1. Types of load-displacement curves illustrating determination of P_S and P_Q.

The test will not be valid if $P_{max}/P_Q > 1.10$, where P_{max} is the maximum load the specimen was able to sustain. In the geometrical construction, the 5 per cent secant offset line represents the change in compliance due to crack growth equal to 2 per cent of the initial length.

When maximum load P was determined, the value of K_I could be calculated using the stress intensity factor expression for the CT specimen as recommended by ASTM. The ASTM standards for the mode I stress intensity factor (SIF), K_I calibration for the CT specimen is given by Equation 1a and 1b respectively;

$$K_I = \frac{P}{BW^{1/2}} f\left(a_i/W\right) \tag{1a}$$

$$f\left(a_i/W\right) = \frac{\left(2 + a_i/W\right)}{\left(1 - a_i/W\right)^{3/2}} \left[0.886 + 4.64\left(a_i/W\right) - 13.32\left(a_i/W\right)^2 + 14.72\left(a_i/W\right)^3 - 5.6\left(a_i/W\right)^4\right]$$
(1b)

The expression for K_I determination is accurate to within 0.5 per cent, over the entire range of a/W $\left(a/W < 1\right)$ as presented in Janssen et al. [10].
The stress intensity factor as very important property in fracture criteria which depends on the applied load and the material configuration shall be computed for the mode II loading using the expression;

$$K_{II} = \tau_{n\theta}\sqrt{\pi a} \tag{2}$$

where $\tau_{n\theta}$ is the shear stress parallel to the crack shall be determined using the stress transformation by method of equation. From the wedge method of stress transformation, we have that; the force in the y direction is given by;

$$P = -\left(\sigma_{yy}\sin\theta + \tau_{xy}\cos\theta\right)\left(\Delta B\cdot\Delta t\right) \tag{3}$$

From equilibrium of forces in the t direction on the force wedge, we obtain the shear stress, $\tau_{n\theta}$ as a function of σ_{yy}, τ_{xy} and θ; where the shear plane, t inclination angle, $\theta = 38.7°$, $\sigma_{xx} = 0$.

$$\tau_{n\theta} = -\sigma_{xx}\cos\theta\,\sin\theta + \sigma_{yy}\sin\theta\,\cos\theta + \tau_{xy}\left(\cos^2\theta - \sin^2\theta\right) \tag{4}$$

The theory proposed by Waddoups et al. stated in Gdoutos is based on the generalised concept of the process zone that the actual crack length is extended by the length of the process zone which is taken equal to a damage zone at the crack tip. Hence, for a crack length of a, the critical stress, σ_C shall be determined according to the stress intensity factor criterion, expressed by;

$$\sigma_C = \frac{K_{IC}}{\sqrt{\pi(a+\ell)}} \tag{5}$$

where ℓ is the damage zone at each crack tip and it will be determined from experiment near failure along the crack ligament.

3.3. Analysis of Stress Field near the Crack Tip

The study of stress and displacement fields near the crack tip is very important, because these fields govern the fracture process that takes place at the crack tip and the damage zone. In this section, study of the stresses and displacements near the crack tip for the crack opening deformation modes was analysed, using the Westerguaard equation for stress distribution in the y-direction. The equation is given by;

$$\sigma_y = \frac{K_I}{\sqrt{2\pi r}}\cos\frac{\theta}{2}\left(1 + \sin\frac{\theta}{2}\sin\frac{3\theta}{2}\right) \tag{6}$$

where K_I is the mode I stress intensity factor, σ_y is the stress at a location, r around the crack at angle, θ.

3.4. The Charpy Impact Test

The purpose of the Charpy impact test is to measure the energy absorption capacity of the reinforced polyester composite materials [11]. A notched bar of reinforced composite specimen was supported as a simple beam so that the vertical faces away from the point of impact and is struck at the middle using a hammer as incorporated on the test equipment. The impact test had a setup similar to the 3PB test and this is the most appropriate for the composite material, which damage and fracture in a brittle manner because of the case of the presence of micro defect or

a surface scratch; and the stress concentrated at these regions as this will accelerate the failure rate under sudden impact force. The energy which is absorbed by the blow is determined by a measuring device on the machine. The size of the tested specimen and the experiment setup is shown in the figures below;
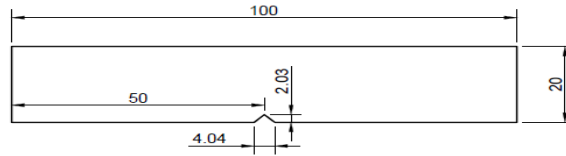
Figure 2. ASTM standard Notched Charpy Impact Test specimen.
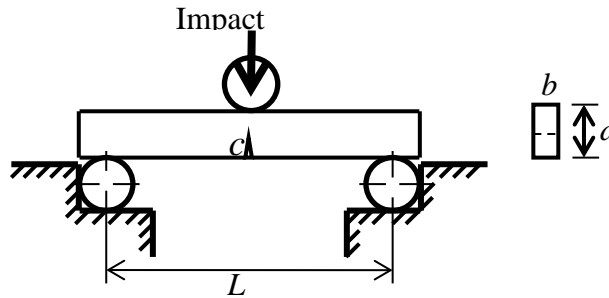
Figure 3. Charpy Impact Test Specimen setup.

3.5. Test Procedures for the Determination of Mode I Stress Intensity Factor, K_I

Before the determination of K_I, the CT specimen composition and manufactured were as shown in section 3.2, marked out as shown in figure 4 below. Hence, the CT specimen was drilled to make provision for the pins through which the load was introduced on the specimen, using a U-bracket which is attached to the Universal Testing Mechanic.
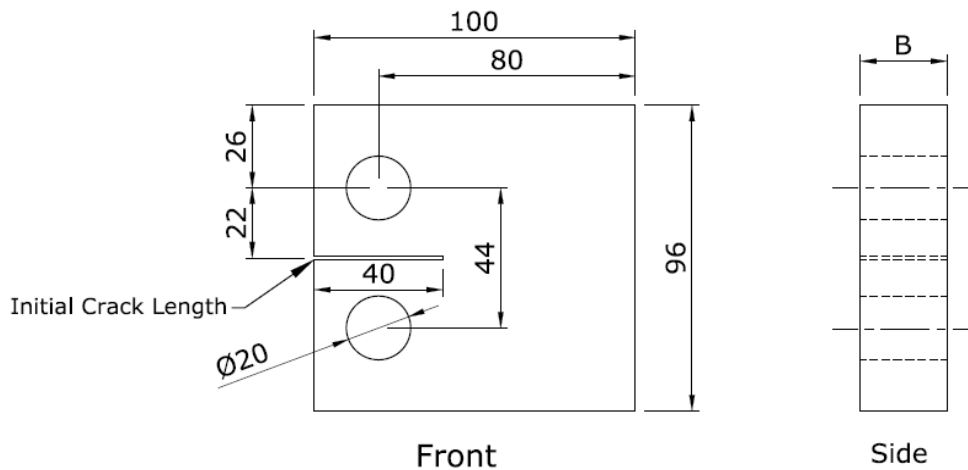
Figure 4. ASTM standard precracked Compact Tension (CT) specimen.

3.6. Analysis of Stress Field near the Crack Tip

The study of stress and displacement fields near the crack tip is very important, because these fields govern the fracture process that takes place at the crack tip and the damage zone. In this section, study of the stresses and displacements near the crack tip for the crack opening deformation modes was analysed, using the Westerguaard equation for stress distribution in the y-direction. The equation is given by;

44

$$\sigma_y = \frac{K_I}{\sqrt{2\pi r}} \cos\frac{\theta}{2}\left(1 + \sin\frac{\theta}{2} \sin\frac{3\theta}{2}\right) \tag{7}$$

where K_I is the mode I stress intensity factor, σ_y is the stress at a location, r around the crack at angle, θ.

4. RESULTS AND DISCUSSIONS

4.1. Load, P (kN) versus Displacement, δ (m) Test Data and Plots

The load – displacement plot was obtained for all specimens from experimental data, and this provided the platform for the fracture mechanics analysis on each specimen, containing varied fibre volume fraction and form, using the compact tension specimen, as shown above under tensile load condition on the universal testing machine. As the load was gradually applied and varied at a constant rate of 0.55mm per minute, then the crosshead vertical displacement data obtained as well as the increase in crack length as it propagated along the ligament and a successive interval of 5mm. These measurements were successful carried out by marking the crack growth front as it advanced. The determination of the maximum load, P lead to the determination of the stress intensities.

4.2. Data Analysis of Stress, σ_y Distribution in the Neighbourhood of Crack

Figure 5-18 shows the stress distribution around locations ahead of crack for different specimen. In the analysis of damage zone crack region around the crack tip as it propagates, there was an attempt to account for the fact that, the stress distribution cannot simply be cut off above σ_y as shown below. For the analysis to be straightforward there were some assumptions which were made that; plane stress state was being considered, that the material behaviour was linearly elastic and the plastic zone shape was circular. The occurrence of the damage zone makes the crack behave as if it were longer than its physical size.
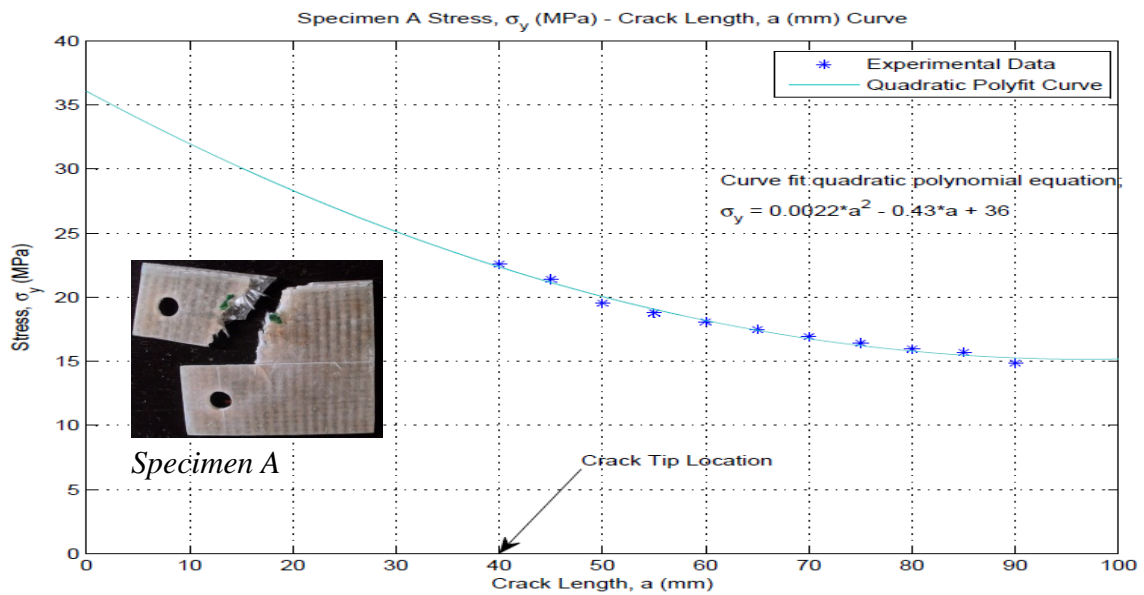
Figure 5. Stress Distribution around locations ahead of crack, a (mm) for Specimen A.
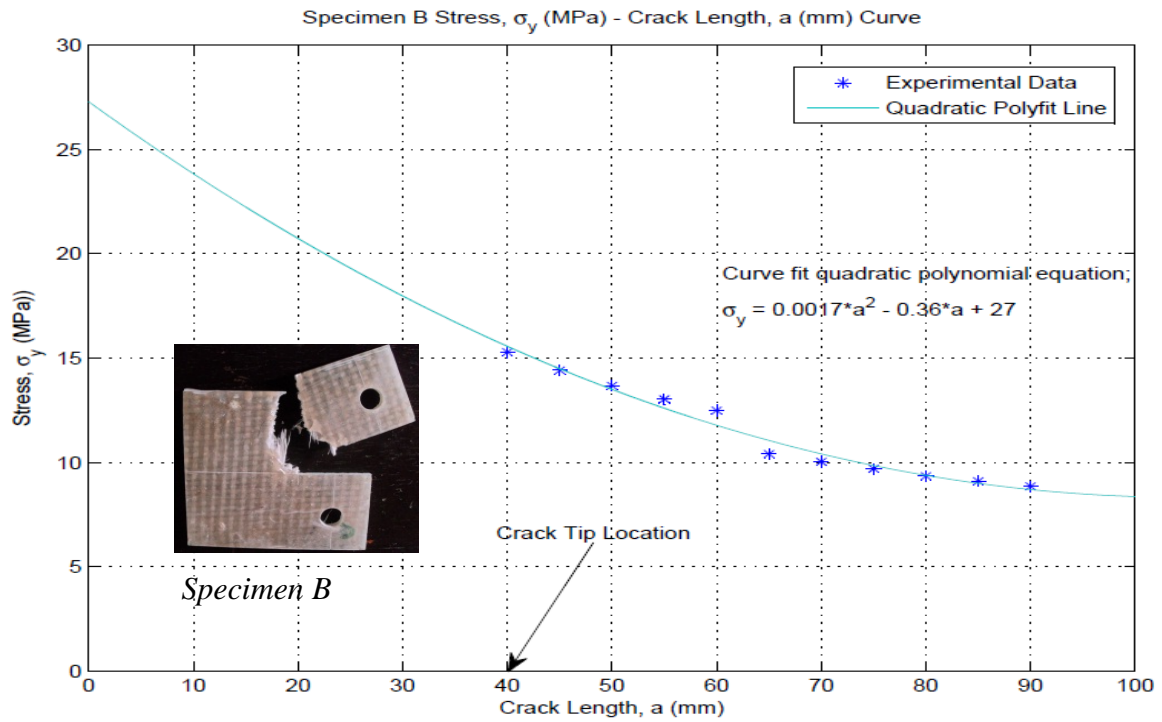
Figure 6. Stress Distribution around locations ahead of crack, a (mm) for Specimen B.
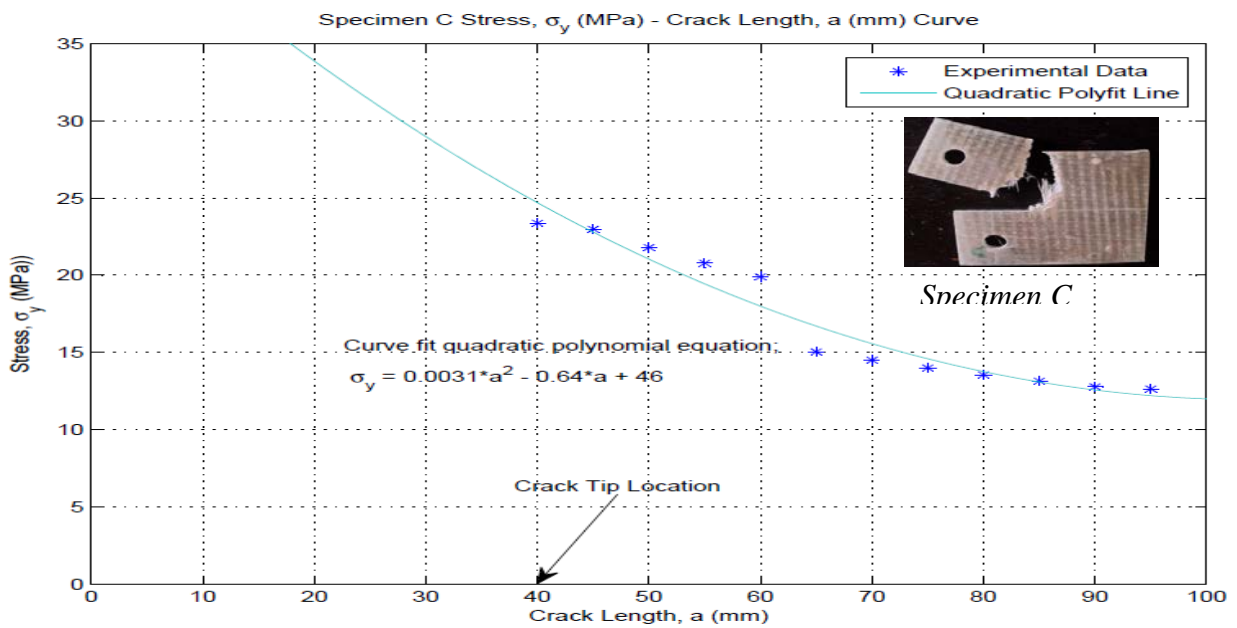
Figure 7. Stress Distribution around locations ahead of crack, a (mm) for Specimen C.
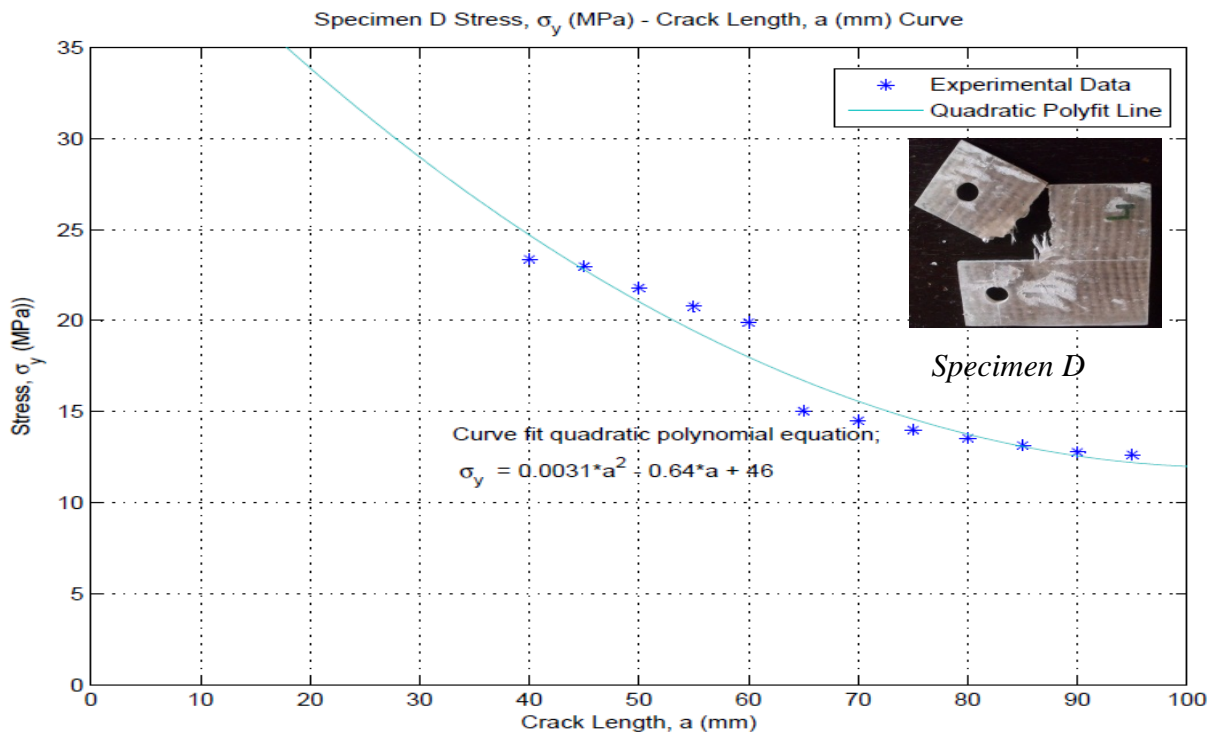
Figure 8. Stress Distribution around locations ahead of crack, a (mm) for Specimen D.
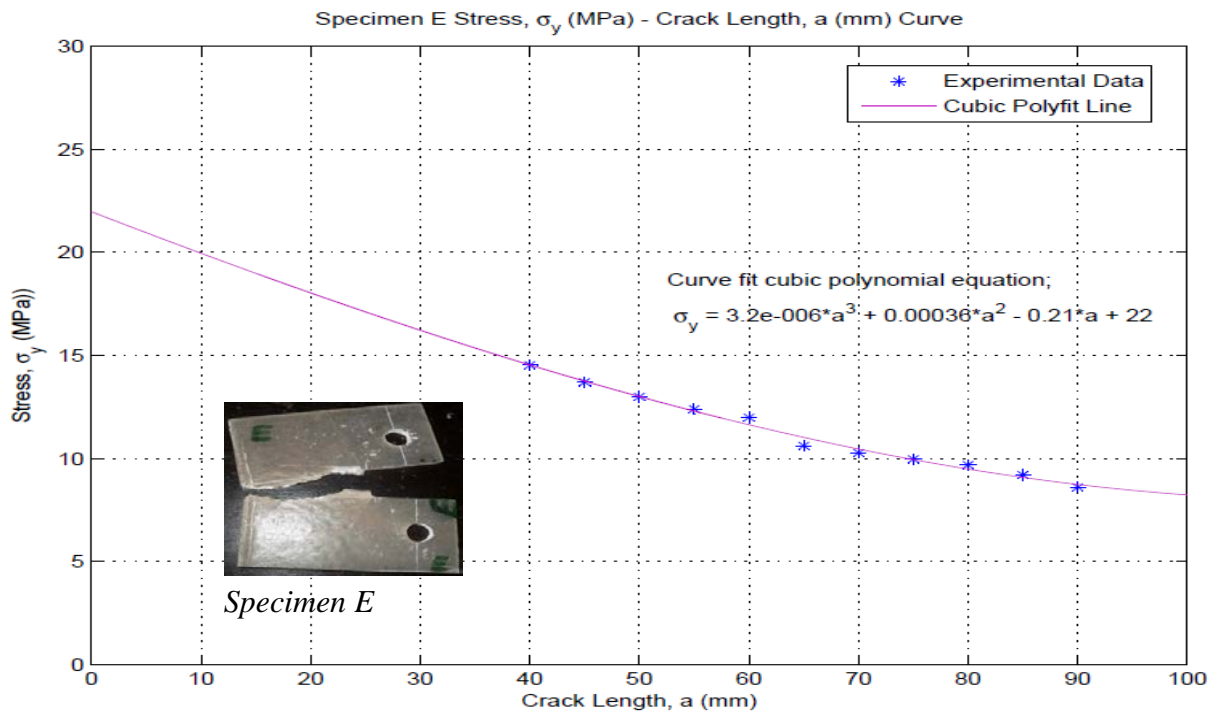
Figure 9. Stress Distribution around locations ahead of crack, a (mm) for Specime.
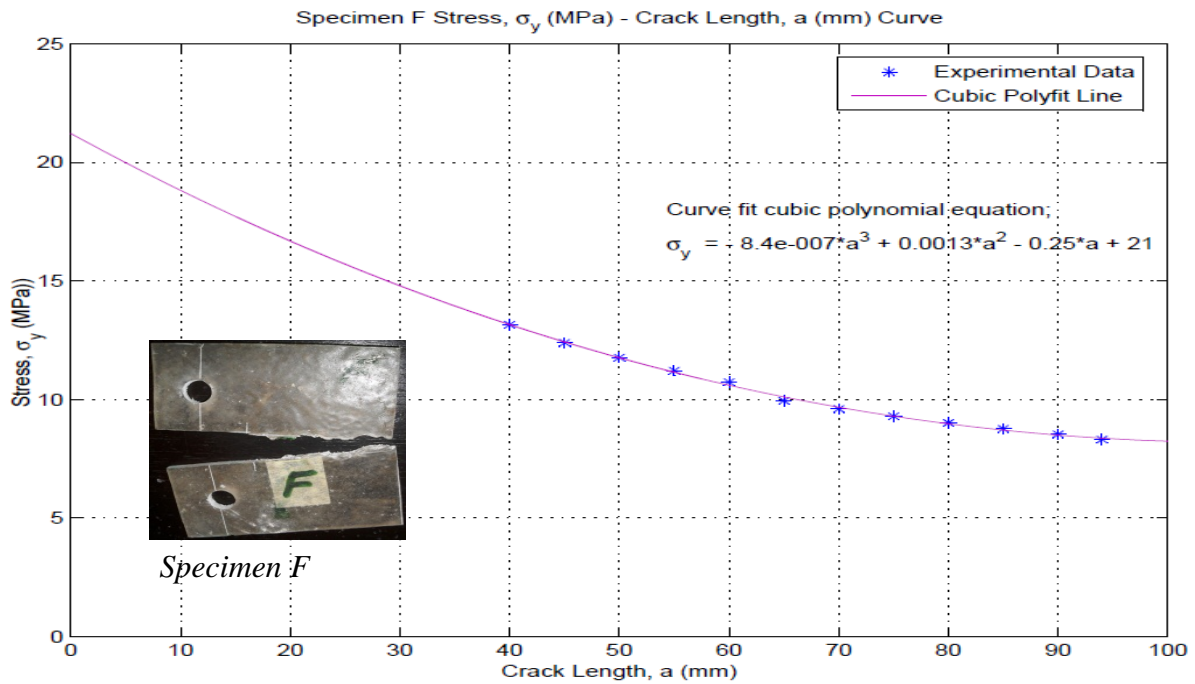
Figure 10. Stress Distribution around locations ahead of crack, a (mm) for Specimen F.
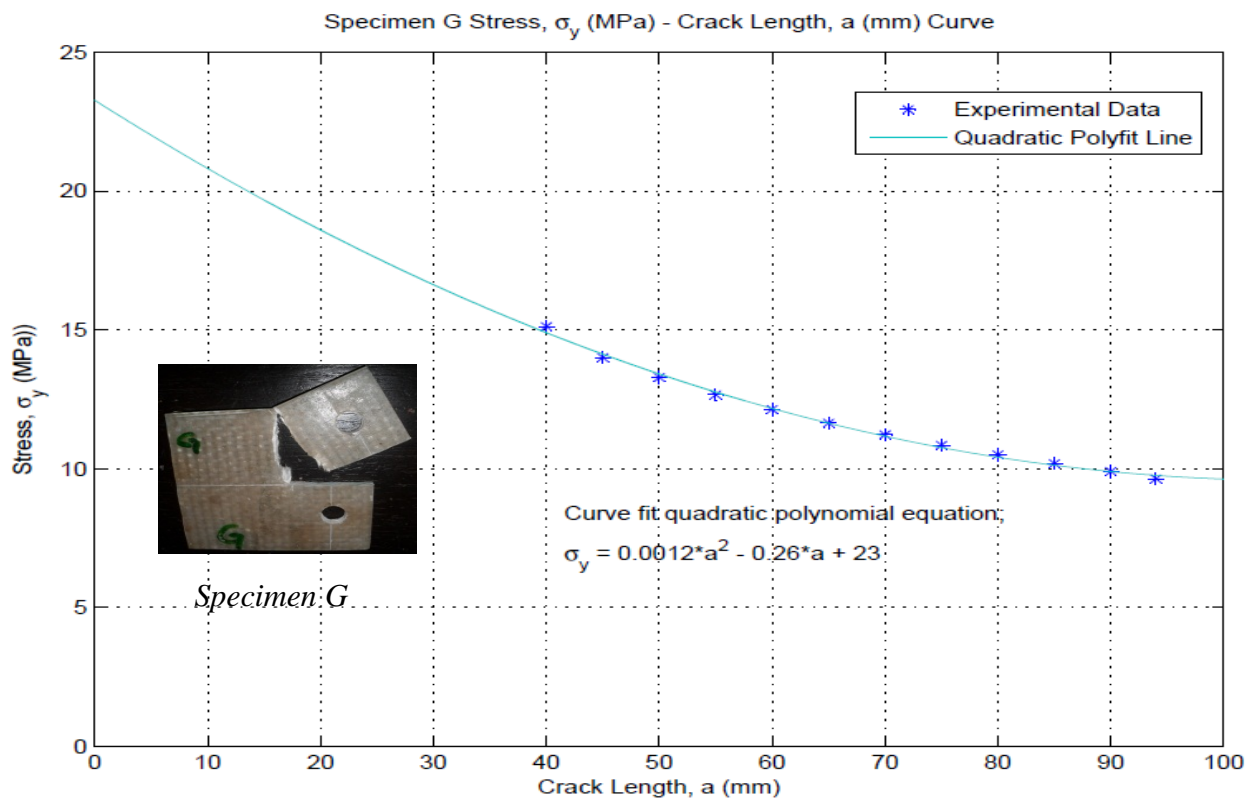
Figure 11. Stress Distribution around locations ahead of crack, a (mm) for Specimen G.
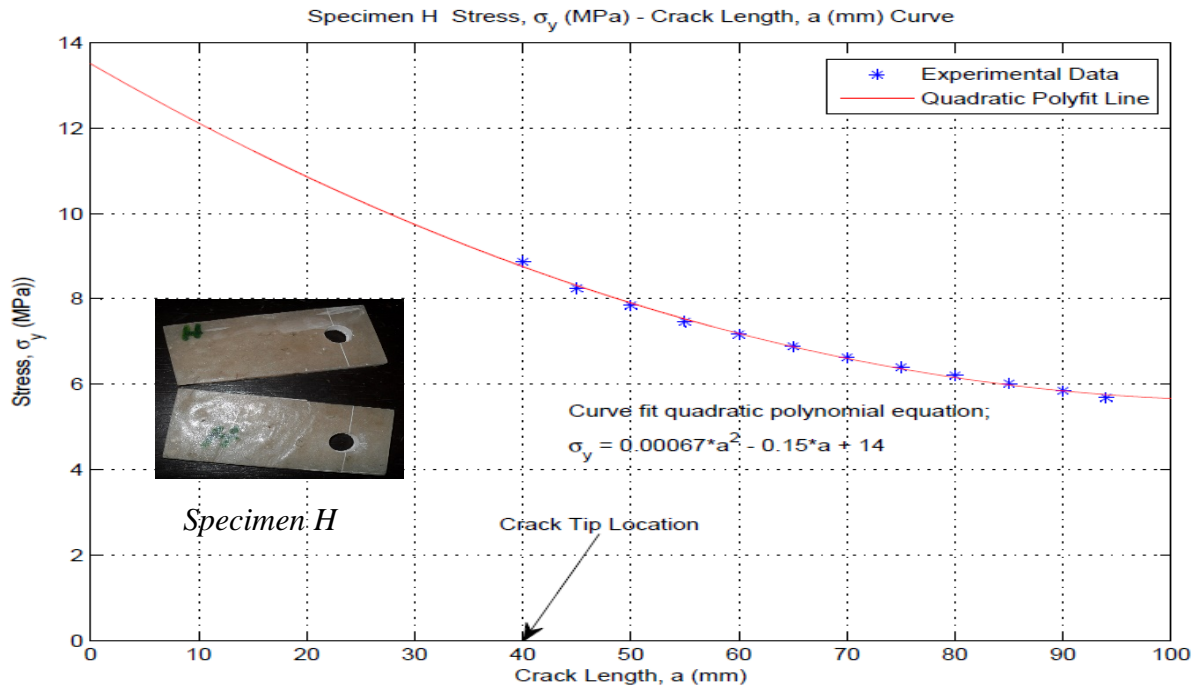
Figure 12. Stress Distribution around locations ahead of crack, a (mm) for Specimen H.
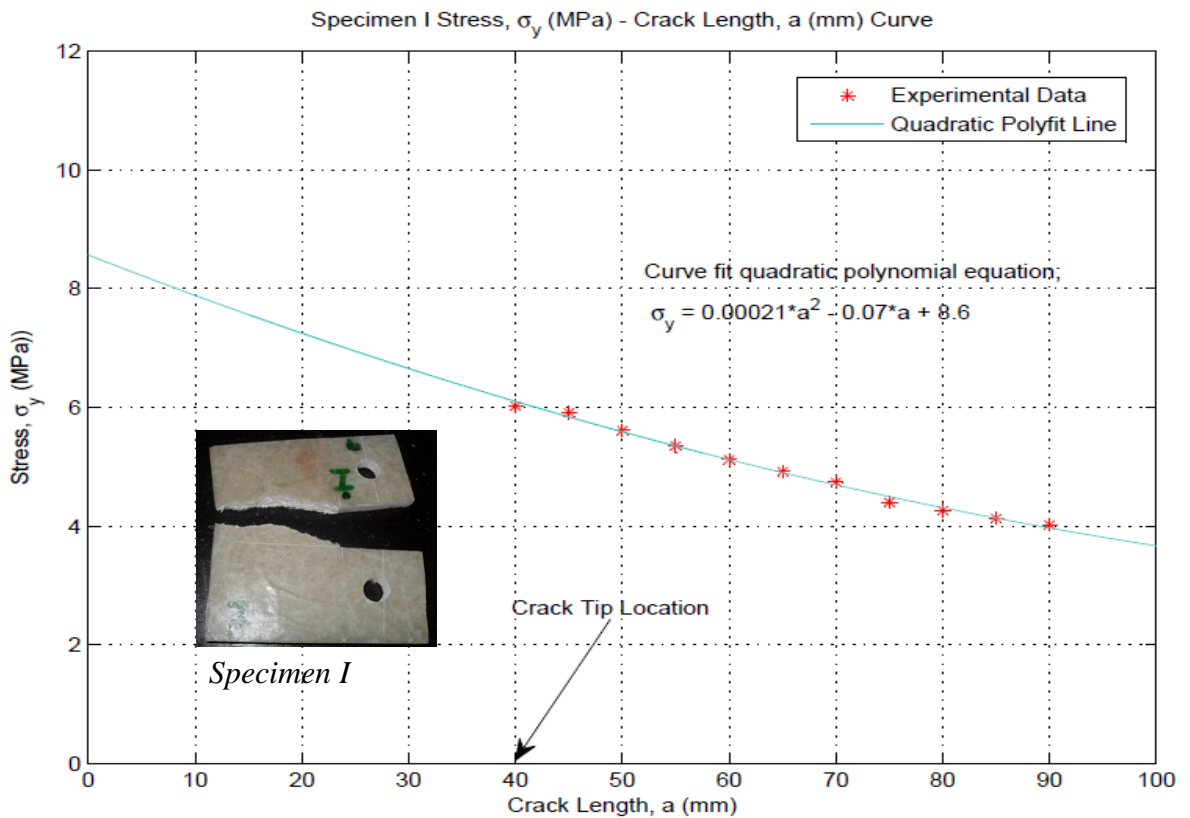
Figure 13. Stress Distribution around locations ahead of crack, a (mm) for Specimen I.
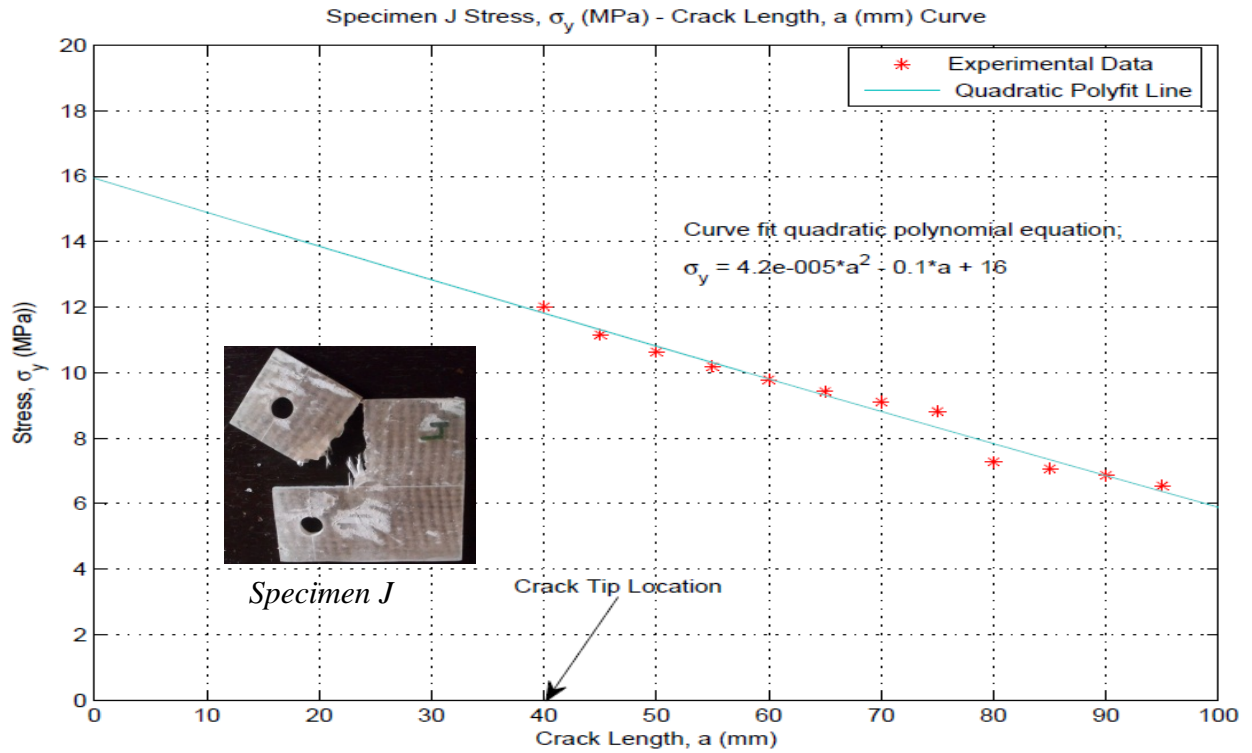
Figure 14. Stress Distribution around locations ahead of crack, a (mm) for Specimen J.
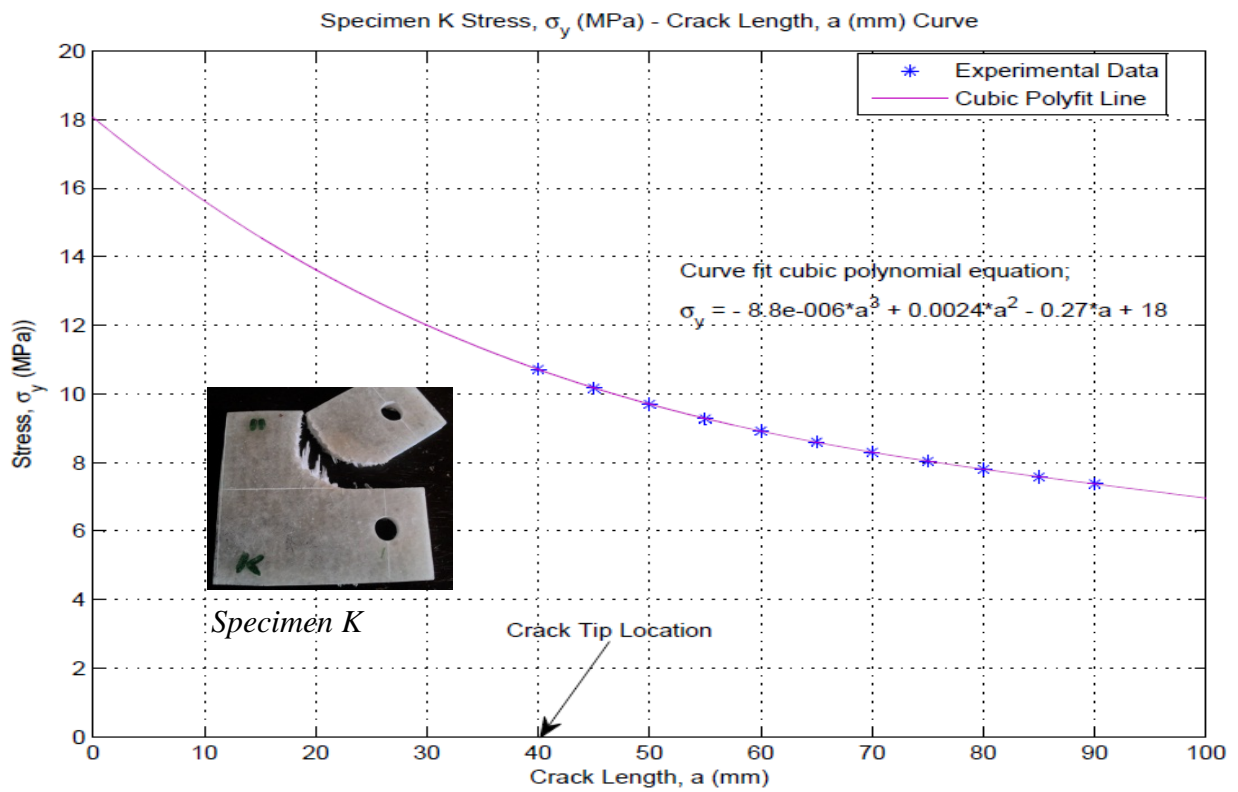
Figure 15. Stress Distribution around locations ahead of crack, a (mm) for Specimen K.
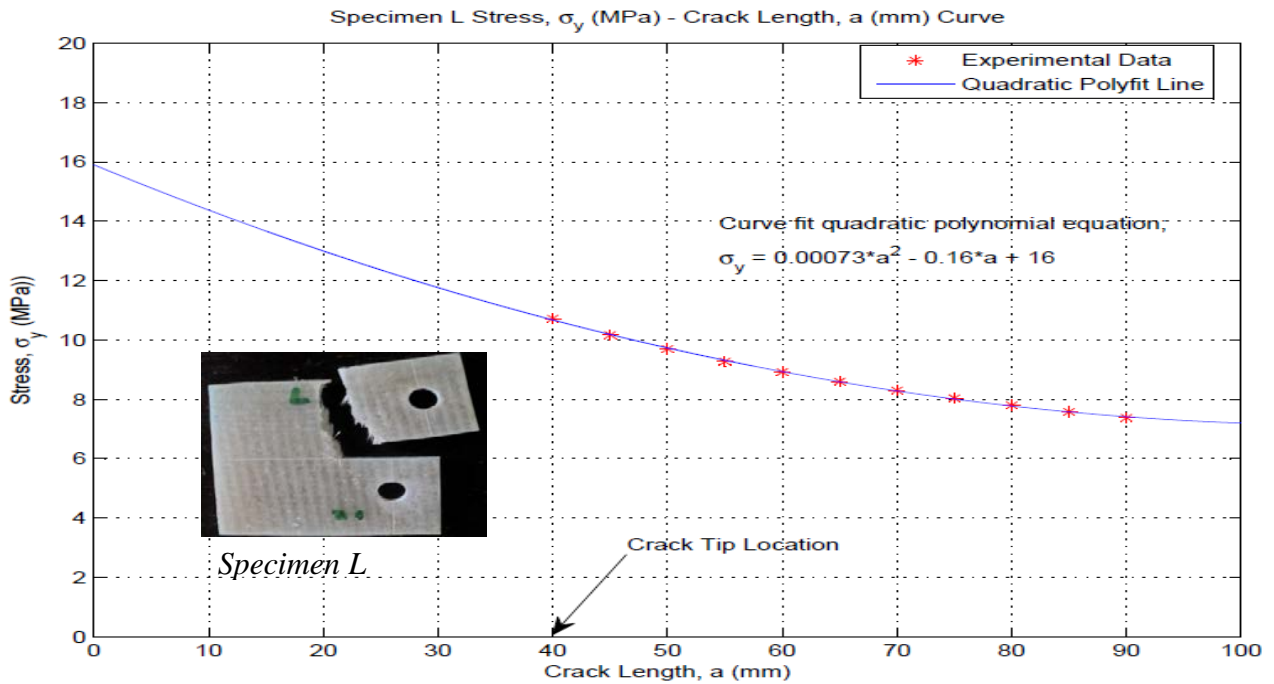
Figure 16. Stress Distribution around locations ahead of crack, a (mm) for Specimen L.
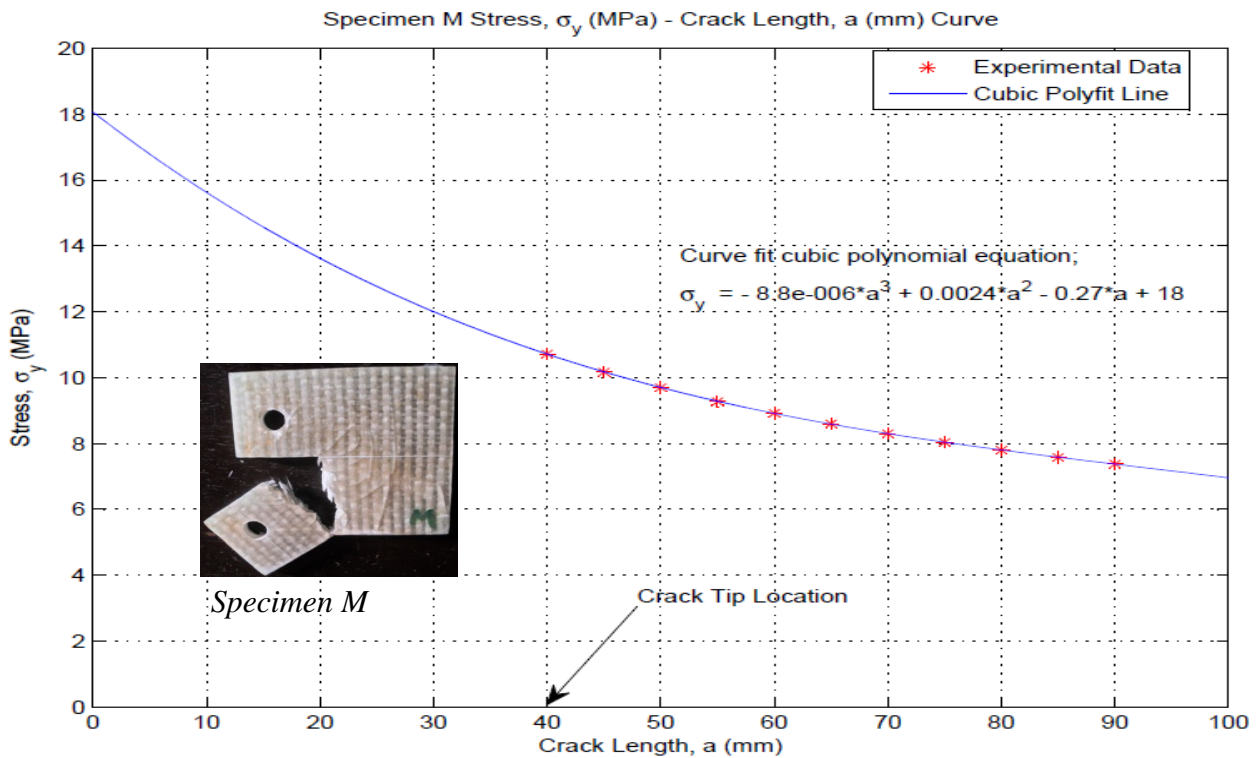
Figure 17. Stress Distribution around locations ahead of crack, a (mm) for Specimen M.

51
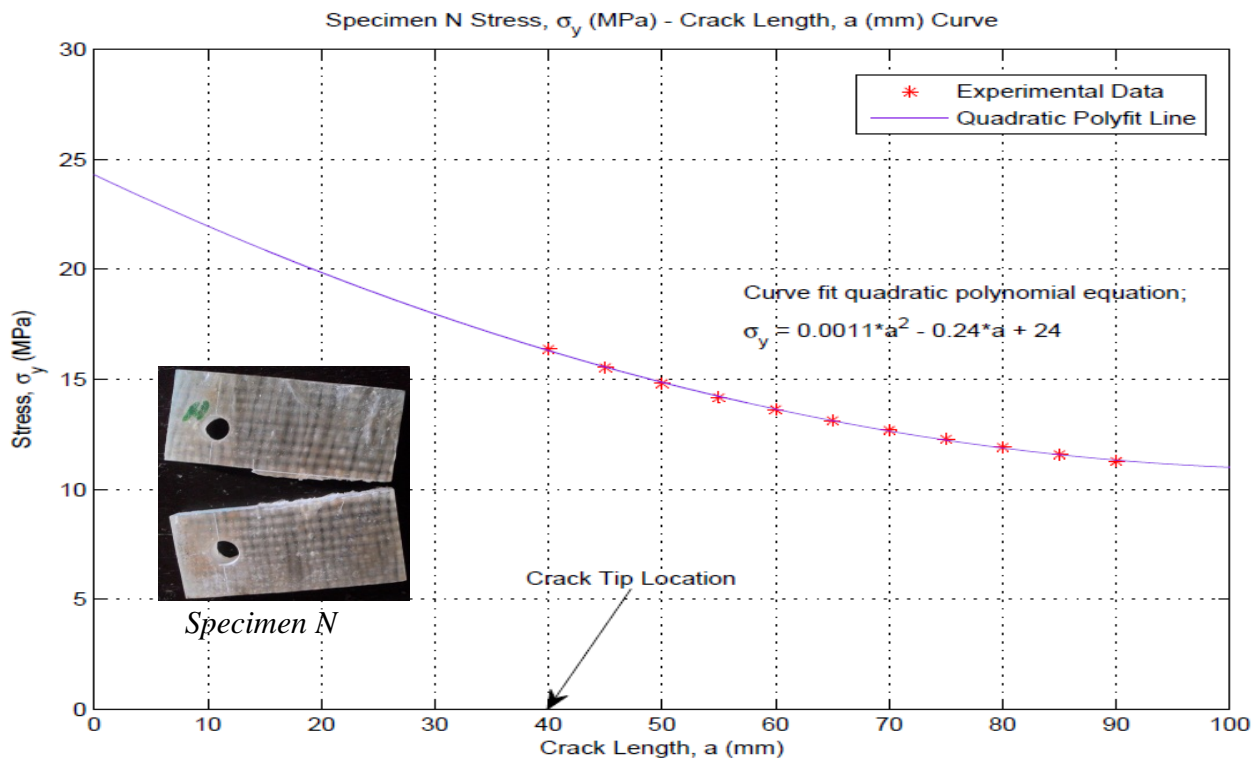
Figure 18. Stress Distribution around locations ahead of crack, a (mm) for Specimen.
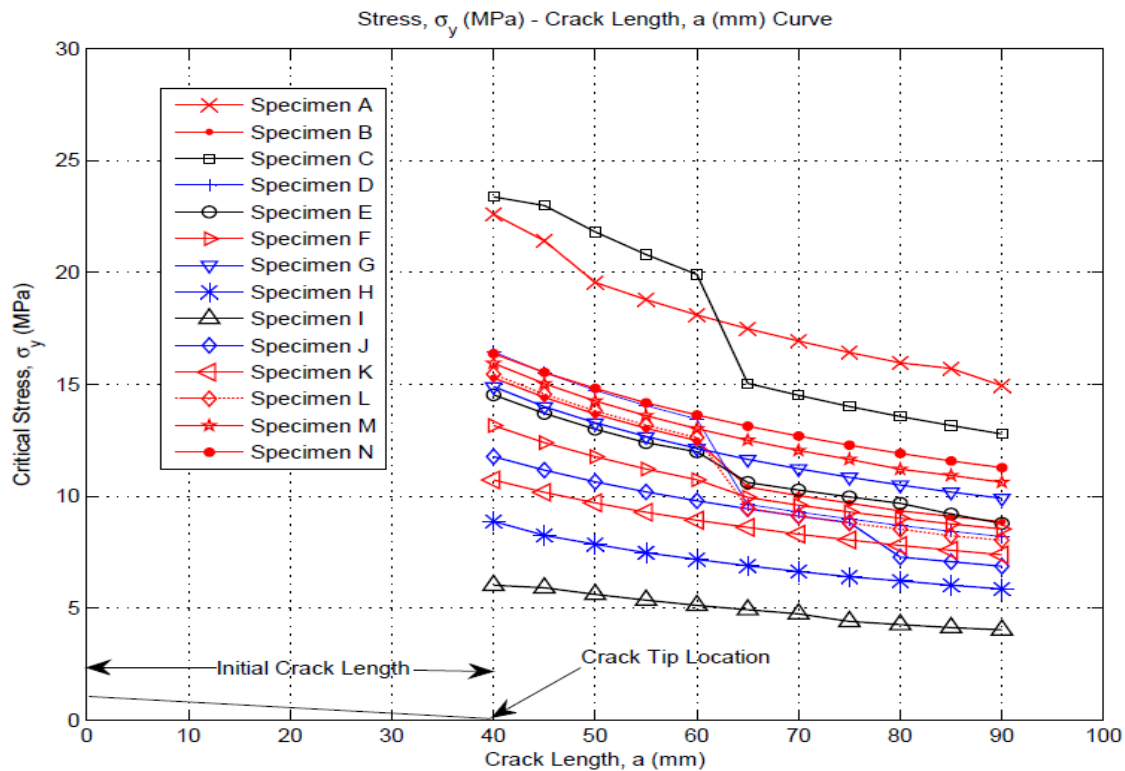
Figure 19. Stress Distribution around locations ahead of crack, a (mm) for all Specimens.

4.3. Interpretatıon of Results

Using equation 7 to model the stress distribution near the crack tip, it could be shown that the region around the neighbourhood of the crack tip experience higher stress state than other regions not around this vicinity. This was expressed in the stress distribution versus crack length

curve as shown in figures 5 – 18, and figure 19 showing the variation in stress distribution for all the specimens. Taking a look at the fracture mode of the CT specimens under mode I loading condition, it was observed that fracture of specimens containing woven roving namely; specimen A, B, C, D, G, , J, K, and M with the exception of specimen N, was not all along or in the direction of the original crack. The crack was observed to change direction as it propagate at an angle that was almost at 90° to the horizontal, without any crack growth in the initial crack direction, although this was not the case for all of them as some were seen to grow in the initial crack direction before change direction. The change in crack growth direction was a resistance posed by crack arrest from fibre bridging. This was also observed from the curves to result a decreased in the stress at the location. This could be explained as a change in direction as the crack grows will require a reduced stress level to grow the crack in that direction as the stress intensity at these locations are excessively higher. But for specimens E, F, H, I with the exception of specimen N contained soft and hard mat reinforcements. The cracks were observed to grow along the initial crack direction as a result of the reinforcement composition as this followed the LEFM principle. This could be raced to the form and mechanical properties of the fibre used which could not resist the crack growth efficiently. This shows that composites containing woven roving reinforcement were better fracture resistant composite material than soft and hard reinforcement mats. The weaving pattern of the woven roving was a key factor which contributed to its distinguished performance. From figure 13, it be shown that specimen I which contained 12 plies of soft mat reinforcement required the least stress magnitude to grow the crack, while specimen C which contained 2 plies of woven roving and one ply of hat mat experienced the highest critical stress.

5. CONCLUSIONS

It was observed from the stress intensity and critical stress versus crack length curve, that the crack tip is where the maximum stress exists but also, the location of the minimum stress intensity factor. This is an indication that glass reinforced polyester composites has the tendencies to resist damage and crack propagation when exposed to sudden impact force, if the internal structure and surface are void of defects and microcracks resulting from blisters, foreign particle, holes and fibre-matrix debonds, i.e. the energy required to grow the crack will be inactivated or equal to zero. During sudden impact force, the effect was found to be transferred in a wave-like fashion through and across the entire region and cross section of the material, and this result to bending the material which gives rise to matrix cracking before the debonding of fibres, thereby exposing them to tensile stress especially with the tip of defect experiencing the maximum stress. The stress intensity factor versus thickness curve reveals that the size effect also manifests in composite materials. This was revealed in the decreasing trend of the plot as the thickness increased, and that the thickness range best for tailoring reinforced polyester composite was 3-4mm. The critical stress was observed to be very high for reinforced polyester composite specimens with smaller thickness compared to those with higher thickness, which showed lower critical stress values.

REFERENCES

[1]Radif, Z. S. and Ali, A. Fracture Toughness of Kenaf Mat Reinforced Polyester Composite. *Pertanika Journal of Science and Technology.* 99(1), 177-187, 2001.
[2]Làszló, P. K. and George, S. S. Mechanics of Composites Structures. *Cambrige University Press: New York.* 20-45, 2003.
 [3]Edelugo, S. O. The Timed Response of Different Types of GRP Laminates on Exposure to Various Strenght of Alkaline and Acidic Environments. *Journal of Advanced Material.* 41(2), 79–87, 2009.
[4]Dhakal, H. N., Zhang, Z. Y., Richardson, M. O. W. and Errajhi, O. A. Z. The Low Velocity Impact Response of Non-woven Hemp Fibre Reinforced Unsaturated Polyester Composites. Advanced Polymer and Composites

(APC) Research Group, Department of Mechanical and Design Engineering, University of Portsmouth. Retrieved from www.elsevier.com, 2006.

[5[Szekrényes, A. Overview on the Experimental Investigation of the Fracture Toughness in Composite Materials. *Hungarian Electronic Journal of Sciences*. 12, 30-38, 2007.

[6]Williams, J. G. Linear Fracture Mechanics. *Advances in Polymer Science, Springer Varlag, Berlin, Heidelberg, New York*. 27, 69 – 82, 1978.

[7]Mandel, J. A., Pack, S. C. and Tarazi, S. Micromechanical Studies of Crack Growth in Fibre Reinforced Materials. *Engineering Fracture Mechanics*. 16, 741-754, 1982.

[8]Okorie, B. A. Lecture Notes on Fracture and Fracture Mechanics. Mechanical Engineering Department, University of Nigeria, Nsukka, 2010.

[9]Parhizgar, S., Zachary, L. W. and Sun, C. T. (1982). Application of the Principle of Linear Fracture Mechanics to the Composite Materials. *International Journal of Fracture Mechanics*. 20, 3-15, 1982.

[10]Janssen, M., Zuidema, J. and Wanhill, R. J. H. Fracture Mechanics. (2nd Edition). New York: Spon Press. 2004.

[11]Garo, A. C. and Trotman C. K. Effect of Water on Fracture Toughness of Reinforced Composites. *Engineering Fracture Mechanics Journal,* 24, 34-42, 1980.

International Journal of Engineering and Innovative Research

http://dergipark.gov.tr/ijeir

COMPARATIVE ANALYSIS OF MALE AND FEMALE ADULT FOOT DEMOGRAPHIC DATA IN NIGERIA

Stella Isioma Monye[1] , Samuel Ayodeji Omotehinse[1*] , Godwin Ovuworie[1]

[1]University of Benin, Faculty of Engineering, Department of Production Engineering, Benin City, Nigeria.

*Sorumlu Yazar: drsamayodeji@gmail.com

ABSTRACT: Anthropometric measurements form the bedrock for the design of products for consumers' use, therefore, accurate knowledge of the different dimensions and the methods of measurements are key to obtaining veritable data. The evolving nature of the population has made it imperative for a regular up - to - date foot demographic data to be developed and established. As there is paucity of such data, this study seeks to cover this gaping hole. This study adopted the traditional measurement method which entailed the use of anthropometric instruments by five (5) researchers to manually take body measurements of four hundred (400) adult subjects comprising 200 male and 200 female. The participants were within the age bracket of 18-55 years from University of Benin, Benin-City excluding the foreigners, pregnant women, children and individuals with musculoskeletal disorders (MSDS). Stratified random sampling technique was employed in selecting the subjects to be measured. Twenty-seven foot anthropometric data were taken excluding age and weight. The resulting data were descriptively analyzed using SPSS version 16 and paired sample t-test. Result of the descriptive statistics gave the mean age, weight and height of the pooled sample of the population as; 26.47 ± 7.65 years, 63.40 ± 14.07kg and 170.52 ± 8.82cm respectively. The result also revealed that stature is significantly higher in males than in females. The results of the t-test showed that foot length and foot breadth of males differ significantly from those of the females (16.785 and P<0.001), (20.468 and P<0.001). The implication of this is that the foot demographic data established would aid the design of prosthesis and footwear for better functionality.

Keywords: Demographic data, Foot Anthropometry, Prosthesis, Footwear, Descriptive statistics

1. INTRODUCTION

Data on modelling foot anthropometric dimensions for the design of prosthesis and footwear in Nigeria are rare. This situation has therefore established a yawning crevasse for the development of foot anthropometry that can serve as baseline for the design of prosthesis and footwear. Foot anthropometry has shown that foot dimensions vary widely with individuals and the import is that the design of foot wears including prosthesis must consider those variations in order to achieve the desired fitness. The need to also understand the biomechanics associated with the normal foot before any foot orthosis or surgical intervention can be applied is considered necessary. It is instructive to note that prosthesis in this context is referred to as an artificially made limb or part of the body that is used to replace a part of the body that is missing either due to amputation or lack of development while an orthosis is a device used to correct, accommodate, or enhance the use of a body part. However, this study is only concerned with prosthesis. Research interest in Foot anthropometry dates back to the 20th century. Seminal works on foot anthropometry include those by: [1] who examined the postural mechanism of

the human foot. Kondo [2] measured the foot of the students (5-18 years old) in Tokyo using stratified three-stage sampling and found out that foot growth ends in the order of height, breadth and length, that growth of foot stops sooner than stature. Foot measurement for shoe construction with reference to the relationship between foot length, foot breadth and ball girth was carried out by [3]. His study compared the ratios of ball girth/foot length and foot breadth/foot length between the Japanese male subjects and the French male. Wunderlich and Cavanagh [4] analyzed gender differences in foot shape in a large sample of young individuals. Univariate t-tests and multivariate discriminant analyses were employed in assessing the reliability of classification into gender classes, the significant difference between men and women for each foot and leg dimension. Their results showed that for a given stature, men have longer and broader feet than women. They differ at the first toe, lateral side of the foot, the arch and the ball of the foot. They also opined that during the manufacture of women's sport shoes, these differences should be taken into consideration. Also, [5] quantified the change in three dimensional foot shape under different weight- bearing conditions. An optical digitizing system was used to capture the 3-D plantar surface shape of the foot cast, measurements and comparisons were made. The result indicated that the contact area of the foot increased as the weight bearing increased. Likewise, rear foot width, foot length, foot breadth (width) increased while the arch angle, arch height and average height decreased. Ozden et al. [6] conducted a study on stature and sex estimate using foot and shoe dimensions. Xiong et al. [7] modeled foot dimensions so that the characteristic shape of feet, essentially the region of the mid foot can be understood. They noted that the lack of generalized models has been the cause of the difficulty in the application of foot anthropometry to design good fitting footwear. Fifty (50) Hong Kong Chinese adults comprising 24 females and 26 males took part in the study. The results from the application of mathematical models on the various measurements made, showed that foot height showed no direct relationship with foot length. This result is helpful in designing footwear that has an enhanced fit in the height dimension. Kanaani et al. [8] obtained 8 important foot dimensions and established that there is significant correlation between 85% of foot dimensions. The foot images were taken by a digital camera. A fit size to shoe design was developed by [9]. They selected 303 subjects randomly, in Malaysia for the research and it was revealed that there was a significant difference between the length of the right and left foot. Also, the width of the right and left foot also showed significant difference. Salles and Gye [10] also conducted a study on personalized footwear which can be advantageous for population growth including older individuals, people with arthritis or diabetic foot problems. Personalized footwear can potentially provide a perfect fit for the wearer. Previous studies that also focused on foot measurements include [11-12]. On the area of gender differences, Hong et al. [13] concluded that women showed significantly smaller values of foot dimensions in girth, width and height than men. A total of nineteen foot variables were obtained through video filming, including, width, girth, height, length and angle variables. Also, de Castro et al. [14] identified differences between the anthropometric foot variables of older men and women. They concluded that there were differences between some of the anthropometric foot variables of older women and men that must be considered during their footwear design/manufacture. Samaila et al. [15] measured the anthropometric parameters of foot of adult males and females Ga'anda people, in order to find out racial characteristics of their own, determine their difference and to classify their foot shapes. Abdurrahman et al. [16] described foot anthropometric data of high school students in Bandung for the purpose of manufacturing good fitting shoes. Other studies namely, [17-19] focused on: Foot dimensions of a young adult Nigerian, Enugu Campus within the age bracket of 20-28 years; Sexual dimorphism in foot dimensions among adult Nigerians their age ranged between 18 years and above, resident in Port Harcourt; foot anthropometry of the Igbos in Nigeria aged 16-45 years respectively. It is evident from the foregoing that there is a balance of literature especially in the area of

assessment of baseline foot demographic data for Nigerian adult Population. Previous studies focused attention more on the estimation of stature (height), prediction of footwear fit, as well as gender (sex), from foot dimensions/measurements. The aim of this research therefore is to develop a robust, up to date male and female demographic data in Nigeria that can help bridge the gap caused by demographic differences and serve as baseline for the design of prosthesis and footwear.

2. MATERIALS AND METHODS

2.1. Materials

The different anthropometric dimensions were obtained with the following anthropometric tools; A-226 standiometer, small height rod, adjustable rule, sliding caliper, soft metric tape. The weight was in kilogram (kg) while the length, breadth and height dimensions were in centimeters (cm). The data for the study were sourced from University of Benin, Benin-City, Edo State. The University of Benin is well situated and has a good quota sample of the parent population. Twenty – seven (27) foot anthropometric dimensions were obtained excluding age and weight. These measurements were from a total of 400 male and female subjects. Below is the list of the dimensions: Age, Weight, Stature (height), Waist height, Waist thigh length, Thigh girth, Crotch height, Knee height, Knee girth, Calf height, Calf girth, lateral malleolus, medial malleolus, Ankle girth, Foot length, Foot breadth, Heel height, Heel girth, Bimalleolar breadth (BMB), Heel breadth, Joint/ball girth, Foot waist girth, Instep girth, Instep height, Instep length, Ball height, Toe length, Toe height, Toe girth.

2.2. Methods

A total of four hundred (400) adult subjects were measured which included 200 male and 200 female by five (5) notable researchers who are well trained in the field of anthropometry. A pilot study was first conducted where each body dimensions was measured 3 times and the average taken before the final measurement of the region was made. The participants were within the age bracket of 18-55 years and from the University of Benin, Benin-City, Nigeria. Stratified random sampling technique was employed in selecting the subjects to be measured. The following groups of people were excluded from the study: Foreigners, Pregnant Women, Children, Individuals with musculoskeletal disorders (MSDS) and Subjects below 18 and above 55 years. The measurements were done by using standard anthropometric instruments and techniques. The descriptive statistics of the resulting data were analyzed using SPSS version 16. The subjects were required to take off their shoes and stockings. They also showed willingness to partake in the study by consenting to be measured in order to obtain the desired data. The measurements were taken at specific period of the day from 9:00am to 3:00pm to avoid diurnal error. Some of the individual foot diagrams are depicted in Figure 1.
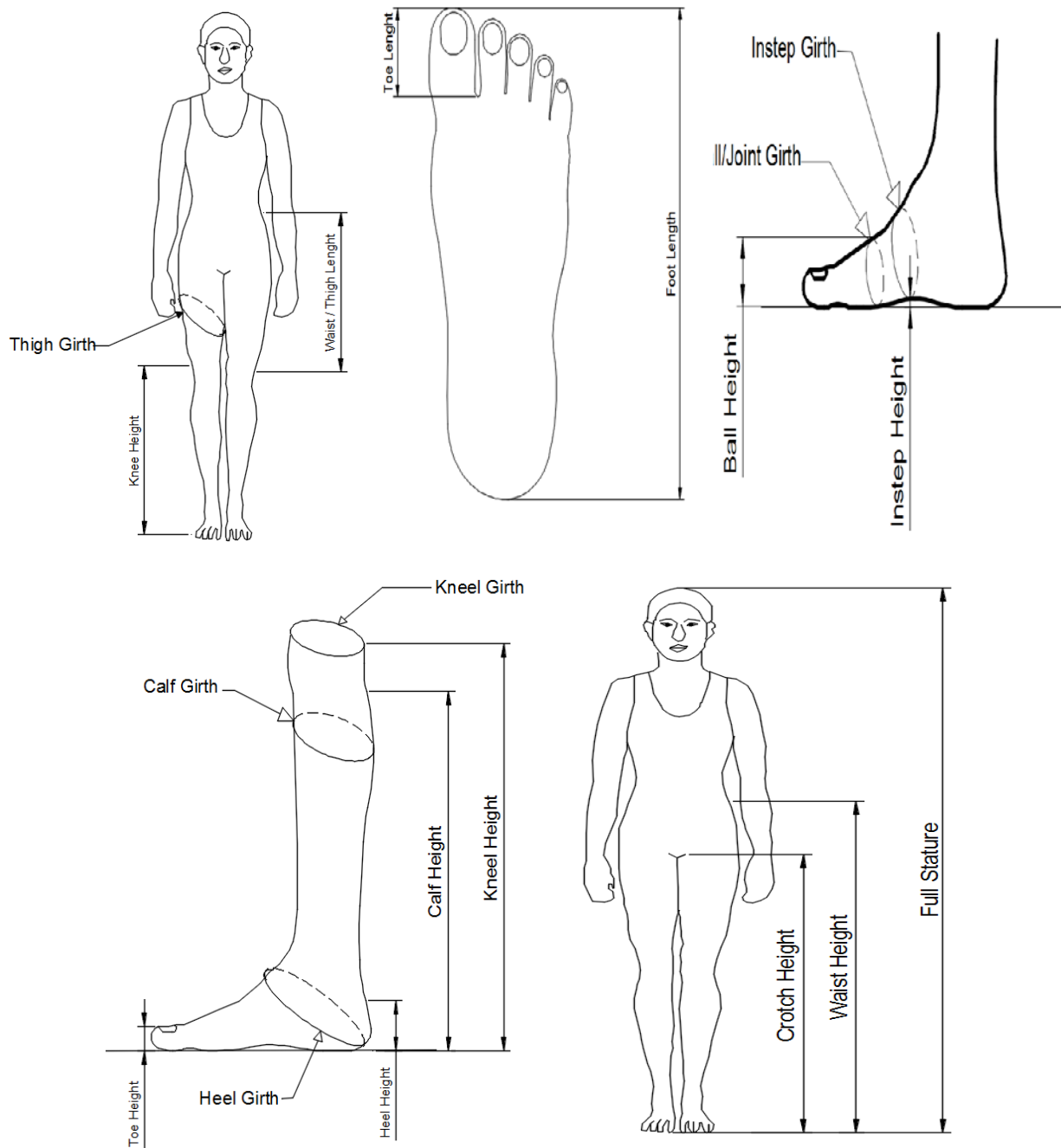
Figure 1. Diagrams showing some of the anthropometric dimensions.

3.   RESULTS AND DISCUSSION

The characteristics of the subjects concerning demographic data are presented in Tables 1, 2 and 3. In addition paired sample t- test was employed to compare the variables between male and female variables as shown in Table 4.

Table 1. Descriptive statistics of females Adult Population.

MEASUREMENTS (Female)	MEAN	SD	MIN	MAX	Percentiles				
					5th	25th	50th	75th	95th
Age	24.74	7.43	18	55	18	20	23	27	44.9
Weight	58.15	13.29	27	120	42.05	49	56	64	79.95
Stature	164.59	6.34	150	182	154.5	160	164	168.2	176.74
Waist Height	103.89	5.1	94.2	119	97	100	104	107.22	112.4
Waist Thigh Length	25.35	3.79	17	38	20	22	25	28	32
Thigh Girth	56.66	7.8	42.5	92	46.05	51.5	55	61	71
Crotch Height	77.09	4.66	65.5	88.5	70.5	73.25	77	79.5	85.5
Knee Height	48.44	3.2	35.5	59.9	44.5	46.6	48.5	50	52.5
Knee Circumference	38.06	4.11	24.5	55	32.52	35.12	38	40.5	45.47
Calf Height	34.85	2.89	29	43	30.02	33	34.55	36.47	40.5
Calf Circumference	35.13	3.54	26	48.5	30	32.5	35	37.5	40.95
lateral malleolus	6.78	0.66	5.5	8	5.8	6.22	6.9	7.3	8
medial malleolus	7.78	0.72	6.4	9.4	6.5	7.2	7.8	8.2	9
Ankle Circumference	26.42	2.31	21.5	36.5	23.5	25	26	27.5	29.97
Foot Length	24.71	1.24	21.54	28.39	22.7	23.09	24.88	25.5	27.24
Foot Breadth	9.29	0.6	7.76	10.86	8.17	8.99	9.26	9.72	10.26
Heel Height	5.23	0.74	3.5	7.4	4	4.8	5.25	5.7	6.4
Heel Circumference	33.19	1.84	28	38	30	32.5	33	34.5	36.19
Bimolleolar Breadth (BMB)	6.48	0.42	5.36	7.67	5.73	6.2	6.49	6.76	7.24
Heel Breadth	5.57	0.53	4.15	6.91	4.61	5.24	5.61	5.86	6.5
Joint/Ball Girth	23.07	1.36	19.7	27	20.8	22.22	23	23.7	25.49
Foot Waist Girth	22.77	1.43	19.3	27	20.5	21.85	22.85	23.5	25.8
Instep Girth	24.01	1.55	19.5	28.5	21.5	23	24	25	26.5
Instep Height	4.17	0.55	2.5	5.8	3.3	3.8	4.2	4.5	5
Instep Length	18.67	1.1	16.5	22	17	18	18.5	19.3	20.5
Ball Height	3.11	0.37	2.2	4.2	2.6	2.9	3	3.4	3.89
Toe Length	7.01	0.56	6	9	6.2	6.5	7	7.3	8
Toe Height	1.92	0.22	1.5	3	1.6	1.8	2	2	2.3
Toe Girth	8.51	0.61	7	10.5	7.5	8	8.5	9	9.4

Table 2. Descriptive statistics of pooled sample (both gender together).

MEASUREMENTS	N	MEAN	SD	MIN	MAX	Percentiles				
						5th	25th	50th	75th	95th
Age	400	26.47	7.64921	18	55	18.0	21.0	25.0	29.0	43.0
Weight	400	63.4025	14.0704	27	138	45.0	54.25	62.0	71.0	89.0
Stature	400	170.518	8.8246	150	193	157.0	163.85	169.5	177.0	185.0
Waist Height	400	106.560	5.82363	94.2	122.5	97.5	102.325	106.0	110.0	117.975
Waist Thigh Length	400	28.4987	4.74322	17	40	21.0	25.0	28.5	32.0	36.0
Thigh Girth	400	55.8212	6.76822	42.5	92	46.5	51.5	55.0	60.0	69.0
Crotch Height	400	76.48	4.80879	65.5	89.5	69.025	72.92	76.35	79.475	85.475
Knee Height	400	49.85	3.42422	35.5	60	44.52	47.5	50.0	52.0	55.5
Knee Circumference	400	37.7635	3.53029	24.5	55	33.0	35.0	37.0	40.0	44.0
Calf Height	400	35.3637	3.02851	29	44.5	30.51	33.5	35.0	37.0	41.38
Calf Circumference	400	35.47	3.37956	23.9	48.5	30.515	33.0	35.5	37.5	40.5
lateral malleolus	400	7.052	0.8375	5.5	10.5	5.905	6.5	7.0	7.5	8.5
medial malleolus	400	8.129	0.85525	6.18	11	7.0	7.5	8.0	8.675	9.5
Ankle Circumference	400	27.29	2.5052	21.5	39	24.0	26.0	27.0	28.2	31.975
Foot Length	400	25.8	1.7018	21.54	30.25	22.99	24.762	25.72	27.035	28.61
Foot Breadth	400	9.8728	0.823	7.76	11.8	8.5	9.24	9.86	10.4375	11.23
Heel Height	400	5.515	0.76611	3.5	7.5	4.0	5.0	5.5	6.0	6.8
Heel Circumference	400	34.769	2.51454	28	44	30.5	33.0	34.5	36.5	39.0
Bimolleolar Breadth (BMB)	400	6.816	0.58007	5.36	8.1	5.96	6.4125	6.77	7.2575	7.74
Heel Breadth	400	5.74	0.57615	4.15	7.36	4.85	5.38	5.72	6.0875	6.77
Joint/Ball Girth	400	24.28	1.80841	19.7	28.2	21.2	23.0	24.2	25.5	27.2
Foot Waist Girth	400	23.97	1.84296	19.3	28	21.0	22.8	24.0	25.5	27.0
Instep Girth	400	25.2625	2.021	19.5	30	22.0	24.0	25.0	26.5	29.0
Instep Height	400	4.239	0.59267	2.5	6	3.3	3.9	4.2	4.6	5.2
Instep Length	400	19.61	1.53411	16.5	25	17.3	18.5	19.5	20.7	22.0
Ball Height	400	3.20925	0.42848	2.2	4.8	2.6	3.0	3.1	3.5	4.0
Toe Length	400	7.32125	0.71186	4.6	9.5	6.2	7.0	7.2	7.8	8.5
Toe Height	400	1.99	0.24949	1.5	3.3	1.7	1.8	2.0	2.0	2.5
Toe Girth	400	9.01175	0.781	7	11.2	8.0	8.5	9.0	9.5	10.295

Table 3. Descriptive statistics of males Adult Population.

MEASUREMENTS (male)	MEAN	SD	MIN	MAX	5th	25th	50th	75th	95th
					Percentiles				
Age	28.19	7.49	18	55	19	23	26.5	30	42.95
Weight	68.65	12.84	46	138	54	60	65	74.75	90
Stature	176.45	6.72	159.5	193	166.2	171.17	176.2	180.87	187.97
Waist Height	109.22	5.27	98	122.5	101	105	109	112.57	118.6
Waist Thigh Length	31.64	3.29	24	40	26	29.25	31.25	34	37
Thigh Girth	54.98	5.43	43	70.5	46.5	51.5	54.5	58.5	64
Crotch Height	75.88	4.89	67	89.5	68	72.27	75.5	79.27	85
Knee Height	51.26	3.05	44.3	60	46.71	48.62	51.4	53.4	56
Knee Circumference	37.47	2.82	32	44.5	33.5	35	37	39	43
Calf Height	35.88	3.08	29	44.5	31	33.5	35.5	38.15	41.4
Calf Circumference	35.82	3.18	23.9	47.5	31.5	33.77	35.5	38	40.5
lateral malleolus	7.32	0.91	5.6	10.5	6	6.7	7	8	8.99
medial malleolus	8.48	0.83	6.18	11	7.1	8	8.5	9	10
Ankle Circumference	28.15	2.4	23.4	39	25	26.5	28	29	32
Foot Length	26.89	1.37	22.99	30.25	24.37	26.1	26.89	27.7	29.49
Foot Breadth	10.45	0.57	8.34	11.8	9.56	10.09	10.41	10.86	11.42
Heel Height	5.8	0.68	4	7.5	4.5	5.4	5.9	6.27	7
Heel Circumference	36.34	2.07	31.5	44	32.71	35	36.2	37.6	39.98
Bimolleolar Breadth (BMB)	7.15	0.52	5.5	8.1	6.3	6.79	7.21	7.57	7.87
Heel Breadth	5.91	0.57	4.26	7.36	5.11	5.47	5.87	6.33	6.89
Joint/Ball Girth	25.49	1.33	22.3	28.2	23.4	24.5	25.4	26.5	28
Foot Waist Girth	25.18	1.36	21.8	28	23	24.1	25.1	26	27.5
Instep Girth	26.52	1.62	23.1	30	24	25.2	26.5	28	29
Instep Height	4.31	0.62	2.6	6	3.4	3.9	4.3	4.77	5.4
Instep Length	20.56	1.3	17.8	25	18.5	19.5	20.5	21.3	23
Ball Height	3.31	0.46	2.2	4.8	2.7	3	3.25	3.5	4
Toe Length	7.63	0.71	4.6	9.5	6.7	7.2	7.7	8	8.89
Toe Height	2.07	0.26	1.7	3.3	1.7	1.9	2	2.2	2.5
Toe Girth	9.51	0.59	8	11.2	8.5	9	9.5	10	10.5

Tables 1, 2 and 3 depict the descriptive statistics of foot measurements of the female, pooled and male sample of the population. The mean age was 24.74 ± 7.43 in females, 28.19 ± 7.49 in males and 26.47 ± 7.65 for the pooled sample. The tables also showed the mean weight to be 58.15 ± 13.29, 68.65 ± 12.84 and 63.40 ± 14.07 for the female, male and both genders together respectively. Similarly, the mean stature in female group was 164.59 ± 6.34 while in male group was 176.45 ± 6.72 and for the pooled sample, 170.52 ± 8.82. The results showed that stature is significantly higher in males than in females which coincide with the result obtained by [11]. For the foot dimensions, the mean foot length for the female was 24.71 ± 1.24 while for male was 26.89 ± 1.37, with the foot length larger in males than in females as compared to that

obtained by [8, 15]. In Table 1, the 50th percentile female was 164cm tall and the stature span was 32cm, from the range of 150cm to 182cm. The 50th percentile male was 176.2cm tall. The tallest male was 193cm, while the shortest was 159.5cm, giving a stature difference of 33.5cm. Also, the 50th percentile for both gender, gave 169.5cm, from 150cm to 193cm with a range of 43cm. The weight was 62kg, with a span of 111kg ranging from 27kg to 138kg. Similarly, the age for the 50th percentile was 25years with a span of 37years from 18years to 55years. The 50th percentile female had a body weight of 56kg from 27kg to 120kg and a span of 93kg. Also the male had a weight of 65kg, the distribution of body weight ranged from 46kg to 138kg and a span of 92kg. For the foot measurements, the 50th percentile female had a foot length of 24.88cm, which ranged from 21.54cm to 28.39cm having a span of 6.77cm. Also, a foot length of 26.89cm was recorded for the 50th percentile male with a span of 7.26cm which ranged from 22.99 cm to 30.25cm compared to 26.92 ± 0.13 and 24.75 ± 0.17 obtained by [18] as well as 27.1 ± 1.3 cm and 25.1 ± 1.1 cm gotten by [17]. For the pooled sample, the foot length had a value of 25.72cm, having a span of 8.71cm ranging from 21.54cm to 30.25cm. The Mean±SD for bimolleolar breadth of the foot 74.47±4.11 obtained by [8] in Iranian men with ages ranging from 18 to 25 differs significantly from 7.15±0.52 obtained in this study in Nigerian Men with ages 18 to 55 years.

Table 4. Comparison of variables between males and females in foot anthropometry

Paired Samples Test									
		Paired Differences							
					95% Confidence Interval of the Difference				
		Mean	Std. Deviation	Std. Error Mean	Lower	Upper	t	df	Sig. (2-tailed)
Pair 1	Age Male - Age Female	3.45000	10.91942	.77212	1.92741	4.97259	4.468	199	.000
Pair 2	Weight Male - Weight Female	1.05050E1	19.01652	1.34467	7.85337	13.15663	7.812	199	.000
Pair 3	Stature Male - Stature Female	1.18620E1	9.65483	.68270	10.51575	13.20825	17.375	199	.000
Pair 4	Waist Height Male - Waist Height Female	5.32850	7.50504	.53069	4.28201	6.37499	10.041	199	.000
Pair 5	Waist Thigh Lenght Male - Waist Thigh Length Female	6.28750	4.63774	.32794	5.64082	6.93418	19.173	199	.000
Pair 6	Thigh Girth Male - Thigh Girth Female	-1.68250	9.96764	.70482	-3.07237	-.29263	-2.387	199	.018
Pair 7	Crotch Height Male - Crotch Height Female	-1.20600	6.68676	.47283	-2.13839	-.27361	-2.551	199	.012
Pair 8	Knee Height Male - Knee Height Female	2.82050	4.53277	.32051	2.18846	3.45254	8.800	199	.000
Pair 9	Knee Circumference Male - Knee Circumference Female	-.58800	5.16046	.36490	-1.30757	.13157	-1.611	199	.109
Pair 10	Calf Height Male - Calf Height Female	1.02950	4.09812	.28978	.45807	1.60093	3.553	199	.000

		Paired Differences							
					95% Confidence Interval of the Difference				
		Mean	Std. Deviation	Std. Error Mean	Lower	Upper	T	df	Sig. (2-tailed)
Pair 1	Calf Circumference Male - Calf Circumference Female	.68450	4.87585	.34477	.00462	1.36438	1.985	199	.048
Pair 2	lateral malleolus Male - lateral malleolus Female	.53350	1.10118	.07786	.37995	.68705	6.852	199	.000
Pair 3	Medial malleolus Male – Medial Malleolus Female	.70590	1.06472	.07529	.55744	.85436	9.376	199	.000
Pair 4	Ankle Circumference Male – Ankle Circumference Female	1.72350	3.44357	.24350	1.24333	2.20367	7.078	199	.000
Pair 5	Foot Length Male - Foot Length Female	2.18365	1.83981	.13009	1.92711	2.44019	16.785	199	.000
Pair 6	Foot Breadth Male - Foot Breadth Female	1.15830	.80030	.05659	1.04671	1.26989	20.468	199	.000
Pair 7	Heel Height Male - Heel Height Female	.57300	.97185	.06872	.43749	.70851	8.338	199	.000
Pair 8	Heel Circumference Male - Heel Circumference Female	3.15200	2.88825	.20423	2.74927	3.55473	15.434	199	.000
Pair 9	Bimolleolar Breadth Male - Bimolleolar Breadth Female	.67410	.66053	.04671	.58200	.76620	14.433	199	.000
Pair 10	Heel Breadth Male - Heel Breadth Female	.33520	.78254	.05533	.22608	.44432	6.058	199	.000

		Paired Differences							
					95% Confidence Interval of the Difference				Sig. (2-tailed)
		Mean	Std. Deviation	Std. Error Mean	Lower	Upper	t	Df	
Pair 1	Joint Ball Girth Male - Joint Ball GirthFemale	2.41300	1.87832	.13282	2.15109	2.67491	18.168	199	.000
Pair 2	Foot Waist Girth Male - Foot Waist Girth Female	2.40700	1.91643	.13551	2.13978	2.67422	17.762	199	.000
Pair 3	Instep Girth Male - Instep Girth Female	2.50800	2.13095	.15068	2.21086	2.80514	16.644	199	.000
Pair 4	Instep Height Male - Instep Height Female	.14000	.85906	.06074	.02021	.25979	2.305	199	.022
Pair 5	Instep Length Male - Instep Length Female	1.89550	1.67627	.11853	1.66176	2.12924	15.992	199	.000
Pair 6	Ball Height Male - Ball Height Female	.19550	.57627	.04075	.11515	.27585	4.798	199	.000
Pair 7	Toe Length Male - Toe Length Female	.62550	.83009	.05870	.50975	.74125	10.657	199	.000
Pair 8	Toe Height Male - Toe Height Female	.14200	.33240	.02350	.09565	.18835	6.042	199	.000
Pair 9	Toe Girth Male - Toe Girth Female	.99850	.87152	.06163	.87698	1.12002	16.203	199	.000

3.1. Statement of Hypothesis

H_0: There are no significant differences between the male and female foot anthropometric dimension.

H_1: There are significant differences between the male and female foot anthropometric dimensions.

3.2. Interpretation of Selected Results

3.2.1. Ankle circumference

Since t-value obtained is 7.078 and falls outside the lower critical value of 1.243 and upper critical value of 2.204, we therefore reject the null hypothesis and infer that there are significant differences between the male and female ankle Circumference.

3.2.2. Heel circumference

Since t-value obtained is 15.434 and is above the lower critical value of 2.749 and higher critical value of 3.555, we therefore reject the null hypothesis and accept the alternate hypothesis that there are significant differences between the male and female heel Circumference.

3.2.3. Foot length

Since t-value obtained is 16.785 which fall outside the lower critical value of 1.927 and the upper critical value of 2.440, we therefore reject the null hypothesis and accept the alternate hypothesis that there are significant differences between the male and female foot length. Our result showed that foot length in males are significantly higher than that of females, same with the result gotten by [15].

3.2.4. Foot breadth

Since the t-value obtained for the foot breadth is 20.468 and this falls outside the two critical values of 1.047 and 1.270, we therefore reject the null hypothesis and conclude that there are significant differences between the male and female foot breadth which also falls within the result obtained by [15, 18].

3.2.5. Calf height and calf circumference

Since the t-value obtained for calf height (1.985) and calf circumference (3.553) falls outside the lower critical value of 0.005 and upper critical value of 1.364 for calf height and a lower critical value of 0.458 and upper critical value of 1.601 for calf circumference, we reject the null hypothesis and accept the alternate hypothesis and conclude that there are significant differences between the male and female calf height and calf circumference. This result can be compare to the one obtained by [4] who stated that after normalization of the measurements by foot length, men and women were found to differ significantly in two calf, five ankle, and four foot shape variables.

Arising from the foregoing, results of the t-test showed that there are significant differences between male and female foot anthropometric dimensions, therefore designs of foot wears and prosthesis should be made differently.

Table 5 and 6 shows the abridged body and foot anthropometric dimensions for Male and Female adults in Nigeria from 18 to 55 years.

Table 5. Abridged Body and Foot Anthropometric Dimensions for male

S/N	SEX	AGE	WEIGHT	STATE OF ORIGIN	STATURE	WAIST HEIGHT	WAIST THIGH LENGTH	THIGH GIRTH	-	-	-	TOE HEIGHT	TOE GIRTH
1	M	36	83	ANAMBRA	179.6	111.8	35	48	-	-	-	2	9
2	M	19	69	DELTA	177.6	114	36.5	54	-	-	-	2.2	10
3	M	30	77	OYO	175	107	32	60	-	-	-	2.3	10
4	M	29	71	ENUGU	170	107.5	34.5	55	-	-	-	2.3	9
5	M	30	92	DELTA	193	122.5	40	60	-	-	-	2	10
6	M	30	74	ANAMBRA	171	108	35	58	-	-	-	1.8	8.5
7	M	42	83	EDO	173	108	37	63	-	-	-	3.3	10
8	M	39	65	EDO	168	104	36	61	-	-	-	1.7	9
-	-	-	-	-	-	-	-	-	-	-	-	-	-
-	-	-	-	-	-	-	-	-	-	-	-	-	-
-	-	-	-	-	-	-	-	-	-	-	-	-	-
198	M	26	55	OYO	165	103.5	28	47	-	-	-	2	8.8
199	M	29	62	EKITI	167	106	28	56	-	-	-	2.4	9.9
200	M	24	66	LAGOS	162	102	30	60.5	-	-	-	2.1	9

Table 6. Abridged Body and Foot Anthropometric Dimensions for Female

S/N	SEX	AGE	WEIGHT	STATE OF ORIGIN	STATURE	WAIST HEIGHT	WAIST THIGH LENGTH	THIGH GIRTH	-	-	-	TOE HEIGHT	TOE GIRTH
1	F	25	57	ANAMBRA	159.5	97.5	30.5	55	-	-	-	2	8
2	F	25	55	IMO	169.5	109.5	28	53	-	-	-	2	8
3	F	20	40	DELTA	157	97	22.5	47	-	-	-	1.8	8.5
4	F	19	62	DELTA	166	108.6	28.5	63	-	-	-	2	9
5	F	28	49	SOKOTO	175	106.5	19	47.2	-	-	-	1.7	8.5
6	F	19	49	ONDO	168.2	107.3	22	47	-	-	-	1.9	7.6
7	F	27	55	DELTA	157.5	98	26	55	-	-	-	1.9	9.4
8	F	20	61	DELTA	164.2	109	32	52.5	-	-	-	2.1	10
-	-	-	-	-	-	-	-	-	-	-	-	-	-
-	-	-	-	-	-	-	-	-	-	-	-	-	-
-	-	-	-	-	-	-	-	-	-	-	-	-	-
198	F	25	75	EDO	181.5	112	22	62.5	-	-	-	3.2	8
199	F	22	60	CROSS RIVER	167	105	26	63.5	-	-	-	3.4	6.2
200	F	20	69	DELTA	171.5	108	25.5	62	-	-	-	3	6.7

4. CONCLUSION

This study has been able to identify the basic demographic differences between male and female adult population in Nigeria from the age bracket of 18-55 years. The pooled demographic changes between the male and female population were also analyzed. It is evident from this study that the anthropometric body dimensions for males and females differ significantly which could be attributed to so many factors such as ethnic and genetic compositions, nutrition, age among others. However, such factors should be critically taken into consideration while designing footwear and prosthesis.

REFERENCES

[1] MacConaill, M. A. (1944). The postural mechanism of the human foot. *Royal Irish Academy*, Vol. 50. pp. 265-278.

[2] Kondo, S. (1953). Growth of the foot of the school boys and girls in Tokyo. *J Anthropology Soc. Nippon*. 63: 22-32.

[3] Baba, K. (1974). Foot measurement for shoes construction with reference to the relationship between foot length, foot breadth, and ball girth. *Journal human ergol*. 3 (2): 149 – 156.

[4] Wunderlich, A.E and Cavenagh, P.R. (2001). Gender differences in adult foot shape implications for shoe design. *Medicine and Science in sports and Exercises*. 33(4): 605-611.

[5] Tsung, B.Y., Zhang, M., Fan, Y.B., Boone, D.A. (2003). Quantitative Comparison of plantar foot shapes under different weight-bearing conditions. *J Rehabil Res Dev*. Vol 40(6): 517-526.

[6] Ozden, H. (2005). stature and sex estimate using foot and shoe dimensions. *Forensic science International*. Vol. 147, issues 2-3: 181-184.

[7] Xiong, S., Goonetilleke, R.S., Witana, C.P, Lee A.E. (2008). Modelling Foot height and foot shape-related dimensions. *Ergonomics*. Volume 51(8): 1272-1289.

[8] Kanaani, J. M., Mortazavi, S. B., Khavanin, A., Mirzai, R., Rasulzadeh, Y., Mansurizadeh, M. (2010). Foot anthropometry of 18-25 years old Iranian male students. *Asian Journal of Scientific Research*: Volume 3(1): 62-69.

[9] Bari, S. B., Othman, M., Salleh, N.M. (2010). Foot anthropometry for shoe design among preschool Children in Malaysia. *Pertanika J. soc. Sci. and Hum*. 18(1): 69-79.

[10] Salles, A.S., and Gyi, D.E. (2010). The specification and evaluation of personalized footwear for additive manufacturing. 3rd Applied Human Factors and Ergonomics(AHFE) international conference. 355-383.

[11] Jitender, K.J (2010). Estimation of height from measurement of foot length in Haryana region. *Journal of Indian Academy of forensic Medicine*, 32 (3): 231 – 233.

[12] Krishnan, K., Sharma, A (2007). Estimation of stature from dimension of hands and feet in a North Indian population. *J. Forensic, Legal Med,* 14: 327 – 332.

[13] Hong, Y., Wang, L., Xu, D.Q., Li, J.X (2011). Gender differences in foot shape: a study of Chinese young adults. *Sports Biomech* 10(2): 85-97.

[14] De Castro, A.P., Rebelatto, J.R., Aurichio, T.R (2011). Effect of Gender on foot anthropometrics, in older people. *Journal of sport Rehabilitation*. 20: 277-286.

[15] Samaila, (2015). comparison of the foot height, length, breadth and foot types between males and females Ga'anda people, adamawa, Nigeria *IOSR Journal of dental and medical sciences* (IOSR-JDMS): Vol. 14, issue 8, version 1, 89-93.

[16] Abdurrahman, I.R., Tahid, A., Fathurachman. (2018). Foot anthropometric profile of High School students in Bandung. *Althea Medical Journal*, Volume 5(2): 93-97.

[17] Obikili, E.N and Didia, B. C (2006). Foot dimensions of a young adult Nigerian population. *Anatomical Society of Eastern Nigeria*, 1: 22-24.

[18] Bob-Manuel, I., Didia, B. (2008). Sexual dimorphism in foot Dimensions Among Adult Nigerians. *The internet Journal of Biological Anthropology*. Vol 3. Num 1: 1-6

[19] Ekezie, J (2013). Foot Anthropometry; A forensic and prosthetic application. *International journal of science and research* (IJSR), Vol. 4, issue 6, pp. 738 – 746.

Smart Home Automation System

Fouad Zaro [1]* , Ali Tamimi [1] , Anas Barakat [1]*

[1] Palestine Polytechnic University, Electrical Engineering Department, Hebron, Palestine.

*Sorumlu Yazar: fzaro@ppu.edu

ABSTRACT: This paper presents a low cost, flexible and scalable Smart Home Automation System based on Arduino Technology and Wi-Fi connection, in addition to apply specific techniques for reduction of power consumption and load management. The system will be accessible anywhere, anytime for controlling and monitoring. This study relies on Arduino Technology and Node-MCU boards, the electrical appliances are connected to a cloud database that communicates with the user by an android application connected to the internet. A prototype for a specific house has been built, the proposed system is able to control all home electrical units and appliances like: lighting, sockets, HVAC units, fire, gas and intruder siren systems, in addition to monitor the real time power consumption, the house PV system generation and the current room's temperature and humidity. Furthermore, the system is able to reduce power consumption using predefined algorithms.

Keywords: Smart Home, Arduino Mega 2560, wireless sensor network, Android, Node-MCU microcontroller, Home Automation.

1. INTRODUCTION

Smart home automation systems (SHAS) are new trend has been started beside all new technological innovation we have today, this trend started when smart appliances became more popular, nowadays we have smartphone, smart tablets, smart cars, smart washing machines and the list goes on. Most of smart appliances became "smart" when you connect them to the internet, to give access and control power over their settings and configurations and give more technical and useful information about the process they do, from this point of view Smart home automation became a thing.

Internet of things (IoT) can be simply described as providing internet connection to hardware devices, circuits or any form of electrical appliances in order to control them from remote devices such as smartphones, which indeed adds the ability to form unique communication and features between these appliances. [1]. Smart home automation system opens the door for safer life, increasing comfort and more control over house energy and consumption which all leads to energy saving and load control [2]. This study is an application of Smart home automation system (SHAS) concept in which we apply Arduino technology to give the control over the whole system, in order to obtain a law cost, flexible, scalable, user friendly and power economical system.

In [3] a full smart home system design presented, the main purpose of this design is to find a solid way to communicate three main elements in the proposed system:

- A website server (User interface to communicate with the system).
- A personal computer as a Server.
- Arduino hardware.

The methodology used in this system depends on a website user interface so the user could interact with the system by sending commands to the server (personal computer), then the server do the processing needed for that command and then send the actuator status to the Arduino hardware. On the other hand, Arduino hardware collects sensors data and sends it back to the server, then the server do the processing needed for these data and decide the best implementation of system's actuators, and send information about the process to the user by website page [4]. The main disadvantage of such system is the dependency on physical PC for the server which limits the flexibility of the system and increases the cost.

In [5], the author presented a concept design of Home Automation system based on internet website, the study aims to control electrical home units using a website accessible from anywhere worldwide, this website connected to a personal computer mounted in the house as a system server, this pc will be connected to a hardware controller from one side using USB or LAN connection, and from the other side the controller will be connected with all electrical equipment's and units, the author provided a full detailed control design and algorithms, but It lakes from any electrical designs like PCB (printed circuit board) or even simulation diagrams or schemes.

In [7],the authors proposed a security protection and monitoring home system using Arduino and NodeMCU boards, the main idea of this approach is to connect multiple PIR sensors, fire sensors, temp and humidity sensor and other switches and sensors to an Arduino board to process received sensors signals then send the processed data to nodeMCU board connected to blink server which is connected to mobile application, the user will be able to monitor several home parameters and control some lights and door look's solenoid, also the user would receive an email if any house intruder detected by the system.

In [8], a full working industrial smart warehouse system was proposed that relied on Arduino mega 2560 board for software processing, actuators control and sensors data acquiring and ESP8266 modules for Wi-Fi connection. The proposed system has two modes online and offline mode, if the system has an internet connection then it could be monitored and controlled from anywhere using a smartphone application, if not then a control panel inside the warehouse will do the job, the system able to monitor several environmental parameter and has movement detection system which automatically activate some electrical appliances like lights, fans and gates, also it has fire/smoke alarm system. The authors assured that the system was robust, reliable, easy to use and efficient using just an Arduino board.

In [9], the author built a simple yet effective system for a PLC controlled room plant using Arduino board, the main idea here is to extend the current system setup to a wireless approach in which the Arduino board collects the main room plant's parameters and send it wirelessly to an android device then store them in an SQL database, the results were very effective, reliable and most important with a very low additional cost, this study showed that a low-cost micro controller such as Arduino uno could replace high-end and high-cost PLC system with a very reasonable price.

In [10], a full Smart home electrical monitoring system proposed using Arduino boards, the system relied mainly on ZMPT101T voltage transformer and ACS716 current sensor, the

system achieved was 96.7% accurate in comparison with fluke digital multimeter, the most interesting result that the system is able to reduce the instantaneous house power (electrical consumption) by 10% during peak hours which highly satisfying using such low-cost system, worth to be mentioned that the system work with predefined algorithms that reads users activity and power consumption and manages all connected electrical load in a such manner that reduces the house consumption smartly and wisely without affecting the user activities.

The author of [13] introduced a smart home activity prediction system called Sequence Prediction via Enhanced Episode Discovery (SPEED), this prediction system guarantees a prediction accuracy of 88.3% which is very accurate compared to other prediction systems like LeZi, IPAM and others, the main idea of this algorithm that it depends on common home activities patterns and scenarios, the main advantage of applying such systems to smart home systems (SHS) is improving the SHS efficiency and usability.

In [15] the author used ZigBee wireless network for modeling and analysis for the smart home, where the process on his study is divided for three main types : coordinator, router and terminal node. The author used petri-nets and PIP-2 to the analysis of the system where he have studied the workflow system framework. The petri-nets aims to achieve high security and reliability system data transfer that simulate the resource flow situation in the smart home system, using resource place and transition sequence of Petri Net model to analyze the accessibility of model and verify the non-deadlock and security and other property of the smart home system.

In [16] the author used raspberry-pi micro-controller board for monitoring temperature and humanity using Bluetooth and GSM modules. The study contains many modules which are: Raspberry Pi, EnOcean control protocol transceiver module, Internet access module, data storage module. Each sensor is connected to the smart home controller which is connected to the Wi-Fi where the Wi-Fi sends the data to the server and the server sends the data to the PC. The author used java programming languages to program the user interface on the web The study main disadvantage of the system that it have one purpose only which is measuring the humidity and temperature. The study is not cast effective also where it need PC connected to it to monitor the data and save it.

In [18] the author designed low cast smart home system where it is controlled using web server. In this study Arduino nano is used as the main controller for the system. The user can control devices such as lights and Fans speed using relay module, where the status of the devices is monitored on LCD (2*8) screen and on the web server. The main disadvantage of this study that it cannot control many devices where the Arduino nano doesn't have too much input and output pins, the system also cannot be controlled outside the house where it's connected to the web server using ESP8266 Wi-Fi chip.

In [19] the author used Arduino as the main controller for the system and used the Node-MCU module to connect to the internet using HTTP requests from the android phone where the system can be controlled from anywhere in the world. The system communication is based on HTTP communication using API requests where it has four main commands (put, get, post, delete). The app was programed using java language. The problem with this study that it cannot be installed in the house easily where the author have tested the system on breadboard and the main disadvantage for the system that the user don't take any feedback from the system for the status of the devices.

In [20] the author used ESP8266 Wi-Fi module based smart home, where its used as the main controller for the system . The ESP8266 acts as web server with port address of 80 characters. In this study the author used a password and user name in the application to verify the appliances and secure their data where only the authorized person can enter and control the home from the smart phone app. The problem with the Node-MCU ESP8226 module that it doesn't have too much input and output ports which means that it cannot control many devices.

2. SYSTEM STRUCTURE AND DESIGN

Our smart home approach was designed to achieve 3 main objectives

- Low-cost system.
- Flexibility.
- Efficiency.

And to achieve these objectives the system was divided into three main circuits (Master, Indoor-slave and Outdoor-slave), each circuit has its own PCB design, electrical components and software and all work separately so the working of any doesn't affect others. Figure 1 illustrates the main system layout.
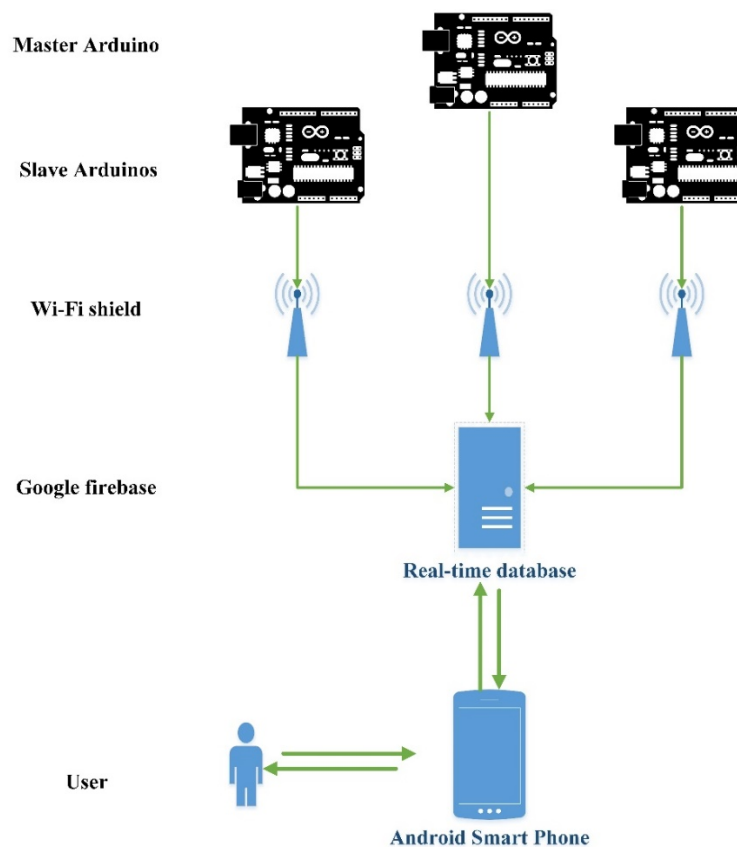
Figure 1. System layout.

2.1. Hardware design

As mentioned before the system contains 3 main circuits, each circuit has 2 Microcontrollers, actuators, sensors and electrical power elements.

- Microcontrollers: the circuit relies on 2 microcontrollers, Arduino mega 2560 microcontroller which process all user commands and activates the circuit's actuators as desired and process all received sensors signals and send it to the NodeMCU

microcontroller is responsible for sending and receiving data from/to a cloud database and Arduino microcontroller.

- Electrical components:
 A. Relay (10A/16A)
 B. DC power supply
 C. Buck converters (LM2596 DC-DC buck converter step-down).
 D. Multi buffer IC (ULN2004a).
 E. Gas/Fire sensor (MQ).
 F. PIR sensor.
 G. Humidity and temperature sensor (DH11).
 H. Light sensor (LDR).
 İ. Current sensor (ACS712).
 J. Voltage transformer (ZMPT101B).
 K. Real time clock (RTC).
 L. 4 channel logic level converters.

- PCB boards: Each circuit has two PCB boards, shield board which contains NodeMCU microcontroller and RTC (real time clock) ship, and logic level shifter, the main board contains the power supply, Arduino microcontroller, and all circuit actuators and sensors.

2.1.1. Master Circuit

Figure 4 illustrates master circuit layout.

Figure 2. Master circuit layout.

- Microcontrollers:
  - 1x Arduino Mega 2560.
  - 1X NodeMCU (ver.3).
- Electrical Components:
  - 1 x Alarm relay (10A).

72

- o 1 x Buck converter.
- o 1 x power supply.
- o 4 x ACS712 current sensor.
- o 2 x ZMP101b voltage transformer.
- o 1 x RTC.
- o 8 x LED and resistors.
- • PCB boards: Shield (figure 5 a-b) and main PCB boards (figure 6 a-b).

Figure 3. a-b front & back views of shield board.

Figure 4. a-b front & back views main master board.

2.1.2. Indoor-slave

Figure 7 illustrates master circuit layout.

Figure 5. Indoor-slave circuit layout.

- Microcontrollers:
  - o 1x Arduino Mega 2560.
  - o 1X NodeMCU (ver.3).
- Electrical Components:
  - o 6 x relay (10A).
  - o 14 x relay (16A).
  - o 3 x Buffer IC.
  - o 3 x Buck converter.
  - o 1 x power supply.
  - o 2 x ACS712 current sensor.
  - o 1 x ZMP101b voltage transformer.
  - o 1 x RTC
  - o 1 x LDR, 1x MQ2 & 1 x DH11.
  - o 55 x LED and resistors.
- PCB boards: Shield and main PCB boards (figure 8 a-b).

Figure 6. a-b front & back views Indoor-slave main board layout.

- Outdoor-slave

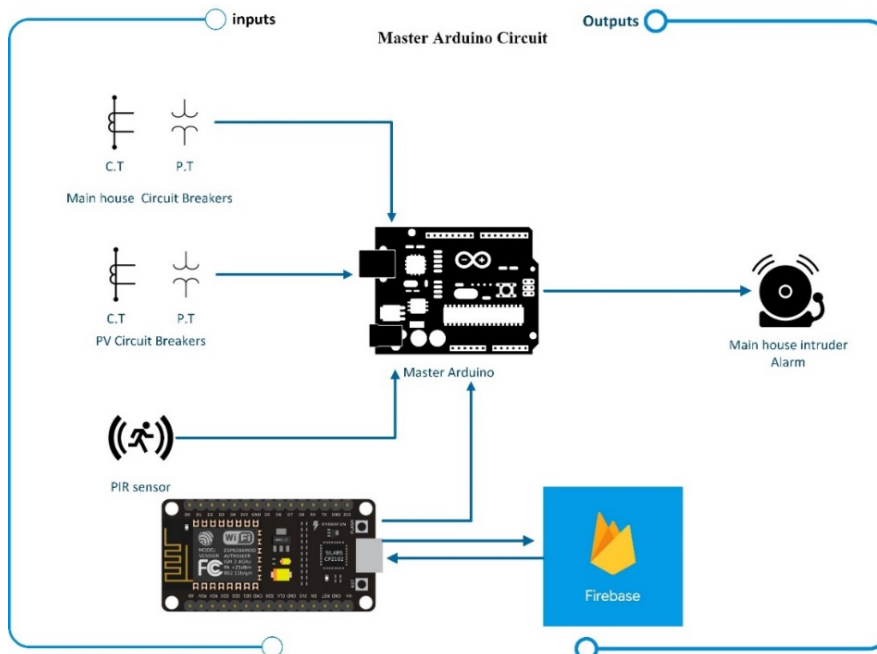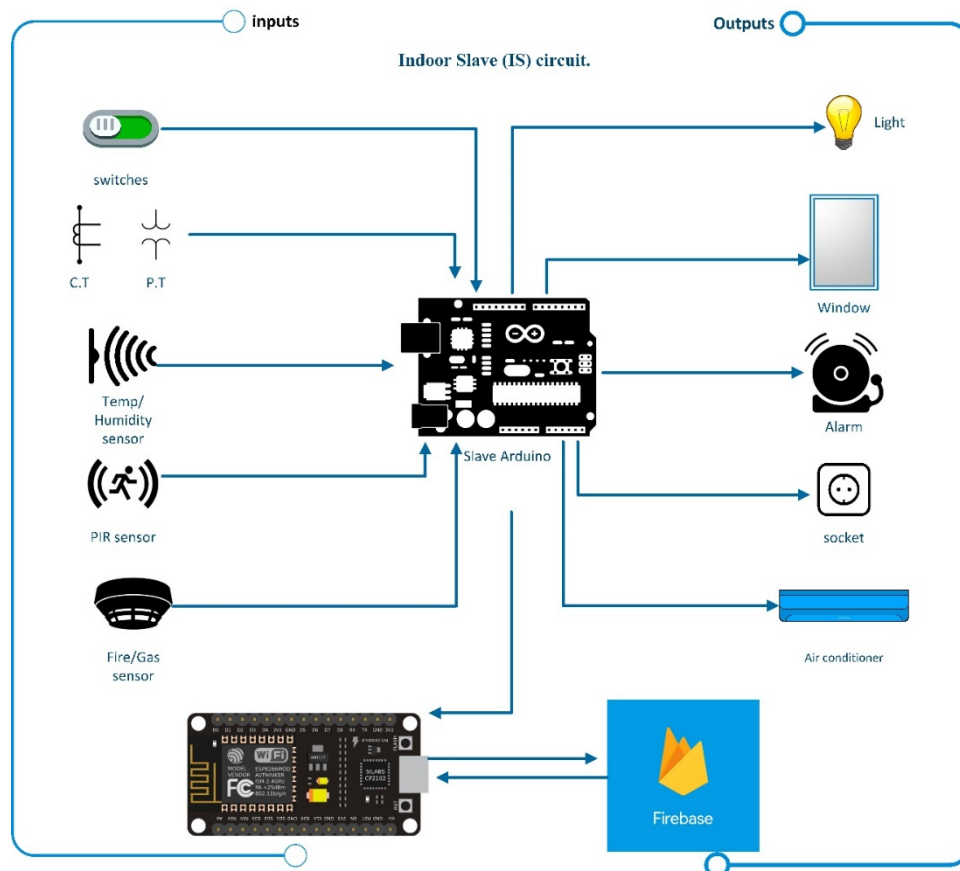Figure 9 illustrates master circuit layout.

Figure 7. Indoor-slave circuit layout.

- Microcontrollers:
  - o 1x Arduino Mega 2560.
  - o 1X NodeMCU (ver.3).
- Electrical Components:
  - o 11 x relay (10A).
  - o 10 x relay (16A).
  - o 3 x Buffer IC.
  - o 3 x Buck converter.
  - o 1 x power supply.
  - o 2 x ACS712 current sensor.

- o 1 x ZMP101b voltage transformer.
- o 1 x RTC.
- o 1 x LDR, 1x MQ2 & 1 x DH11.
- o 55 x LED and resistors.

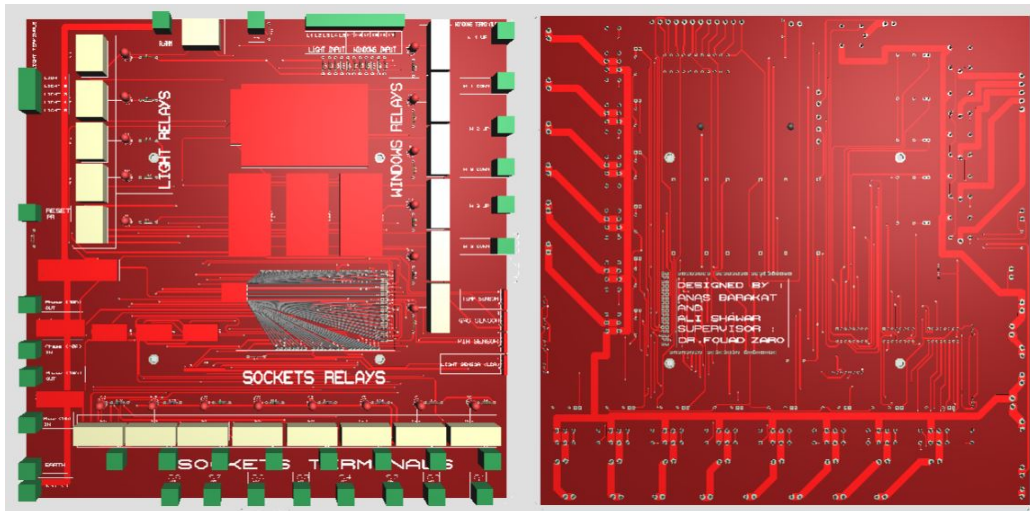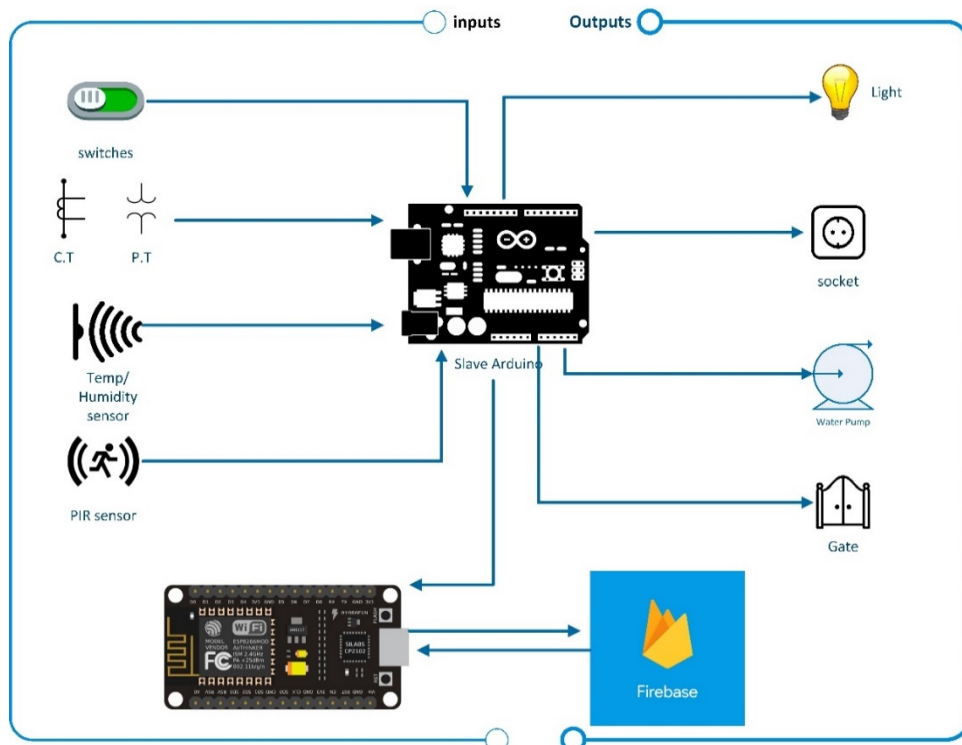- PCB boards: Shield and main PCB boards (figure 8 a-b).

Figure 8. a-b front & back views Indoor-slave main board layout.

2.2. Software design

In this section we are listing all software programs (Tables 1&2) used in designing our system's hardware and software and the main flowcharts of each circuit describing the main processes and techniques used in the system.

Table 1. programming languages used.

Programming Language	Use
Arduino IDE software based on C/C++	Arduino programming
Http Commands + AT commands	Google firebase real-time database
android SDK based on Java	android Application programming

Table 2. software programs used.

Program	Use
Proteus version 8.1	Design Main Electrical Circuits PCB schemes
AutoCAD 2016	Design Case Study House
Shapr3D (based on CAD Software)	Design Wall mounted covers for PCB boards
Microsoft Visio 2016	Design study Diagrams and Flowcharts

Figures 11-14 show the flowcharts for the system's main circuit boards and the android application. Master circuit will act as a monitor device for both house electrical consumption and PV system production and includes an intruder siren system capable to detect movement for different 14 PIR distributed all over the house sensors.

The master circuit equipped with Hall Effect current sensor will be described later in this report and with V.Ts for both
- Main house circuit breaker.
- Main PV system circuit breaker.

The board read both RMS value for both voltage and current, and then calculate the power by 10 sec refresh rate, and calculate the consumption/production energy for recent day, month and send them to the database, in which all the data stored in specific variable, then these data read by the android application and presented in statistics page.
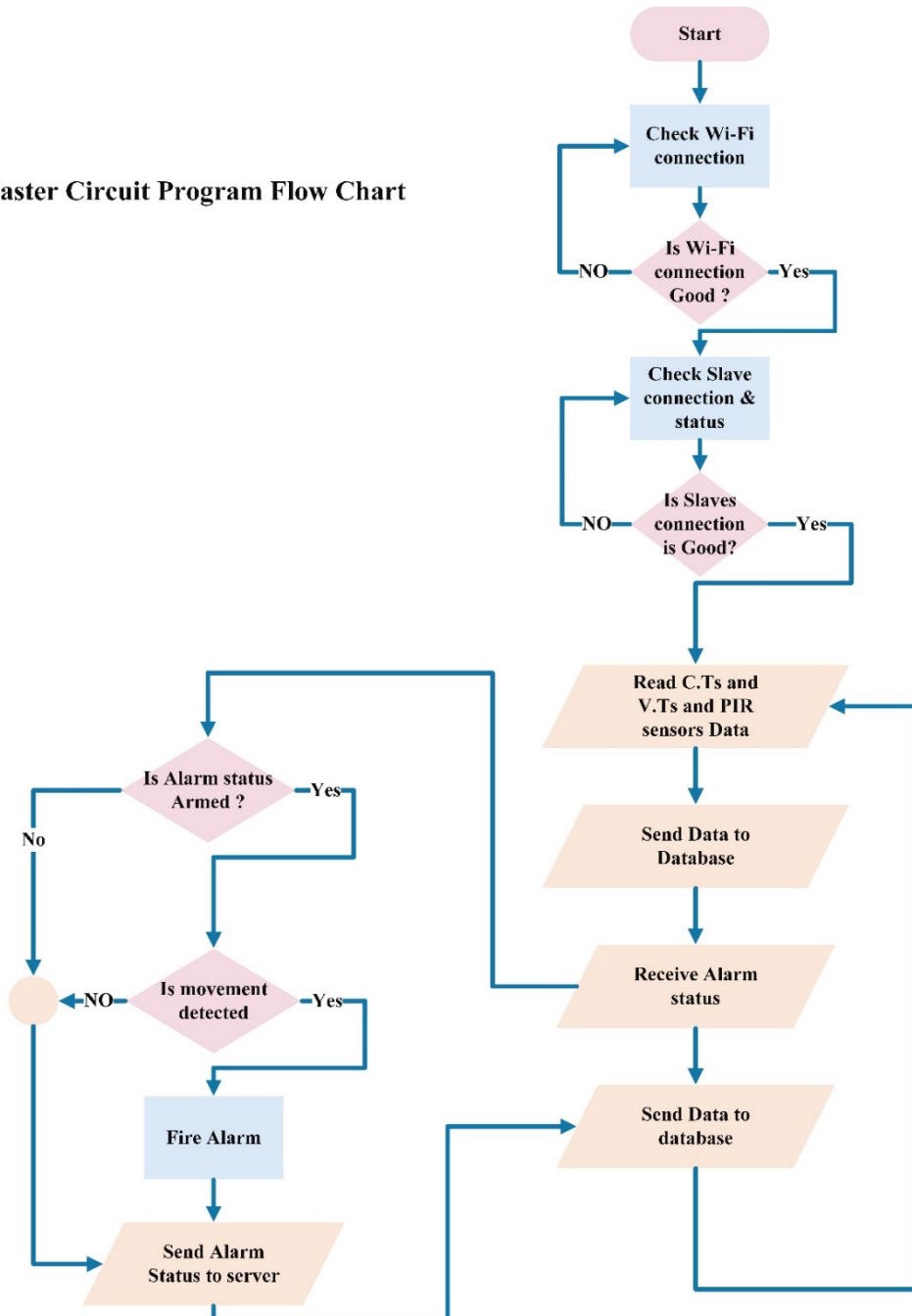

Figure 9. Master flowchart.

In Figure 11, we illustrate the main software algorithm for the master circuit board in the system:

- When the master board start working for the first time, it checks the internet connection as programmed before by the end user.
- After the board receives a robust and stable internet connection it checks the slave's boards connection to make sure that each part of the house is connected and properly working.
- Then the board starts reading each C.T and V.T values to detect the real R.M.S value for the voltage and the current of both the main circuit breaker of the house and the main breaker of the connected PV system (if available).
- Then based on previous readings the board calculates the consumed and produced (power and energy) of the house, then the board send the data to the server and store them inside its own memory in case of any internet connection problems.
- in parallel to previous process the board checks the alarm status from the database (Armed or Not armed), if the system is armed the board checks each PIR value to detect any human movement, if any is detected, then the intruder alarm system will be fired, and the board will send a notification to the database to be send to the user smartphone.
- Furthermore, master circuit calculate 15 minute KW demand and send it to a public or private (as desired) online google sheet, for electrical distribution calculation, this data is very useful for users consumption reading and building distribution transformer loading curves, transformer diversified demand curves, load duration curve and accurate diversity factor table for electrical utility database, so distribution transformer capacity and expansion calculations will be much more accurate for the government or at least for the local electrical supplier.
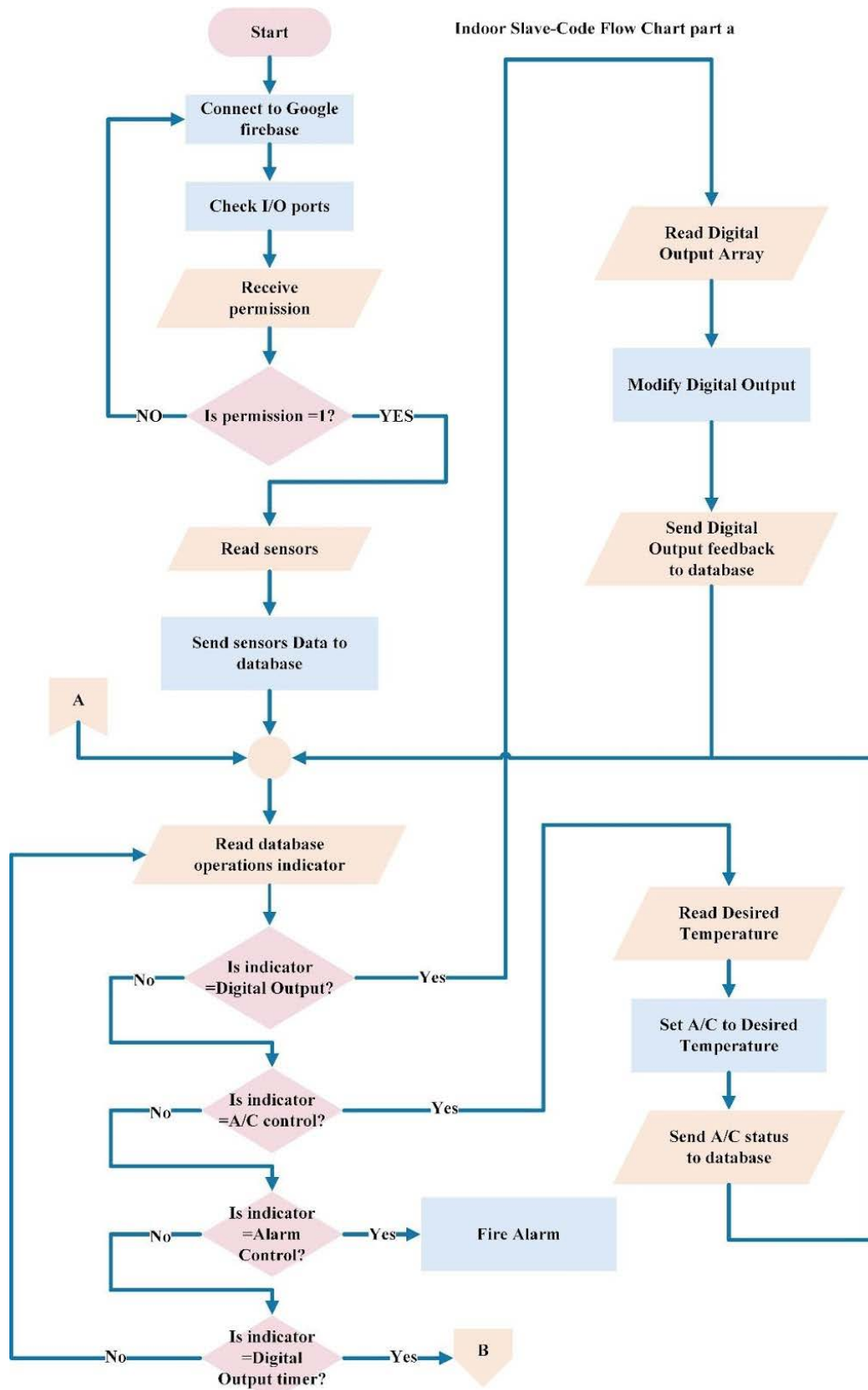
Figure 12. Indoor Slave software Flowchart A.

In Figure 12, we illustrate the main software algorithm for the indoor slave circuit board in the system:

- The circuit initiates the connection with the database using Wi-Fi internet connection, then checks ports status like relays, sensor and actuators, if everything is as expected, the circuit waits the permission to be given by the database to connect.
- After the connection to the Database, the circuit starts reading all sensors data (like: Temperature, humidity, V.T, C.T, PIR, LDR, Gas sensor etc.) and send sensor readings to the database.
- After that the circuit reads consumer commands stored in the database as a serial of characters and numbers (like: daa077664512L99999999w99999999xdab2000220099999999999999999xdac220020 009999999999999999xdad2000220099999999c000x).
- Now each character in the sample above is an indicator, and the serial of numbers are decimals indicates the binary value of each inputs and an encryption for the alarm system and timers for each electrical appliance.
- For HVAC units, the system can read the desired temperature and then decode the temperature to the desired frequency, and then send it to previously programmed IR LED, to turn the HVAC unit on directly to the desired temperature and mode.
- Also the system is programmed with some predefined safety scenarios like if the system detects any toxic gases it automatically open the windows and if any fire is detected the system will activate Fire-Siren system and reach the user by the smartphone application.

Note: for HVAC units, the system is flexible so we can program it to any IR frequency, by other words we could program any IR remote with the system.

Figure 13. Indoor Slave software Flowchart b.

In Figure 13, we illustrate the timer algorithm for the indoor slave circuit board:

In this system, the user is able to define a timer for turning on or off any electrical appliance, for example: The user is able to set a timer to turn the kitchen lights off at 12:00 am, and turn all house's lights on and windows to open on at 7:00 am. Those timers stored in the database as serial of characters and numbers, when the circuit receives these serial it program itself to turn on/off or open/close any electrical appliance as desired.

The main user will communicate with the system using an android application loaded on android smartphone, the application have access specific predefined database for the system, the user will have database link and authentication key, Then the smart app send the authentication key and database link to Google firebase to check access if it's OK then the real-time database let the app control the master and slaves circuits by sending commands and receive information from the system see Figure 14 for android application flowchart.
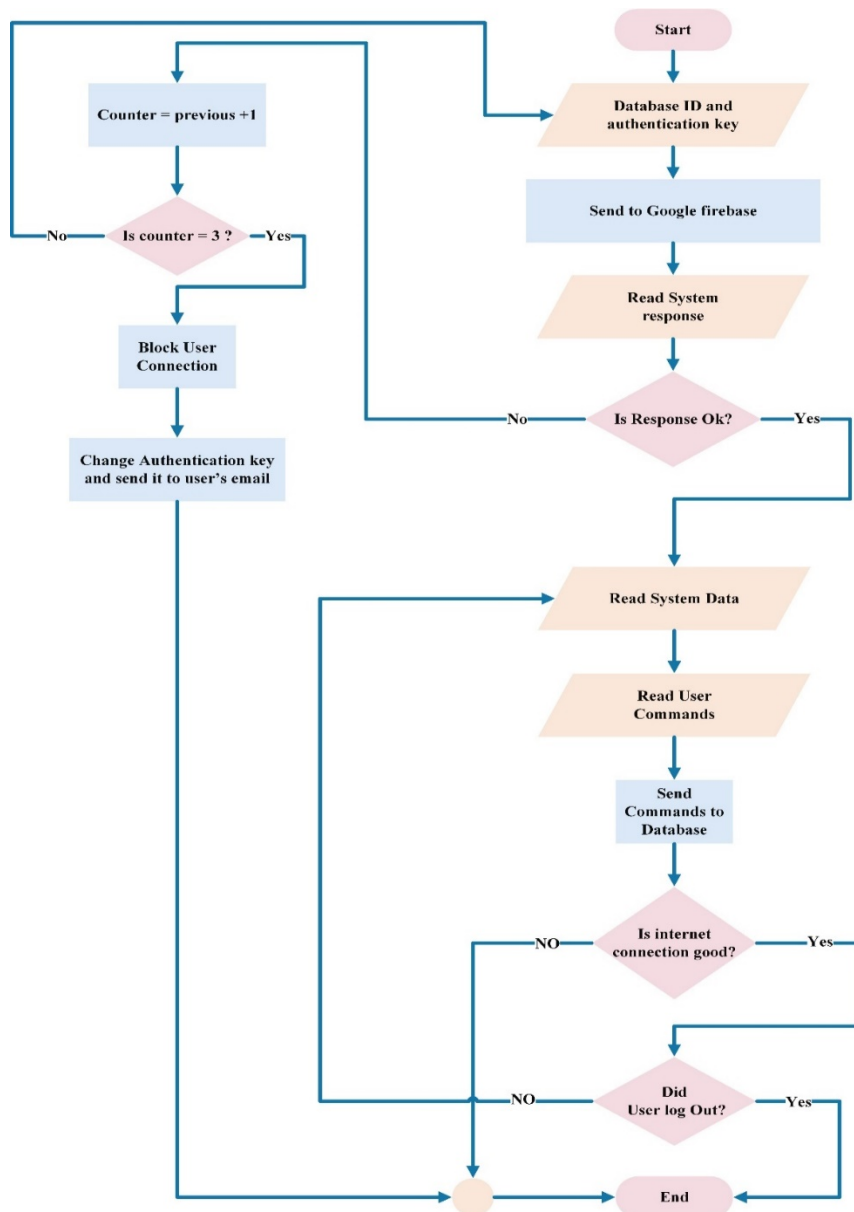

Figure 14. Android app flowchart.

3. IMPLEMENTATION.

In this section we describe the main techniques and how we implemented our system connection, control, electrical consumption measurement and PCB design and calculations.

3.1. System Connection

In this approach we relied on Wi-Fi technology where each circuit of the three has a shield board with NodeMCU controller, the NodeMCU controller provided with Wi-Fi ship that give the microcontroller an internet access which in turn connects the microcontroller to the cloud database (Google firebase).
The system's cloud database has specific name and authentication key, when the NodeMCU connects to Google firebase, google server checks the name and authentication key and gives the NodeMCU access to the system database. Now the microcontroller continually reads cloud's variables and send feedbacks about sensors and devices data and information.

The NodeMCU microcontroller communicates with Arduino microcontroller through I2C communication, this communication provides reliable and robust communication between different manufacturer boards, although it's much simpler than alternative communication types for microcontrollers but yet it's the most used serial communication in microcontroller industry.

3.2. Control

When the user activates an electrical device through the android app, the application generates a series of characters contains an encrypted information about the devices status including the new command then the app sends the data to a specific variable stored in the cloud database, as mentioned before the microcontroller continually read cloud's variables and when a new data is detected the NodeMCU microcontroller send the data to the Arduino Mega 2560 which in turn decrypts the data and activates the desired changes.
In this system the user will be able to control the following:
- Light units.
- Electrical outlets.
- Electrical windows.
- HVAC units the control includes desired temperate and mode (heating or cooling).
- Electrical Gate.
- Electrical water pump.
- And any loads operates with current under 16A.

The user will be able to turn on/off the devices, set desired daily turn on/off time and generate custom buttons able to activate or deactivate any devices as a predefined sequence of activities like (Leave Home button) that automatically deactivate all non-critical devices and close the gate with single button press, typically as any user would do when he leaves his home.
For HVAC unit control, we relied on IR technology, in which we program the system with the AC's remote control IR frequencies for each temperature (18-30) C^0 and mode (heating or cooling).

Also the system will present many electrical and environmental parameters:
- Humidity

- Temperature
- Toxic Gas & fire status.
- House power consumption (watt).
- House monthly consumption (kWh).
- House daily consumption (kWh).
- PV system generation power (Watt).
- PV system monthly generation energy (kWh).
- PV system daily generation energy (kWh).
- PV status. (Normal, need cleaning or need maintenance).

PV status is a technique in which the system will compare the generated energy and peak power of the system daily and compare it with NASA database of the solar hours of system's location and determine whether the system generates the expected energy or not.

3.3. Power and Energy Calculations.

In this section we're illustrating our technique in calculating voltage and current RMS values. For voltage measuring we're using ZMPT101B voltage transformer, that converts voltage from AC range to DC sinusoidal wave form with 2.5v reference value, in order to calculate the RMS value we take 40 samples each cycle (i.e. one sample each 500 micro seconds), then we calculate the RMS value for the measured cycle using the following equation.

$$\text{Vrms/cycle} = \sqrt{\frac{\sum_1^{40} \text{Vsample}^2}{40}} \qquad (3.3.1)$$

And for higher accuracy we take the average RMS value for 12 cycle, this process refreshed each 10 seconds, this calculation process used for both current and voltage and for current measuring we're using ACS712 Hall Effect IC.

Each 10 seconds we calculate the apparent power and add it to energy variables to calculate energy.

$$\text{S (VA)} = \text{Vrms} * \text{Irms} \qquad (3.3.2)$$

To calculate the average power we need to calculate PF (power factor), and to do so we measure the time difference b/t voltage zero crossing sample and current zero crossing sample, as we have 20 sample per cycle

$$1 \text{ x Cycle} = 20\text{ms for 50 hz frequency}$$

And

$$1 \text{ x Cycle} = 360 \text{ degree}$$

For 20 samples per cycle we have

$$1 \text{ x sample} = 1\text{ms} = 18 \text{ degree.}$$

Now we calculate the number of samples b/t voltage zero crossing sample and current zero crossing sample

$$V_0 \text{ sample } \# - I_0 \text{ sample } \# = N. \qquad (3.3.3)$$

Now for power factor angle

$$\theta = 18 * N \qquad (3.3.4)$$

$$PF = \cos(\theta) \tag{3.3.5}$$

Average power

$$P_{avg} = S * PF \tag{3.3.6}$$

$$\text{Energy variable (Watt Hour)} = \text{prevoius value (watt Hour)} + P_{avg}(\text{watt}) * \left(\frac{10}{3600}\right) \tag{3.3.7}$$

3.4. PCB design and calculation

All PCB boards designed using Proteus software ver. 8.1.

For trace's width calculations we have 2 types of traces:

- ❖ Signal trace that represent all signals from-into Arduino boards.
- ❖ Power traces that represent phase traces, 16 Amp phase for power circuits and 10 Amp phase for lighting circuits.

3.4.1. Traces widths

- ❖ For signal trace width we chose 1.2 mm width which is s standard in PCB design.
- ❖ For 10 Amp trace we chose 3.75 mm width.
- ❖ For 16 Amp trace we chose 4.5 mm width.

3.4.2. Calculations

First, the Area is calculated:

Area [mils^2] = (Current [Amps]/ (k*(Temp_Rise [deg. C])^b))^(1/c) (3.4.2.1)

Then, the Width is calculated:

Width [mils] = Area [mils^2]/ (Thickness [oz]*1.378[mils/oz]) (3.4.2.2)

For IPC-2221 external layers: k = 0.048, b = 0.44, c = 0.725

- For 16A traces:

Area $=\left(\frac{16}{0.048*50^{0.44}}\right)^{1/0.725} = 281.01(\text{mils}^2)$

Width $=\frac{281.01}{1*1.378} = 204(\text{mils})$

204 mils =5.18/2=2.56 mm

Average Ambient Temp. =50 C° Temp. Rise = 20 C°.

- For 10A traces:

Area $=\left(\frac{10}{0.048*50^{0.44}}\right)^{1/0.725} = 146.95(\text{mils}^2)$

Width $=\frac{146.95}{1*1.378} = 107(\text{mils})$

107 mils =2.71 /2=1.355mm

Average Ambient Temp. =50 C^o Temp. Rise = 20 C^o.

4. DISCUSSION

This paper demonstrates that a low cost, flexible and scalable smart home automation system based on Arduino technology and Wi-Fi connection has been designed, implemented and established, each PCB circuit had been printed and tested thermally and it could withstand without any external cooling in environment with ambient temperature up to 45 C^0 .

Furthermore, this specific system has been implemented on a small room unit and tested for more than 6 months, all circuits worked perfectly fine, with command success rate of 99%, and the speed of processing the command was on average 1.5 second, and the average time for receiving the feedback of the processed command takes on average 2.7 seconds.

In comparison with other smart home systems our system will cost quarter the cost of other systems such as (ABB, Siemens, Belkin), these systems use master unit to control all the devices where each device has independent circuit that control and connect it to the master unit, this method will increase the price a lot where the total number of the circuits used is large.

5. CONCLUSION

 The proposed system consists of many sub-systems that controlled by Arduino and Node-MCU microcontroller as a main controlling system, in addition, to apply specific techniques for the reduction of power consumption and load management. All equipment connected to a cloud database that communicates with the user by an android application connected to the internet. The system is accessible anywhere, anytime for controlling and monitoring issues. The performance of the communication system works well, although it is highly dependent on the internet provider.

A prototype for a specific house has been built, the proposed system is able to control all home electrical units and appliances like lighting, sockets, HVAC units, fire, gas and intruder siren systems perfectly, in addition, to monitor the real-time power consumption, the house PV system generation and the current room's temperature and humidity. Furthermore, the system is able to reduce power consumption using predefined algorithms.

The proposed architecture of SHAS increases the safety protection to the user; the system uses a low voltage activating switches rather than the conventional electrical switches. Moreover, implementing Wi-Fi connection in master and slave control boards that allows the system installs in a simpler way. Furthermore, any Smartphone based on Android and support Wi-Fi can be used to access, monitor and control the devices at home. Future works will focus on controlling the application of home devices by voice commands.

REFERENCES

[1] G. Kortuem, F. Kawsar, V. Sundramoorthy, and D. Fitton, "Smart objects as building blocks for the internet of things," IEEE Internet Computing, vol. 14, no. 1, pp. 44-51, 2010.
[2] S. Kumar, "Ubiquitous smart home system using android application," arXiv preprint arXiv:1402.2114, 2014.
[3] A. ElShafee and K. A. Hamed, "Design and implementation of a WIFI based home automation system," World academy of science, engineering and technology, vol. 68, pp. 2177-2180, 2012.
[4] S. Anwaarullah and S. Altaf, "RTOS based home automation system using Android," international journal of advanced Trends in computer science and engineering, vol. 2, no. 1, pp. 480-484, 2013.
[5] R. J. Nunes and J. C. Delgado, "An Internet application for home automation," in Electrotechnical Conference, 2000. MELECON 2000. 10th Mediterranean, 2000, vol. 1, pp. 298-301: IEEE.

[6]   M. Soliman, T. Abiodun, T. Hamouda, J. Zhou, and C.-H. Lung, "Smart home: Integrating internet of things with web services and cloud computing," in 2013 IEEE 5th international conference on cloud computing technology and science, 2013, vol. 2, pp. 317-320: IEEE.

[7]   D. B. Adriano and W. A. C. Budi, "Iot-based Integrated Home Security and Monitoring System," in Journal of Physics: Conference Series, 2018, vol. 1140, no. 1, p. 012006: IOP Publishing.

[8]   Y. Kurnia and J. L. J. b.-T. Sie, "Prototype of Warehouse Automation System Using Arduino Mega 2560 Microcontroller Based on Internet of Things," vol. 1, no. 3, pp. 124-130, 2019.

[9]   T. J. Alexander, "An implementation of mobile control room environment in android platform for industrial applications," in 2015 International Conference on Circuits, Power and Computing Technologies [ICCPCT-2015], 2015, pp. 1-4: IEEE.

[10] I. Abubakar, S. Khalid, M. Mustafa, M. Mustapha, and H. J. A. S. L. Shareef, "Residential Energy Consumption Management Using Arduino Microcontroller," vol. 24, no. 6, pp. 3887-3893, 2018.

[11] S. A. J. F. T. Mohammed, "Designing a Maximum Power Point Tracking System for a Monocrystalline Silcion Solar Module Using the Arduino Microcontroller and Synchronous Buck Converter," vol. 47, no. 3, p. 525, 2019.

[12] C. Mejia, C. Llivisaca, L. I. Minchala, L. Gonzalez, and J. Gonzalez, "Blade stress monitoring in a small wind turbine by using Arduino microcontroller," in 2018 IEEE International Autumn Meeting on Power, Electronics and Computing (ROPEC), 2018, pp. 1-5: IEEE.

[13] M. R. Alam, M. B. I. Reaz, M. M. J. I. T. o. S. Ali, Man,, C.-P. A. Systems, and Humans, "SPEED: An inhabitant activity prediction algorithm for smart homes," vol. 42, no. 4, pp. 985-990, 2011.

[14] S. Zhihua, "Design of Smart Home System Based on ZigBee," in 2016 International Conference on Robots & Intelligent System (ICRIS), 2016, pp. 167-170.

[15] H. Zheng, H. Zhang, and L. Pan, "Modeling and Analysis of ZigBee Based Smart Home System," in 2014 5th International Conference on Digital Home, 2014, pp. 242-245.

[16] X. Wen and Y. Wang, "Design of smart home environment monitoring system based on raspberry Pi," in 2018 Chinese Control And Decision Conference (CCDC), 2018, pp. 4259-4263.

[17] P. Kumar and P. Umesh Chandra, "Arduino and Raspberry Pi based smart communication and control of home appliance system," in 2016 Online International Conference on Green Engineering and Technologies (IC-GET), 2016, pp. 1-6.

[18] S. Mahmud, S. Ahmed, and K. Shikder, "A Smart Home Automation and Metering System using Internet of Things (IoT)," in 2019 International Conference on Robotics,Electrical and Signal Processing Techniques (ICREST), 2019, pp. 451-454.

[19] G. M. M and C. Vyjayanthi, "Implementation of Cost Effective Smart Home Controller with Android Application Using Node MCU and Internet of Things (IOT)," in 2018 2nd International Conference on Power, Energy and Environment: Towards Smart Technology (ICEPE), 2018, pp. 1-5.

[20] R. K. Kodali and K. S. Mahesh, "Low cost implementation of smart home automation," in 2017 International Conference on Advances in Computing, Communications and Informatics (ICACCI), 2017, pp. 461-466.

[21] A. Express. (2018, 01/12/2018). Arduino accesorios. Available: https://www.aliexpress.com/wholesale?catId=0&initiative_id=AS_20181201121635&SearchText=arduino +accesorios

APPENDIX

List of Symbols and Abbreviations

SHAS	Smart Home Automation System.
IoT	Internet of Things
PC	Personal Computer
HVAC	Heating Ventilating Air Conditioning units
UPS	Uninterruptable Power Supply
I/O	Inputs/Outputs
USB	Universal Serial Bus
LAN	Local Access Network
PCB	Printed Circuit Board
I2C	Inter-Integrated Circuit
IP	Internet Protocol
C.T	Current Transformer
P.T	Potential Transformer
IS	Indoor Slave
OS	Outdoor slave
LDR	Light Dependent Resistor
PIR	Passive Infrared Sensor
Kbps	kilobytes per second
SCL	Serial Clock Line
SDA	Serial Data Addressing
ID	Identification
SRAM	Static Random Access Memory
EEPROM	Electrically Erasable Programmable Read-Only Memory
LED	Light Emitting Diode
DC	Direct Current
IR	Infra-Red
RH	Relative Humidity
CAD	Computer-aided drafting
IDE	Integrated Development Environment
Http	Hypertext Transfer Protocol
SDK	Software Development Kit
3D/2D	3 Dimensions/ 2 Dimensions.